Aerosol Characterization over the Southeastern United States Using High Resolution Aerosol Mass Spectrometry: Spatial and Seasonal Variation of Aerosol Composition and Sources with a Focus on Organic Nitrates

Lu Xu[1], Sriram Suresh[1,*], Hongyu Guo[2], Rodney J. Weber[2], Nga Lee Ng[1,2]

[1]School of Chemical and Biomolecular Engineering, Georgia Institute of Technology, Atlanta, GA, USA

[2]School of Earth and Atmospheric Sciences, Georgia Institute of Technology, Atlanta, GA, USA

[*]now at: ExxonMoBil, Omaha, NE, USA

Correspondence to: N. L. Ng (ng@chbe.gatech.edu)

Abstract

We deployed a High-Resolution Time-of-Flight Aerosol Mass Spectrometer (HR-ToF-AMS) and an Aerosol Chemical Speciation Monitor (ACSM) to characterize the chemical composition of submicron non-refractory particles (NR-PM_1) in the southeastern US. Measurements were performed in both rural and urban sites in the greater Atlanta area, Georgia (GA), and Centreville, Alabama (AL) for approximately one year, as part of Southeastern Center for Air Pollution and Epidemiology study (SCAPE) and Southern Oxidant and Aerosol Study (SOAS). Organic aerosol (OA) accounts for more than half of NR-PM_1 mass concentration regardless of sampling sites and seasons. Positive matrix factorization (PMF) analysis of HR-ToF-AMS measurements identified various OA sources, depending on location and season. Hydrocarbon-like OA (HOA) and cooking OA (COA) have important, but not dominant, contributions to total OA in urban sites (i.e., 21-38% of total OA depending on site and season). Biomass burning OA (BBOA) concentration shows a distinct seasonal variation with a larger enhancement in winter than summer. We find a good correlation between BBOA and brown carbon, indicating biomass burning is an important source for brown carbon, although an additional, unidentified brown carbon source is likely present at the rural Yorkville site. Isoprene-derived OA (Isoprene-OA) is only deconvolved in warmer months and contributes 18-36% of total OA. The presence of Isoprene-OA factor in urban sites is more likely from local production in the presence of NO_x than transport from rural sites. More-oxidized and less-oxidized oxygenated organic aerosol (MO-OOA and LO-OOA, respectively) are dominant fractions (47-79%) of OA in all sites. MO-OOA correlates well with ozone in summer, but not in winter, indicating MO-OOA sources may vary with seasons. LO-OOA, which reaches a daily maximum at night, correlates better with estimated nitrate functionality from organic nitrates than total nitrates.

Based on the HR-ToF-AMS measurements, we estimate that the nitrate functionality from organic nitrates contributes 63-100% to the total measured nitrates in summer. Further, the contribution of organic nitrates to total OA is estimated to be 5-12% in summer, suggesting that organic nitrates are important components in the ambient aerosol in the southeastern US. The spatial distribution of OA is investigated by comparing simultaneous HR-ToF-AMS measurements with ACSM measurements at two different sampling sites. OA is found to be

spatially homogeneous in summer, possibly due to stagnant air mass and a dominant amount of regional secondary organic aerosol (SOA) in the southeastern US. The homogeneity is less in winter, which is likely due to spatial variation of primary emissions.

We observed that the seasonality of OA concentration shows a clear urban/rural contrast. While OA exhibits weak seasonal variation in the urban sites, its concentration is higher in summer than winter for rural sites. This observation from our year-long measurements is consistent with 14 years of organic carbon (OC) data from the SouthEastern Aerosol Research and Characterization (SEARCH) network. The comparison between short-term measurements with advanced instruments and long-term measurements of basic air quality indicators not only tests the robustness of the short-term measurements, but also provides insights in interpreting long-term measurements. We find that OA factors resolved from PMF analysis on HR-ToF-AMS measurements have distinctly different diurnal variations. The compensation of OA factors with different diurnal trends is one possible reason for the repeatedly observed, relatively flat OA diurnal profile in the southeastern US. In addition, analysis of long-term measurements shows that the correlation between OC and sulfate is substantially stronger in summer than winter. This seasonality could be partly due to the effects of sulfate on isoprene SOA formation as revealed by the short-term, intensive measurements.

1. Introduction

The southeastern US is an intriguing region to study aerosol formation. Firstly, the fine particulate matter ($PM_{2.5}$) concentration is generally high and often exceeds the National Ambient Air Quality Standards (NAAQS) (Cohan et al., 2007; Blanchard et al., 2013). Secondly, the southeastern US is characterized by large emissions from both biogenic and anthropogenic sources, which makes it an ideal region to study the effects of interactions between biogenic/anthropogenic emissions on organic aerosol formation and air quality. Roughly, half of the land in the southeastern US is covered by forests, which emit large amounts of biogenic volatile organic compounds (VOCs) that are precursors for secondary organic aerosol (SOA) formation (Geron et al., 2000; Guenther et al., 2006). Based on radiocarbon analysis, Schichtel et al. (2008) showed that about 90% of total carbon is biogenic in a rural site in Tennessee.

Similarly, Weber et al. (2007) found that 70-80% of the carbon in water-soluble organic carbon (WSOC, a surrogate for SOA) is of biogenic origin in Atlanta, GA. However, recent studies revealed that the formation of SOA from biogenic VOCs is largely controlled by anthropogenic emissions in the southeastern US (Weber et al., 2007; Xu et al., 2015). Thirdly, a wide range of air quality data has been routinely collected by the SEARCH (SouthEastern Aerosol Research and Characterization) network, including multiple rural and urban sites in the southeastern US from 1999 to 2013 (Edgerton et al., 2005; Hansen et al., 2003; Hidy et al., 2014). Combining short-term field campaigns and long-term measurements is useful because short-term field campaigns with state-of-the-art instruments can better characterize atmospheric processes and provide insights in interpreting the long-term observations. In turn, long-term measurements of basic air quality parameters are helpful when testing the robustness of short-term field campaign results (Hidy et al., 2014).

A number of field studies have been conducted to understand the sources of OA in the southeastern US. Lim and Turpin (2002) showed that ~50% of OC is secondary in urban Atlanta by using an EC tracer method. Blanchard et al. (2008) applied three different empirical models and estimated that the fraction of secondary OC (SOC) in OC is ~20-60% in the southeastern US, which was higher at rural sites compared to urban sites and higher in summer compared to winter. The authors also showed that the estimated SOC/OC ratio highly depends on the estimation methods. By using WSOC as a surrogate for SOC, Weber et al. (2007) showed that SOC accounts for roughly 75% of OC in Yorkville, a rural site in GA, while the contribution of SOC to OC decreases to about 65% in Georgia Institute of Technology, an urban site. However, these studies were based on bulk properties, such as OC and WSOC, which makes it challenging for OC source apportionment beyond separating it into primary and secondary OC. Attempts have been made to apportion OC into different sources based on molecular makers. For example, by using molecular maker-based chemical mass balance modeling (CMB-MM), Zheng et al. (2006) attributed OC into various primary emission sources such as wood combustion and gasoline engine exhaust. However, limited by the number of molecular markers included in the model, the CMB-MM method is insufficient to resolve SOC and often results in high percentages of unexplained OC (Zheng et al., 2002). Also, filter samples collected on a daily basis have been used in most previous studies, which limits the temporal resolution and could introduce uncertainty due to filter sampling artifacts. The Aerodyne Aerosol Mass Spectrometer (AMS)

has been widely used to characterize the chemical composition of submicron non-refractory species with high temporal resolution (Canagaratna et al., 2007; Jayne et al., 2000). Budisulistiorini et al. (2013) deployed an Aerosol Chemical Speciation Monitor (ACSM) (Ng et al., 2011) at the SEARCH Jefferson Street site in downtown Atlanta, GA. Various OA sources were identified by factor analysis in Budisulistiorini et al. (2013), including one source related to isoprene oxidation. However, due to the lower resolving power of ACSM, PMF analysis on ACSM data can have difficulty in separating different primary sources such as cooking and vehicle emission, which have similar mass spectra (Crippa et al., 2014; Mohr et al., 2009). In addition, measurements at both rural and urban sites are needed in order to investigate the spatial distribution of aerosol and various OA subtypes.

Organic nitrates are important atmospheric species as their fate could affect the nitrogen cycle and ozone production (Perring et al., 2013; Mao et al., 2012). Organic nitrates, which are primarily formed from VOCs oxidation by nitrate radicals, or by ozone and hydroxyl radical in the presence of NO_x, have been shown to be an important component of organic aerosol. For example, Rollins et al. (2012) observed that organic nitrates contribute about 27-40% to the OA growth at night in Bakersfield, CA, by using a Thermal-Dissociation Laser-Induced-Fluorescence technique (TD-LIF) (Day et al., 2002). Multiple approaches have also been proposed to estimate organic nitrates from indirect measurements. For example, Farmer et al. (2010) proposed that the concentration of the nitrate functionality (i.e., $-ONO_2$) in organic nitrates could be estimated based on the nitrate functionality fragmentation pattern in the AMS, or the differences between AMS and ion-chromatography (IC) measurements.

In this study, we performed measurements by a suite of instrumentation in multiple sites in the greater Atlanta, GA, area, and Centerville, AL, with a focus on a high-resolution time-of-flight aerosol mass spectrometer (HR-ToF-AMS). Positive matrix factorization analysis is performed on HR-ToF-AMS data to identify distinct OA sources. The contribution of organic nitrates to total OA is estimated by different methods based on HR-ToF-AMS measurements. Measurements were performed in both rural and urban sites to investigate the spatial distribution of aerosol in the southeastern US. In addition, measurements spanning over a year allow us to evaluate the seasonal variation of aerosol composition. These results are supported by long-term

144 measurements from the SEARCH network and provide further insights into interpreting historic
145 measurements.

146

147 **2. Method**

148 Measurements were conducted at the following sites as part of two field campaigns:

149 2.1 Southern Oxidant and Aerosol Study (SOAS)

150 The Southern Oxidant and Aerosol Study (SOAS, http://soas2013.rutgers.edu/) is a
151 collaborative field campaign that took place from 1 June to 15 July 2013. The sampling site
152 (32.94°N, 87.18°W) is a SEARCH network site near Centreville, in rural Alabama, as shown in
153 Fig. 1. The site is located in a forested area away from large urban cities (55km SE of Tuscaloosa
154 and 84 km SW of Birmingham, AL). Detailed meteorological conditions of the sampling site can
155 be found in Hidy et al. (2014). In brief, the sampling period was characterized by high relative
156 humidity (>50% all the time), warm temperatures (daily maximum 28.6 °C at 15:00 local time),
157 and light winds (Xu et al., 2015).

158 2.2 Southeastern Center for Air Pollution and Epidemiology study (SCAPE)

159 This extensive field study was part of the Southeastern Center for Air Pollution and
160 Epidemiology (SCAPE, http://scape.gatech.edu/), which is an EPA-funded joint research center
161 between Georgia Tech and Emory University, focusing on the study of air quality and the health
162 effects of air pollutants (Verma et al., 2014; Winquist et al., 2014; Russell et al., 2014). Four
163 sampling sites in both rural and urban areas are selected, as shown in Fig. 1. Detailed description
164 of each sampling site can be found in Verma et al. (2014) and Hansen et al. (2003). Briefly,

165 • Roadside site (RS site) is on the Georgia Tech campus and adjacent (within 5 m) to the
166 Interstate 75/85 (8 lanes each direction). According to Georgia Department of
167 Transportation, about 95% of the traffic fleet on the Interstate 75/85 is light-duty gasoline
168 vehicles.

- Georgia Tech site (GT site) is also on the Georgia Tech campus, but 840 m away from the roadside site. The GT site is located on the top floor of the Ford Environmental Science & Technology Building, which is 30-40 m above ground.
- Jefferson Street site (JST site) is a central SEARCH network site, which is about 2 km west of the Georgia Tech site. This site is situated in Atlanta's urban area and surrounded by a mixed residential and commercial neighborhood and is considered representative of urban Atlanta.
- Yorkville site (YRK site) is the SEARCH rural pair to the JST site located approximately 80 km northwest of JST. This site is situated in a mixed forested – agricultural area and immediately surrounded by pastures for cattle grazing.

We outfitted a trailer with a large suite of instrumentation (described in section 2.3) and conducted measurements from May 2012 to February 2013, with roughly one month at each site, and repeated it in different seasons. The sampling periods are listed in Table 1.

While the trailer was rotated between multiple sites, we also deployed an Aerosol Chemical Speciation Monitor (ACSM, described in section 2.3.2) (Ng et al., 2011) at the Georgia Tech site from May 2012 to February 2013. The paired and simultaneous measurements using an ACSM at the Georgia Tech site and a High Resolution Time-of-Flight Aerosol Mass Spectrometer (HR-ToF-AMS, described in section 2.3.1) rotating among four different sites allow for investigating spatial distributions of aerosol loading and composition in the greater Atlanta area. It is noted that from 20 July to 4 September 2012, both the HR-ToF-AMS and the ACSM were deployed at the Georgia Tech site for instrument inter-comparison.

2.3 Instrumentation

2.3.1 High Resolution Time-of-Flight Aerosol Mass Spectrometer (HR-ToF-AMS)

An Aerodyne High-Resolution Time-of-Flight Aerosol Mass Spectrometer (HR-ToF-AMS) was rotated among different sites in this study to characterize the composition of ambient submicron non-refractory particulate matter (NR-PM_1). A detailed description of the HR-ToF-AMS can be found in the literature (Canagaratna et al., 2007; DeCarlo et al., 2006). In brief, the HR-ToF-AMS focuses ambient particles with vacuum aerodynamic diameter smaller than 1μm into a narrow beam via an aerodynamic lens. The submicron particles are then impacted on a hot

198 tungsten surface (~600°C), where non-refractory species are flash vaporized. The resultant
199 vapors are ionized using 70eV electron impact ionization and analyzed by a time-of-flight mass
200 spectrometer. During sampling, a PM_1 cyclone was used to remove coarse particles. A nafion-
201 dryer was placed upstream of the HR-ToF-AMS to dry the particles (relative humidity <20%) in
202 order to eliminate the potential influence of relative humidity on particle collection efficiency
203 (CE) at the vaporizer (Matthew et al., 2008). Gas-phase interference was eliminated by
204 subtracting the signals when the HR-ToF-AMS sampled through a HEPA filter, which was
205 performed regularly on a daily basis at different times of the day. Ionization efficiency (IE)
206 calibrations were performed with 300nm ammonium nitrate particles, on a weekly basis. The
207 composition-dependent CE was applied to the data based on Middlebrook et al. (2012). We
208 operated the HR-ToF-AMS in two ion optical modes (V and W) with different sensitivity and
209 spectra resolution, but only V mode data are reported in this study considering the low intensity
210 of W mode data. The average sampling time was set at two minutes. The data analysis was
211 performed using the standard AMS analysis toolkits SQUIRREL v1.53 and PIKA v1.12 in Igor
212 Pro 6.34 (WaveMetrics Inc.). Default RIE values were used for the HR-ToF-AMS data.
213 Elemental ratios, such as atomic oxygen-to-carbon ratio (O:C), hydrogen-to-carbon ratio (H:C),
214 and organic mass-to-organic carbon ratio (OM:OC), are determined by following the latest
215 procedures recommended by Canagaratna et al. (2015). Canagaratna et al. (2015) improved the
216 estimation from Aiken et al. (2008), which has been widely used in the literature to estimate
217 elemental ratios, by including composition-dependent correction factors. Caution is required
218 when comparing the elemental ratios in this study with values reported in the literature, which
219 typically used the Aiken estimation. Nitrate signals (NO^+ and NO_2^+) and sulfate signals (SO^+,
220 SO_2^+, etc) are not included in the elemental ratio calculations. Oxidation state (OS) is calculated
221 as 2*O:C – H:C (Kroll et al., 2011).

222 2.3.2 Aerosol Chemical Speciation Monitor (ACSM)

223 An Aerosol Chemical Speciation Monitor (ACSM) was stationary at the Georgia Tech
224 site from 10 May 2012 to 28 February 2013. Similar to the HR-ToF-AMS, the ACSM also
225 provides continuous, quantitative measurements of NR-PM_1 (Ng et al., 2011). The mass
226 resolving power of ACSM (~200) is lower than that of the HR-ToF-AMS (~2000 in V mode)
227 due to use of a low cost residual gas analyzer (RGA) quadrupole mass spectrometer in ACSM

(Ng et al., 2011). In addition, the time resolution of ACSM (~30min) is longer than that of HR-ToF-AMS (~2min). The response factor (RF) of the ACSM was also determined by using 300nm ammonium nitrate particles (Ng et al., 2011). The relative ionization efficiency (RIE) values used for organics, nitrate, and chloride are 1.4, 1.1, and 1.3, respectively. RIE values of 4.18 and 0.59 were used for ammonium and sulfate, which were determined from IE calibrations by using ammonium nitrate and ammonium sulfate particles.

2.3.3 Co-located Instruments

In addition to the HR-ToF-AMS, we deployed various instruments in the trailer while performing measurements at multiple sites (Verma et al., 2014). Instruments of interest to this study include a PILS-LWCC-TOC system (Particle Into Liquid Sampler - Liquid Waveguide Capillary Cell - Total Organic Carbon analyzer), a seven-wavelength Aethalometer and a multi-angle absorption photometer (MAAP). The PILS-LWCC-TOC system continuously (i.e., 15min resolution) measured the light absorption spectra of water-soluble organic components. The detailed working principle of the PILS-LWCC-TOC system can be found in Hecobian et al. (2010). In brief, water-soluble species are first dissolved in water in a PILS (Weber et al., 2001). The liquid sample from the PILS is then injected into a Liquid Waveguide Capillary Cell, where the absorption spectra are collected over wavelengths of 200 to 800nm. The average light absorption between 360 to 370 nm is used as a measure of brown carbon light absorption. Black carbon concentration was measured by either a seven-wavelength Aethalometer or a multi-angle absorption photometer (MAAP). For the Aethalometer, measurements at 660nm were chosen to represent the black carbon concentration, because 660nm is closest to the wavelength utilized by the MAAP. The measured data were corrected for loading effects (Virkkula et al., 2007). The temporal resolutions are 2 min and 1 min for Aethalometer and MAAP, respectively.

At the Jefferson Street (JST) and Yorkville (YRK) sites, a suite of instruments was operated by the SEARCH Network. Detailed descriptions about the collocated instruments can be found in Hansen et al. (2003) and Edgerton et al. (2005). In brief, O_3 concentration was measured by a UV-absorption analyzer with a temporal resolution of 1min. NO and NO_x were measured by a chemilumnescence analyzer (1min temporal resolution), where the NO_2 concentration was calculated by subtracting NO from the total NO_x. $PM_{2.5}$ sulfate and OC were continuously measured by a Fe reduction/UV-fluorescence analyzer and an oxidative combustion

(R&P 5400) analyzer, respectively. The temporal resolution is 5min and 60min for $PM_{2.5}$ sulfate and OC, respectively. Meteorological conditions, such as temperature, relative humidity (RH), solar radiation, and wind speed were also recorded.

2.4 Positive Matrix Factorization (PMF) Analysis

Positive Matrix Factorization (PMF) is a mathematical technique to solve bilinear unmixing problems (Paatero, 1997; Paatero and Tapper, 1994). PMF analysis has been widely applied in the aerosol community for source apportionment (Ulbrich et al., 2009; Jimenez et al., 2009; Zhang et al., 2010; Lanz et al., 2007; Ng et al., 2010; Beddows et al., 2015; Jaeckels et al., 2007; Visser et al., 2015). For the data measured by AMS, PMF analysis represents the observed data matrix as a linear combination of various factors with constant mass spectra but varying concentrations across the dataset (Ulbrich et al., 2009; Zhang et al., 2011). To determine the sources of organic aerosol, PMF analysis was performed on the high-resolution organic mass spectra (*m/z* 12 - 200) obtained by the HR-ToF-AMS for each sampling dataset. We generated the organic data matrix and error matrix from PIKA v1.12 and pretreated the error matrix by using PMF Evaluation Toolkit (PET) software following the procedure described in Ulbrich et al. (2009). Variables (i.e., *m/z*'s) with a signal-to-noise ratio less than 0.2 are removed and variables with a signal-to-noise ratio ranging between 0.2 and 2 are downweighted by a factor of 2. We downweighted the errors of O^+, HO^+, H_2O^+, and CO^+, which are related to CO_2^+ signal, to avoid excessive weighting of CO_2^+. In addition, for four datasets (JST_May, CTR_June, YRK_July, and GT_Aug), the error of CHO^+ is downweighted by a factor of 4. This is because that PIKA v1.12 appears to underestimate CHO^+ error, possibly caused by the overlap of the CHO^+ (*m/z* 29.0027) ion with its adjacent N_2 isotope ion (j15NN, *m/z* 29.0032). For the other three datasets (JST_Nov, YRK_Dec, and RS_Jan), CHO^+ is not included in the PMF analysis due to its occasional negative signal, which is likely caused by a low CHO^+ signal in winter. At times, the CHO^+ concentration is near the detection limit, so a shift in threshold might cause the CHO^+ signal to be treated as noise. PMF solutions were carefully evaluated according to the procedure outlined in Zhang et al. (2011). For each dataset, the optimal solution was determined after examining the residuals of PMF fits, interpretability of factor's diurnal trend, factor correlation with external tracers, and characteristic signatures of factor mass spectrum. The rotational ambiguity of solutions was examined by changing the parameter FPEAK and the robustness of

288 solutions were evaluated by starting PMF with different initial conditions (parameter SEED).
289 The key diagnostic plots for all datasets are shown in Fig. S1. An FPEAK value of 0 is used for
290 all datasets in our PMF analysis on organic mass spectra, because the use of FPEAK values that
291 are different from 0 do not improve the correlations between PMF factors with external tracers.

292 2.5 Estimation of organic nitrates contribution to ambient OA

293 As direct measurements of organic nitrates are not available, we estimate the
294 concentration of particle-phase organic nitrates at each site based on HR-ToF-AMS
295 measurements in this study. It is important to note that total nitrates measured by the HR-ToF-
296 AMS (denoted as $NO_{3,meas}$) is the nitrate functionality ($-ONO_2$), which could arise from both
297 inorganic and organic nitrates. Here, we apply two independent methods in separating the
298 measured total nitrates into nitrate functionality from inorganic and organic nitrates. In the
299 following discussion, we use the subscripts $_{meas,\ inorg,}$ and $_{org}$ to denote nitrate functionality ($-ONO_2$)
300 or fragments (NO^+ and NO_2^+) from total nitrates (measured), inorganic nitrates (calculated), and
301 organic nitrates (calculated), respectively.

302 The first method is based on the NO^+/NO_2^+ ratio (denoted as NO_x^+ ratio method for
303 discussions hereafter) in the AMS mass spectra (Farmer et al., 2010). Due to the extensive
304 fragmentation caused by 70eV electron ionization in the HR-ToF-AMS, the nitrate functionality
305 ($-ONO_2$) fragments to produce NO^+ and NO_2^+ ions. Previous laboratory studies have shown that
306 the NO^+/NO_2^+ ratio in the aerosol mass spectrum is substantially higher for organic nitrates than
307 ammonium nitrate (AN) (Bruns et al., 2010; Fry et al., 2009; Sato et al., 2010; Farmer et al.,
308 2010; Boyd et al., 2015), which is the major source of PM_1 inorganic nitrates in the southeast US
309 that can be detected by the AMS (Guo et al., 2015; Allan et al., 2004). For example, while the
310 NO^+/NO_2^+ ratio is about 2.4 for ammonium nitrate, the ratio ranges from 5 to 10 for SOA
311 derived from isoprene+$NO_3^{\bullet}$ and β-pinene+$NO_3^{\bullet}$ reactions, respectively (Bruns et al., 2010; Boyd
312 et al., 2015). In addition to organic nitrates produced from biogenic VOC oxidation, Sato et al.
313 (2010) showed that the NO_x^+ ratio of organic nitrates from the photooxidation of aromatic
314 hydrocarbons is also clearly higher than that of ammonium nitrate (3.8-5.8 vs 1.1-2.8). Based on
315 the differences in NO_x^+ ratio between organic and inorganic nitrates, Farmer et al. (2010)
316 proposed that the concentrations of NO_{org} and $NO_{2,org}$ can be estimated from NO_{meas} and $NO_{2,meas}$
317 by Eq. 1 and 2.

$$NO_{2,org} = \frac{NO_{2,meas} \times (R_{meas} - R_{AN})}{R_{ON} - R_{AN}} \quad \text{Eq. 1}$$

$$NO_{org} = R_{ON} \times NO_{2,org} \quad \text{Eq. 2}$$

R_{meas} is the NO_x^+ ratio from observation. R_{AN} is the NO_x^+ ratio for pure ammonium nitrate (AN), which has been reported to depend on instrument performance and vary between different instruments (Farmer et al., 2010; Rollins et al., 2010). In this study, we determine the R_{AN} of each dataset from Ionization Efficiency (IE) calibrations using 300nm ammonium nitrate particles. We find that R_{AN} varies between 1.73 and 2.93 (Table 2), which is within the range (1.1 – 3.5) reported in the literature (Sato et al., 2010; Farmer et al., 2010; Sun et al., 2012b; Fry et al., 2013). R_{ON} is the NO_x^+ ratio for organic nitrates. Similar to R_{AN}, R_{ON} also varies between instruments (Boyd et al., 2015; Bruns et al., 2010; Fry et al., 2009). Thus, the R_{ON} values reported in the literature cannot be directly applied in our datasets. In order to circumvent this issue, Fry et al. (2013) assumed that the R_{ON}/R_{AN} value is instrument independent. The authors further obtained R_{ON} by multiplying R_{AN} determined from in-field IE calibrations with R_{ON}/R_{AN} determined from six organic nitrate standards (average value = 2.25) . However, the reported R_{ON}/R_{AN} values in the literature vary for different organic nitrates. For example, while the average R_{ON}/R_{AN} value is 2.25 for the organic nitrate standards in Farmer et al. (2010), the R_{ON}/R_{AN} ranges from 3.70 to 4.17 for organic nitrates produced from β-pinene oxidation by nitrate radicals (Boyd et al., 2015; Bruns et al., 2010; Fry et al., 2009). Considering the large variations in R_{ON}/R_{AN} values and unknown contributions from different organic nitrates, we apply the NO_x^+ ratio method to obtain an estimation range by using extreme R_{ON} values. We select organic nitrates formed from isoprene and β-pinene oxidation as representative because of their large abundance in the southeastern US, potential to produce organic nitrates, and because that they cover a wide range of R_{ON}/R_{AN} values (i.e., 2.08 for isoprene and 3.70-4.17 for β-pinene) (Boyd et al., 2015; Bruns et al., 2010; Fry et al., 2009). The organic nitrates derived from other biogenic VOCs (i.e., α-pinene, limonene, 3-carene, etc) are not considered due to either their lower ambient concentrations in the SE US or lower organic nitrate yields compared to isoprene and β-pinene (Xu et al., 2015). Though the photooxidation of aromatic VOCs could also produce organic nitrates, their R_{ON}/R_{AN} ratio is close to that of isoprene organic nitrates (Sato et al., 2010). Multiplying the average R_{AN} (i.e., 2.28±0.40) of all datasets in this study by the

347 average R_{ON}/R_{AN} ratio of isoprene (i.e., 2.08) and β-pinene organic nitrates (i.e., 3.99±0.25) in
348 the literature (Boyd et al., 2015; Bruns et al., 2010; Fry et al., 2009), within one standard
349 deviation we selected 5 (i.e., 4.74±0.83) and 10 (i.e., 9.10±1.69) as the lower and upper values of
350 R_{ON}. It is important to note that R_{ON} values of 5 and 10 likely correspond to upper and lower
351 bounds of the $NO_{3,org}$ concentrations estimated by the NO_x^+ ratio method. The assumption that
352 R_{ON}/R_{AN} is instrument independent warrants further study.

353 The second method is based on PMF analysis (denoted as PMF method). In addition to
354 PMF analysis on organic mass spectra (denoted as PMF_{org}), we have also performed PMF
355 analysis on organic mass spectra together with NO^+ and NO_2^+ ions (denoted as $PMF_{org+NO3}$).
356 Such analysis could provide useful insights regarding the relative contributions of organic and
357 inorganic nitrates. For instance, Sun et al. (2012b) and Hao et al. (2014) performed PMF
358 analysis on merged mass spectra with both organic and inorganic signals from HR-ToF-AMS
359 measurements. The authors showed that the NO^+ and NO_2^+ fragments are distributed among a
360 nitrate inorganic aerosol (NIA) factor and other organic aerosol factors.

361 In this study, the selection of optimal solutions for PMF analysis on the merged mass
362 spectra (i.e., $PMF_{org+NO3}$) is discussed in detail in the Supplement. In brief, in addition to
363 examining the typical diagnostic plots (Fig. S3), the optimal solutions are selected by comparing
364 the time series (Fig. S5), mass spectrum (Fig. S5), and mass concentration (Fig. S6) with results
365 from PMF_{org}. After determining the optimal solution of $PMF_{org+NO3}$, the concentrations of
366 "nitrate functionality from organic nitrates" (i.e., $NO_{3,org}$) are calculated by summing up the
367 nitrate signals (i.e., NO^+ and NO_2^+) from all OA factors by the following equations.

368 $$[NO^+_{org}]=\sum([\text{OA factor}]_i \times f\_NO_i) \quad \text{Eq. 3}$$

369 $$[NO^+_{2,org}]=\sum([\text{OA factor}]_i \times f\_NO_{2,i}) \quad \text{Eq. 4}$$

370 where $[\text{OA factor}]_i$ is the mass concentration of the *i*th OA factor, f_NO_i and $f\_NO_{2,i}$ are the
371 mass fraction of NO^+ and NO_2^+, respectively, in the *i*th OA factor. For both the NO_x^+ ratio
372 method and PMF method, we calculate the concentration of $NO_{3,inorg}$ (i.e., nitrate functionality
373 from inorganic nitrates) by subtracting $NO_{3,org}$ (i.e., nitrate functionality from organic nitrates)
374 from $NO_{3,meas}$ (i.e., total measured nitrates).

3. Results

Table 1 lists the meteorology parameters (temperature, relative humidity, and wind speed), gas-phase concentrations of NO, NO_2, and O_3, and aerosol composition of the seven datasets reported in this study. The average RH is above 60% for all the datasets, with little seasonal variation, which is consistent with previous observations (Ford and Heald, 2013). The high RH in the southeastern US has direct impacts on particle water content and particle acidity. Recently, Guo et al. (2015) showed that particle water and acidity are mainly driven by the variability of RH, although particle composition also plays a role. The average wind speed is relatively constant (1.3–3.4 m s^{-1}) throughout the year at all sites. NO_x (NO and NO_2) and black carbon (BC), which are tracers for anthropogenic emissions, are lower in the rural Yorkville (YRK) site than the urban Jefferson Street (JST) site. In YRK, the NO_x level is low (i.e., average concentration < 0.3 ppb) in all seasons. In contrast, at the urban JST site, the NO_x level is elevated in winter compared to summer, indicating more anthropogenic emissions, or less dispersion, in winter at urban sites.

Fig. 2 shows the composition of non-refractory submicron particulate matter (NR-PM_1) for all datasets. Organics are the dominant components, which account for more than 50% of NR-PM_1 mass at all sites throughout the year. Although dominant, the concentration of organic aerosol varies substantially among sites and seasons. The seasonal variation of OA mass concentration is small for the urban JST site (9.1 μg m^{-3} in May vs 7.9 μg m^{-3} in November); however, the OA concentration is about 4 times higher in summer than winter for the rural YRK site (11.2 μg m^{-3} in July vs 3.2 μg m^{-3} in December). The difference in seasonality of OA between urban and rural sites is likely due to the varying strength of different OA sources, which will be discussed in detail in section 4.4.2. In terms of diurnal variation, the OA diurnal trend is relatively flat in summer and peaks at night in winter (Fig. 3). The diurnal variation of OA is largely influenced by the changes in planetary boundary layer height and changes in contributions to total OA from various sources, which will be discussed in detail in section 4.4.1. The campaign-average mass spectra of OA from all datasets are similar, as shown in Fig. S7. In order to assess the degree of oxidation of OA, average f_{44} (the ratio of *m/z* 44 to total OA signal) and f_{43} (the ratio of *m/z* 43 to total OA signal) of each dataset is plotted in the triangular space as

404 defined by Ng et al. (2010) in Fig. 4. The OA from all datasets locate in the middle part of the
405 triangle, indicating they are moderately oxidized and have a similar degree of oxidation.

406 Following organics, sulfate (SO_4) has the second largest contribution to total NR-PM_1
407 mass at all sites (Fig. 2). Average SO_4 concentration varies between 3.0 to 4.0 μg m^{-3} at different
408 sites in summer and decreases to 1.4~1.7 μg m^{-3} in winter. The SO_4 concentration at most sites
409 (except JST_Nov and RS_Jan) reaches a daily maximum in the afternoon (Fig. 3), which is
410 likely caused by the strong photooxidation of SO_2 or sulfate entrainment from aloft when the
411 boundary layer height is the highest in the afternoon (Weber, 2003). In contrast to SO_4, where the
412 concentration is higher in summer, total nitrate concentration is elevated in winter. While the
413 average concentration of total nitrates is 0.3-0.4 μg m^{-3} (2-3% of total NR-PM_1, Fig. 2) in
414 summer, it almost triples in winter (0.8-1.4 μg m^{-3}) with elevated mass fraction in total NR-PM_1
415 (10-16%). The reason for the seasonal variation of the total nitrates will be discussed in section
416 4.2.2.

417 **4. Discussion**

418 4.1 OA source apportionment

419 In this section, we focus on the OA source apportionment based on results from PMF
420 analysis on organic mass spectra only (i.e., PMF_{org}). We resolved various factors, including
421 hydrocarbon-like OA (HOA), cooking OA (COA), biomass burning OA (BBOA), isoprene-
422 derived OA (Isoprene-OA), more-oxidized oxygenated OA (MO-OOA), and less-oxidized
423 oxygenated OA (LO-OOA) at multiple sites in different seasons. Based on the inferred volatility
424 from O:C ratios, the two oxygenated OA factors (i.e., MO-OOA and LO-OOA) are typically
425 named as low-volatility OOA (higher O:C and lower volatility) and semi-volatile OOA (lower
426 O:C and higher volatility) (Ng et al., 2010; Jimenez et al., 2009). However, recent studies
427 showed that O:C ratios are not always well-correlated with aerosol volatility (Hildebrandt et al.,
428 2010; Xu et al., 2014). Thus, in this study, we use the terms "more-oxidized OOA" (MO-OOA,
429 O:C ranges between 0.66 and 1.05, with an average of 0.87) and "less-oxidized OOA" (LO-OOA,
430 O:C ranges between 0.44 and 0.62, with an average of 0.54) (Fig. S10). This terminology has
431 been used in several previous studies (Setyan et al., 2012; Xu et al., 2015).

4.1.1 HOA

Hydrocarbon-like organic aerosol (HOA) is a surrogate of primary OA from vehicle emissions. Among all the OA factors, HOA is the least oxidized with oxidation state (OS) ranging from -1.86 to -1.39 (Fig. 4). The mass spectrum of HOA is characterized by hydrocarbon-like ions (C_xH_y family) as shown in Fig. S2, which is similar to the mass spectrum of freshly emitted traffic aerosol (Zhang et al., 2005). HOA is only identified at urban sites with evident morning and evening rush hour peaks (Fig. 5). HOA also shows good correlation with black carbon (R ranges from 0.70 to 0.83) (Fig. S2), further supporting the primary nature of this OA subtype.

For the sites where HOA is identified, HOA accounts for 9-15% (daily average) of total OA (Fig. 6). Even for the roadside (RS) site, which is within 5 meter of the Interstate 75/85, HOA only contributes 15% of total OA. Low contributions of HOA to total OA near highways have been observed in several prior studies (Sun et al., 2012a; DeWitt et al., 2014). For example, DeWitt et al. (2014) found that HOA only comprised 20% of total OA based on HR-ToF-AMS measurements in a high diesel environment (near a highway) in Paris, France. The small contribution of HOA could arise from the types of vehicles on road, the rapid dilution of vehicle emissions, or the high level of regional background OA. Firstly, roughly 95% of the traffic fleet on I75/85 is light-duty gasoline vehicles, according to Georgia Department of Transportation. Unlike diesel vehicles which have large emissions of POA and BC, gasoline vehicles have a larger emission of VOCs (e.g., toluene and benzene) (Platt et al., 2013). Secondly, in addition to vehicle type, the evaporation of POA emitted from vehicles would further decrease its mass concentration. Robinson et al. (2007) showed that POA from vehicle emissions is indeed semi-volatile, which would evaporate substantially upon dilution from tailpipe to ambient conditions (a dilution ratio of 10^3 to 10^4). Thirdly, HOA tends to contribute a small fraction of OA because of the high level of regional background OA in the greater Atlanta area. For example, OOA factors (i.e., LO-OOA and MO-OOA) compromise 47-79% of OA as shown in Fig. 6. The effect of wind direction on HOA concentration is expected to be small considering the close proximity of the roadside sampling site to the highway.

460 4.1.2 COA

461 The mass spectrum of cooking organic aerosol (COA) is characterized by prominent
462 signals at ions $C_3H_5^+$ (*m/z* 41) and $C_4H_7^+$ (*m/z* 55) (Fig. S2), which could arise from the heating
463 of seed oil (Allan et al., 2010). Another feature of COA is its unique diurnal trend. For three out
464 of four datasets (except JST_Nov) where a COA factor is identified, the COA factor exhibits a
465 small peak at lunch time and a large peak at dinner time (Fig. 5). The COA factor is identified in
466 urban sites (JST, GT, and RS) throughout the year, with the average mass fraction varying from
467 12-20%. A prior study by Zheng et al. (2002) estimated that meat cooking accounts for 5-12% of
468 $PM_{2.5}$ organic carbon in the southeastern US by using a chemical mass balance receptor model.
469 The range reported by Zheng et al. (2002) is similar to our study, considering the differences in
470 sampling periods, particle size range, and estimation method. The COA factor has also been
471 detected in many megacities around the world (Huang et al., 2010; Allan et al., 2010; Slowik et
472 al., 2010; Mohr et al., 2012; Crippa et al., 2013), indicating cooking is an important OA source in
473 megacities.

474 We note that the COA factor was not resolved in Budisulistiorini et al. (2013), in which
475 the authors performed PMF analysis on the data collected by an Aerosol Chemical Speciation
476 Monitor (ACSM) at the JST site in 2011 summer and fall. The lack of a COA factor in the
477 analysis by Budisulistiorini et al. (2013) could be a result of the lower resolution (unit mass
478 resolution) of the ACSM compared to HR-ToF-AMS. Previous studies have suggested that COA
479 is not easily differentiated from HOA due to the similarity of their mass spectra in unit mass
480 resolution data (Crippa et al., 2014; Mohr et al., 2009).

481 4.1.3 Isoprene-OA

482 The Isoprene-OA factor is characterized by prominent signals at $C_4H_5^+$ (*m/z* 53) and
483 $C_5H_6O^+$ (*m/z* 82) in its mass spectrum (Fig. S2), which resembles that of isoprene SOA formed
484 via isoprene epoxydiols (i.e., IEPOX) uptake in the presence of hydrated sulfate in laboratory
485 experiments (Lin et al., 2012; Budisulistiorini et al., 2013; Nguyen et al., 2014; Liu et al., 2015).
486 For our datasets, Isoprene-OA is only identified in warmer months (May - August) and accounts
487 for 18-36% of total OA (Fig. 6). The seasonal variation of Isoprene-OA factor is consistent with
488 that of isoprene emissions, which are high in summer and nearly zero in winter (Guenther et al.,
489 2006). The identification of the Isoprene-OA factor is further supported by its correlation with

methyltetrols, which are products formed from isoprene oxidation and likely via IEPOX uptake. For the Centreville dataset where methyltetrols were continuously measured by a semi-volatile thermal desorption aerosol gas chromatograph (SV-TAG) (Isaacman et al., 2014), the correlation coefficient (Pearson's R) between the Isoprene-OA factor and methyltetrols is found to be 0.68 (Xu et al., 2015).

The f_{C5H6O+} (the ratio of $C_5H_6O^+$ to total signal) in isoprene-OA factor, which is used as a characteristic marker for SOA formed via IEPOX uptake in the literature, ranges from 0.9% - 2.3% in this study. This range is similar to the values from other ambient data (Budisulistiorini et al., 2013; Chen et al., 2014; Robinson et al., 2011a; Slowik et al., 2011), but lower than that from laboratory-generated fresh SOA from IEPOX uptake (3.6% from Liu et al. (2015)). We note that the f_{C5H6O+} is higher at rural sites (1.9% for YRK_July and 2.3% for CTR_June) than urban sites (0.9% for JST_May and 1.4% for GT_Aug). Similarly, Liu et al. (2015) observed that the mass spectrum of laboratory-generated SOA from IEPOX uptake has a stronger correlation with that of Isoprene-OA factor from remote regions (Amazon and Borneo) than urban regions (Atlanta, US). The identification of an Isoprene-OA factor at urban sites in the current study has interesting implications. The compound IEPOX is thought to be an oxidation product of isoprene where the organic peroxy radicals react with hydroperoxy radicals (Paulot et al., 2009). In urban areas, one would expect the majority of organic peroxy radicals to react with NO_x, considering the relatively high NO_x level (~15.4 ppb for JST_May in Table 1). However, a recent laboratory study by Jacobs et al. (2014) found that the oxidation of isoprene-derived hydroxynitrates in the presence of NO_x could also produce IEPOX. Thus, Isoprene-OA observed in urban sites could be locally produced. Another possible source for Isoprene-OA at urban sites is advection from rural sites. This could explain the lower f_{C5H6O+} in the Isoprene-OA factor in urban sites, because the compounds which give rise to the $C_5H_6O^+$ signal can be further oxidized during transport. However, the lifetime of the Isoprene-OA factor and the changes in its mass spectral features with chemical aging are largely uncertain. The contribution of advection is probably small as it is unlikely that advection would result in a consistent diurnal profile of Isoprene-OA, which reaches a daily maximum in the afternoon observed not only in this study (Fig. 5), but also in other regions, such as Amazon (Chen et al., 2014) and Borneo forest (Janssen et al., 2013; Robinson et al., 2011a). In addition, Robinson et al. (2011a) only observed the Isoprene-OA factor in data obtained from afternoon flights, but not in morning flights through airborne

measurements in the Borneo forest, implying that the Isoprene-OA formation is rapid and local. Another possibility for the lower f_{C5H6O+} at the urban sites is that Isoprene-OA factor from the urban sites may contain isoprene SOA produced via other pathways, in addition to the IEPOX uptake pathway. Isoprene SOA formed via RO_2+NO pathway only has a negligible signal at $C_5H_6O^+$ (Kroll et al., 2006; Xu et al., 2014), so that the mixing of Isoprene SOA via different pathways may lower the f_{C5H6O+} in the Isoprene-OA factor. Moreover, seasonality may also have an influence on the lower f_{C5H6O+} at the urban sites since the sampling periods at the urban sites are May and August, when the isoprene concentration is relatively lower than that during the sampling periods at the rural sites (i.e., June and July).

For all the sites where an Isoprene-OA factor is resolved, the Isoprene-OA factor is found to be well-correlated with sulfate (R ranging from 0.73 to 0.88, Fig. S2). Xu et al. (2015) showed that the formation of isoprene-OA in the southeastern US is largely controlled by the abundance of sulfate, instead of the particle water content and/or particle acidity. While many prior laboratory studies show that particle acidity plays an important role in IEPOX uptake (Gaston et al., 2014; Surratt et al., 2007), results from ambient observations suggest that particle acidity is critical, but not the limiting factor in isoprene OA formation in the southeastern US, which is likely due to the consistently high particle acidity in the southeastern US (Guo et al., 2015; Xu et al., 2015). Guo et al. (2015) showed that the daily average particle pH throughout the southeastern US ranges between 1.1 and 1.3 in summer time. In the afternoon, when the isoprene mixing ratio is highest and photochemistry is strongest, the particle pH is even lower, ranging between 0 and 0.75 due to lower particle water content. A recent chamber study (Gaston et al., 2014) showed that decreasing pH from 4.63 to 0.5 could greatly enhance IEPOX uptake by up to 150 times, but the enhancement is much weaker (a factor of 2) when furthering decreasing the pH from 0.5 to -0.27, the range of which is relevant to ambient particle pH (0-0.75) in the summer afternoon in the southeastern US (Guo et al., 2015). Similarly, another laboratory study also showed that the effect of particle acidity on IEPOX uptake is minor when the particle pH is low (Nguyen et al., 2014). By comparing the reactive uptake of IEPOX by using wet $(NH_4)_2SO_4$ seed (pH ~3.5) and wet $MgSO_4$+H_2SO_4 mixture seed (pH~0-1 with large uncertainty), Nguyen et al. (2014) found that the reactive partitioning coefficient of IEPOX increases by only 1.5 times as pH decreases from 3.5 to 1 ($H^+_{(aq)}$ increases by two or three orders of magnitude). Taken together, laboratory studies revealed that while increasing particle acidity could greatly enhance

IEPOX uptake when pH is high, the sensitivity of IEPOX uptake to particle acidity is minor when pH is low. This is likely caused by isoprene OA formation from IEPOX uptake being limited by nucleophiles instead of catalyst activity under low pH (Eddingsaas et al., 2010; Piletic et al., 2013), although a low pH is needed to enhance these reactions. We also note that the co-variation between particle acidity and sulfate is not considered in previous laboratory studies (Gaston et al., 2014; Surratt et al., 2007), so the effect of particle acidity could possibly be confounded with the effect of sulfate and warrants further investigation.

4.1.4 BBOA

The mass spectrum of biomass burning organic aerosol (BBOA) is characterized by prominent signals at ion $C_2H_4O_2^+$ (*m/z* 60) and $C_3H_5O_2^+$ (*m/z* 73). These two ions are largely produced by levoglucosan, which is formed from the breakdown of cellulose in biomass burning (Schneider et al., 2006). In addition, Heringa et al. (2011) showed that SOA produced during the aging of primary biomass burning emissions could contribute to these two ions. In this study, BBOA accounts for 9-22% of the OA (Fig. 6). The BBOA factor is mainly resolved in winter datasets, which is consistent with the EPA reported Georgia fire season in late winter (January – March) (Hidy et al., 2014) and the large enhancement in levoglucosan concentrations in winter compared to summer in Georgia (Zhang et al., 2010). BBOA is also identified in JST_May, which may arise from residential wood burning near JST site. The contribution of BBOA to total OA is slightly smaller than the values reported in other studies. Zhang et al. (2010) estimated that biomass burning accounted for 27% of $PM_{2.5}$ mass in winter over the southeastern US by performing PMF analysis on 10 species extracted from filter samples. The differences in biomass burning contribution to OA between this study and Zhang et al. (2010) are likely due to different estimation methods, sampling years (i.e., 2012-2013 vs. 2007), and sample size cut (i.e., PM_1 vs. $PM_{2.5}$).

It is important to note that the BBOA reported in this study likely only represents the relatively fresh OA from biomass burning. For example, laboratory studies revealed that the oxidation of levoglucosan is fast in both the gas and aqueous phases (Zhao et al., 2014; May et al., 2012; Hennigan et al., 2011). The fast oxidation of levoglucosan can result in the rapid decay of signals at $C_2H_4O_2^+$ (*m/z* 60) and $C_3H_5O_2^+$ (*m/z* 73), causing the mass spectrum of BBOA to lose its characteristic signature. In addition, laboratory studies by Hennigan et al. (2011) and

Grieshop et al. (2009) showed that the mass spectrum of OA from biomass burning becomes increasingly similar to that of MO-OOA after photochemical aging. Ambient measurements in the eastern Mediterranean by Bougiatioti et al. (2014) showed evidence that BBOA could be rapidly converted to OOA in less than a day. Thus, aged OA from biomass burning could be apportioned to the MO-OOA factor.

Recent studies have revealed that OA from biomass burning is an important source for brown carbon (Washenfelder et al., 2015; Andreae and Gelencsér, 2006; Zhang et al., 2010; Lack et al., 2013), which has important impacts on climate (Feng et al., 2013; Liu et al., 2014). For four (out of five) datasets where BBOA is resolved by PMF analysis in this study, the Pearson's correlation coefficient (R) between BBOA and brown carbon is greater than 0.69, with the best correlation observed at JST_Nov (R=0.90) (Fig. 7). The correlation coefficient between BBOA and brown carbon is only 0.47 for YRK_Dec, which is likely caused by other brown carbon sources at the YRK site. This hypothesis is supported by summer measurements at YRK. In YRK_July, we observed a large abundance of brown carbon, which reached a daily maximum at around 2pm (Fig. S8); however, a BBOA factor is not resolved for YRK_July, indicating that brown carbon, in this case, could arise from sources other than biomass burning. Hecobian et al. (2010) suggested that SOA from aqueous phase reactions may be an important source for brown carbon in summer based on analysis of ~900 filters collected in 2007 in the southeastern US. A recent laboratory study showed that SOA from IEPOX reactive uptake could be light-absorbing and potentially an important source for brown carbon (Lin et al., 2014). However, Isoprene-OA factor, which is related to the IEPOX uptake pathway studied in Lin et al. (2014), only shows weak correlation (R ranges from 0.22 to 0.50) with brown carbon, as shown in Fig. S9. As suggested by Washenfelder et al. (2015), the difference between ambient observation and laboratory studies is possibly caused by the fact that the IEPOX-derived absorbing chromophores do not dominate the Isoprene-OA mass. However, further studies are warranted to resolve this difference.

4.1.5 MO-OOA

Two oxygenated OA factors (MO-OOA and LO-OOA) with high, but differing O:C ratios, were identified in both rural and urban sites throughout the year. MO-OOA contributes 24-49% of total OA mass (Fig. 6). This factor has the highest O:C ratio, indicating that it is

612 highly oxidized. It has been shown that as OA ages in the atmosphere, the mass spectra of OA
613 from different sources become increasingly similar to each other and resemble that of MO-OOA
614 (Jimenez et al., 2009; Ng et al., 2010). Thus, MO-OOA likely represents a highly aged organic
615 aerosol from multiple sources, which causes the identification of specific sources of MO-OOA to
616 be challenging. In addition to a high degree of oxidation, other notable features of MO-OOA are
617 its diurnal profile and ubiquitous presence. As shown in Fig. 5, in most datasets except RS_Jan,
618 the diurnal profile of MO-OOA reaches a daily maximum in the afternoon. The daytime increase
619 in MO-OOA would become more prominent after considering the dilution caused by boundary
620 layer height expansion during the day. The similar diurnal profile has also been observed in a
621 number of studies (Aiken et al., 2009; DeWitt et al., 2014; Hildebrandt et al., 2010; Huang et al.,
622 2010; Setyan et al., 2012). Moreover, not only in this study in which MO-OOA is identified in
623 different sites and seasons, MO-OOA (or the OOA factor in general) was also identified in
624 datasets obtained at multiple sites around the world, pointing to the ubiquitous nature of this OA
625 subtype (Jimenez et al., 2009; Ng et al., 2010).

626 Possible sources of this factor have been proposed in the literature. Firstly, a number of
627 studies proposed that the source for MO-OOA is long-range transport (Li et al., 2015; Hayes et
628 al., 2013; Robinson et al., 2011b; Raatikainen et al., 2010). This proposed mechanism could
629 explain the high degree of oxidation of MO-OOA because the aerosol gets progressively more
630 oxidized during advection, but it is unlikely to explain the well-defined diurnal profile of MO-
631 OOA (peaks in the afternoon). Secondly, humic-like substances (HULIS) are proposed to be
632 synonymous with MO-OOA because the mass spectrum and the degree of oxidation of HULIS
633 resembles those of MO-OOA (Ng et al., 2010; El Haddad et al., 2013). A recent study by
634 Paglione et al. (2014) performed factor analysis on NMR measurements of water-soluble organic
635 carbon extracted from filters collected in the Netherlands and resolved a factor with mass
636 spectral features that are similar to HULIS. Further, the authors showed that this HUILS factor
637 correlates with the most-oxidized OOA factor (O:C = 0.98) resolved from PMF analysis of their
638 HR-ToF-AMS measurements, providing a linkage between HULIS and MO-OOA. Thirdly, the
639 oxidation of vehicle emission or fuel combustion in general might also contribute to MO-OOA
640 mass, but such contribution is uncertain. On one hand, multiple studies have shown that the
641 photooxidation of gas-phase species from direct vehicle emissions or POA evaporation could
642 rapidly produce secondary OA, which resembles the mass spectrum of oxygenated OA factors

and could be 1-2 orders of magnitude higher than the primary OA emissions (Nordin et al., 2013; Presto et al., 2014; Jathar et al., 2014; Platt et al., 2013). In addition, a previous study by Liu et al. (2011) showed that the carboxylic acids measured by FTIR are exclusively associated with fossil fuel combustion and correlate with the PMF resolved OOA factor from HR-ToF-AMS measurements in coastal California. On the other hand, Zotter et al. (2014) showed that >69% of MO-OOA originated from non-fossil sources in LA basin based on a combination of radiocarbon analysis and AMS PMF analysis. By using the same method, DeWitt et al. (2014) showed that the majority of carbon in OOA is non-fossil even in an environment heavily influenced by traffic emissions, suggesting the source of MO-OOA is not vehicle emissions. Lastly, aged biomass burning is also a possible source for MO-OOA as discussed above in section 4.1.4.

One interesting observation in this study is that MO-OOA is well-correlated with ozone in summer (R = 0.73 for JST_May and YRK_July), but not in winter (R = -0.059 and -0.27 for JST_Nov and YRK_Dec, respectively) (Fig. 8), implying that the sources of MO-OOA may vary with seasons. Considering the large biogenic VOC emissions in summer, the summer MO-OOA may be related to the oxidation of biogenic VOCs. Recently, Ehn et al. (2014) for the first time observed that monoterpene oxidation could produce large quantities of compounds with extremely low vapor pressure. As these compounds have very high O:C (~0.7), it is possible that they serve as an important source for MO-OOA. The identification of the sources of winter MO-OOA could be aided by the radiocarbon analysis. For example, if the majority of MO-OOA in winter has non-fossil sources, it could suggest that aged OA from biomass burning is an important source for MO-OOA, because biomass burning is enhanced and the emissions of biogenic VOCs are low in winter.

4.1.6 LO-OOA

Similar to MO-OOA, less-oxidized oxygenated organic aerosol (LO-OOA) is also observed in both rural and urban sites throughout the year. LO-OOA comprises 19-34% of total OA (Fig. 6). A key feature of LO-OOA is that it consistently exhibits a daily maximum at early morning and at night, in all datasets (Fig. 5). The similar diurnal variation of LO-OOA has also been observed in previous field measurements and thought to be primarily driven by the semi-volatile nature of LO-OOA. The LO-OOA factor identified in multiple prior field measurements has been observed to correlate with ammonium nitrate, a semi-volatile species which mainly

673 partitions into the particle phase at night when the temperature is relatively low (Jimenez et al.,
674 2009; Sun et al., 2012a; Zhang et al., 2011; Ulbrich et al., 2009). However, in this study, LO-
675 OOA only shows moderate correlation with total NO_3 (i.e., $NO_{3,meas}$) measured by the HR-ToF-
676 AMS in summer datasets (R ranges between 0.56 and 0.76) and is not correlated in winter
677 datasets (R ranges between 0.14 and 0.46) (Fig. 9 and Table 2).

678 While LO-OOA is only moderately, or sometimes poorly correlated, with $NO_{3,meas}$ in this
679 study, we find improved correlation between LO-OOA and "nitrate functionality from organic
680 nitrates" (i.e., $NO_{3,org}$) (Fig. 9 and Table 2). $NO_{3,org}$ is estimated by using the NO_x^+ ratio method,
681 as described in section 2.5. An R_{ON} value of 10 is applied in this case since different R_{ON} values
682 would only affect the estimated concentration of $NO_{3,org}$, but not the correlation between LO-
683 OOA and $NO_{3,org}$. For most datasets, LO-OOA correlates better with $NO_{3,org}$ than total nitrates.
684 The biggest improvement is seen in JST_Nov, where the correlation coefficient increases from
685 0.14 to 0.63. However, we also note that the correlation becomes worse for YRK_Dec and
686 RS_Jan, which is likely caused by the small contribution of organic nitrates to total nitrates,
687 resulting in a larger uncertainty in the NO_x^+ ratio method (Bruns et al., 2010). In addition, the
688 correlations between LO-OOA and $NO_{3,org}$ for YRK_Dec and RS_Jan are weakened by the
689 negative $NO_{3,org}$ concentration estimated from the NO_x^+ ratio method (Fig. 9). The negative
690 values are a result of smaller R_{meas} than R_{AN}, at times (see Eq. 1), which is likely caused by
691 variations in instrument performance (Farmer et al., 2010; Rollins et al., 2010).

692 4.2 Nitrates source apportionment

693 4.2.1 Estimation of organic nitrates

694 The NO_x^+ ratio method and PMF method are applied to estimate the concentration of
695 "nitrate functionality from organic nitrates" (i.e., $NO_{3,org}$) at different sites. The concentration of
696 $NO_{3,org}$ and the mass fraction of $NO_{3,org}$ in total measured NO_3 (i.e., $NO_{3,meas}$) estimated from
697 both methods are shown in Fig. 10. Both the NO_x^+ ratio method and the PMF method show a
698 similar seasonality in the contribution of $NO_{3,org}$ to $NO_{3,meas}$ (denoted as $NO_{3,org}/NO_{3,meas}$), which
699 is higher in summer than winter. However, we observe noticeable differences between the two
700 methods. In the following, we first discuss the uncertainties associated with NO_x^+ ratio method
701 and PMF method. Then, we discuss how the uncertainties affect the comparison between the two

methods, and provide a "best estimate" range of $NO_{3,org}$ based on the two methods. Lastly, we use the "best estimate" range of $NO_{3,org}$ to calculate the contribution of organic nitrates to OA by assuming the molecular weight (MW) of organic nitrates.

For the PMF method, the uncertainty is mainly associated with the identification of a nitrate inorganic aerosol (NIA) factor. The NIA factor is resolved in most datasets, except CTR_June and YRK_July. The mass spectrum of the NIA factor is similar to the corresponding factor in Sun et al. (2012b) (Fig. S4). Specifically, it is dominated by NO^+ and contains some organic signals such as CO_2^+ and $C_2H_3O^+$, indicating the NIA factor has a potential interference from organics. The mass fraction of organic signals in the NIA factor varies across sites, with a higher value in warmer months (~70% in JST_May and GT_Aug) than colder months (16%-38% in JST_Nov, YRK_Dec, and RS_Jan) (Fig. S11). The fact that the NO^+/NO_2^+ ratio of the NIA factor resolved from warmer months is higher than that of pure ammonium nitrate (Fig. S12) is also indicative of organic nitrate interference in the NIA factor. Conversely, the NO^+/NO_2^+ ratio of the NIA factor resolved from colder months is closer to that of pure ammonium nitrate, suggesting less interference from organics. Thus, for the sites where a NIA factor is identified, the presence of organic nitrates in the NIA factor would result in an underestimation of $NO_{3,org}$, and the underestimation is larger for warmer months (i.e., JST_May and GT_Aug). For CTR_June and YRK_July, the NIA factor is not resolved from $PMF_{org+NO3}$ analysis, likely due to a small concentration of inorganic nitrates. For example, the concentrations of organics and total nitrates (i.e., $NO_{3,meas}$) are 5.0 and 0.1 μg m^{-3}, respectively, for CTR_June. Even if one assumes that all the measured nitrates arise from inorganic nitrates, the nitrates/organics ratios is only 2%, making it difficult for PMF to retrieve the NIA factor accurately (Ulbrich et al., 2009). Thus, for CTR_June and YRK_July, the small amount of $NO_{3,inorg}$, which is not retrievable by PMF, was attributed to OA factors so that the PMF method would slightly overestimate $NO_{3,org}$.

For the NO_x^+ ratio method, considering the large variation in NO_x^+ ratio for different organic nitrates, the largest uncertainty is associated with the value of R_{ON}. Ideally, the time-dependent R_{ON} values should be applied. However, this is challenging because the determination of time-dependent R_{ON} requires measurements of every ambient organic nitrate species, which are not available. Knowing this, we apply R_{ON} values of 5 and 10 in our analysis to provide the upper and lower bounds of the estimated $NO_{3,org}$ concentration for the NO_x^+ ratio method as

discussed in section 2.5. It is noted that for Centreville, we applied a third method to calculate the concentration of $NO_{3,org}$, which is based on the differences between HR-ToF-AMS measurements (NO_3 from both organic and inorganic species) and PILS-IC measurements (NO_3 from inorganic species only) (Xu et al., 2015; Bae et al., 2007; Orsini et al., 2003). This method, denoted as AMS-IC method, is only applied for Centreville because the PILS-IC was not deployed in the SCAPE study. In order to match the HR-ToF-AMS particle cut size (i.e., PM_1), a PM_1 cyclone was deployed at the inlet of PILS-IC. However, due to the transmission efficiency of PM_1 cyclone, PILS-IC measurements might include contributions from particles larger than 1μm (i.e., inorganic NO_3 in mineral dust). Interferences from water-soluble refractory particles (e.g., calcium or sodium nitrate) are likely small given the concentration of sodium measured by the PILS-IC with a PM_1 cyclone, for example, was negligible and mostly below its detection limit (0.07 μg m^{-3}) (Fig. S13). As shown in Fig. 11, The $NO_{3,org}$ estimated by the AMS-IC method falls within the range of NO_x^+ ratio method, which is defined by R_{ON} values of 5 and 10, indicating the feasibility of using these two values as the upper and lower bounds to estimate $NO_{3,org}$ for the NO_x^+ ratio method.

Based on the uncertainties of the PMF method and the NO_x^+ ratio method, we could explain the differences between the two methods and further combine them in order to narrow the estimation range. According to the extent of agreement between the two methods, all seven datasets are grouped into three categories: summer months (CTR_June and YRK_July), transition months (JST_May and GT_Aug), and winter months (JST_Nov, YRK_Dec, and RS_Jan).

For winter months, the PMF method shows good agreement with the NO_x^+ ratio method with a R_{ON} value of 10 for JST_Nov and YRK_Dec. This is consistent with the observations that the interference of organic nitrates in the NIA factor is small in winter datasets (Figs. S11 and S12) and isoprene emission is negligible in winter (Guenther et al., 2006). Thus, results from the NO_x^+ ratio method with R_{ON} = 5 (i.e., isoprene organic nitrates) are likely unrealistic. With this in mind, we combine the results from the PMF method and the NO_x^+ ratio method with R_{ON} = 10 as the "best estimate" range of organic nitrates for JST_Nov and YRK_Dec. For RS_Jan, the NO_x^+ ratio method predicts negative $NO_{3,org}$ due to R_{meas} being smaller than R_{AN} at times (Eq. 1). In this case, the PMF method is selected as the "best estimate". Taken together, the mass fraction

762 of organic nitrates (i.e., $NO_{3,org}/NO_{3,meas}$) is 0.19-0.21, 0.11-0.21, and ~0.10 for JST_Nov,
763 YRK_Dec, and RS_Jan, respectively.

764 For summer months, the PMF method predicts that all the measured nitrates are from
765 organic nitrates (i.e., $NO_{3,org}/NO_{3,meas}$ = 1, Fig. 10), because a NIA factor is not resolved from
766 PMF analysis and all the measured NO_3 are distributed in the OA factors. The $NO_{3,org}$ estimated
767 from the PMF method falls within the upper (i.e., R_{ON} = 5) and lower bound (i.e., R_{ON} = 10) of
768 the NO_x^+ ratio method (Fig. 10). For CTR_June, the NO_x^+ ratio method with R_{ON} value of 5
769 predicts a $NO_{3,org}/NO_{3,meas}$ ratio that is greater than 1, which results from the assumed R_{ON} value
770 (i.e., 5) being smaller than R_{meas}, at times (Eq. 1). Thus, the PMF method and the NO_x^+ ratio
771 method with R_{ON} = 10 define the upper and lower bound, respectively. Accordingly, the "best
772 estimate" range of $NO_{3,org}/NO_{3,meas}$ is 0.80-1 and 0.63-1 for CTR_June and YRK_July,
773 respectively.

774 For transition months (i.e., JST_May and GT_Aug), the PMF method and the NO_x^+ ratio
775 method show large discrepancies. Compared to the PMF method, the NO_x^+ ratio method predicts
776 1.5–2.5 times higher $NO_{3,org}$ concentration depending on the site and R_{ON} value. This is likely
777 caused by the PMF method under-predicting $NO_{3,org}$, owing to the attribution of some organic
778 nitrates to the NIA factor. Thus, we select the NO_x^+ ratio method with R_{ON} values of 5 and 10 as
779 the "best estimate" range. Accordingly, $NO_{3,org}/NO_{3,meas}$ ranges 0.55-0.76 and 0.64-0.99 for
780 JST_May and GT_Aug, respectively.

781 We also calculate the contribution of organic nitrate molecules to OA from the "best-
782 estimate" range of nitrate functionality (i.e., $NO_{3,org}$). We assume that particle-phase organic
783 nitrates have an average molecule weight of 200 and 300 g mol^{-1} (Rollins et al., 2012), which
784 provides an lower and upper bound for estimating concentrations of organic nitrates. As shown
785 in Fig. 10, organic nitrates contribute about 5-12% to total OA for summer datasets (CTR_June
786 and YRK_July) and 9-25% to total OA for winter datasets (JST_Nov, YRK_Dec, and RS_Jan),
787 suggesting that organic nitrates are important components of total OA in the southeastern US.

788 Figure 12 shows the diurnal variation of $NO_{3,org}$ based on the NO_x^+ ratio method with an
789 R_{ON} value of 10. For most of the datasets, $NO_{3,org}$ starts increasing after sunset, which is mainly
790 caused by the oxidation of VOCs by nitrate radical at night. The daily maximum of $NO_{3,org}$

appears in mid-morning (i.e., ~8am), which is likely because photooxidation of VOCs in the presence of NO (i.e., RO_2+NO pathway) also contributes to organic nitrate when the NO concentration is highest.

4.2.2 Nitrate seasonal variation

As shown in table 1 and Fig. 2, the total nitrate concentration is higher in winter (0.8-1.4 μg m^{-3}, 10-16% of total NR-PM_1) than in summer (0.3-0.4 μg m^{-3}, 2-3% of total NR-PM_1). Based on the NO_x^+ ratio method, $NO_{3,inorg}$ is greatly enhanced in winter relative to summer. For example, the concentration of $NO_{3,inorg}$ increases from 0.22 μg m^{-3} (average of upper and lower bound of the NO_x^+ ratio method) in May to 1.6 μg m^{-3} in November for the JST site. Similarly, $NO_{3,inorg}$ shows a 10-fold increase for YRK_Dec compared to YRK_July.

The seasonal variation of inorganic nitrates could possibly be caused by its semi-volatile nature and varying NO_x emissions. Based on volatility measurements by a thermal denuder, Huffman et al. (2009) showed that ammonium nitrate is very volatile and its gas/particle partitioning is largely affected by temperature. The average temperature in summer is about 15 °C higher than that in winter (Table 1). According to laboratory measurements of ammonium nitrate volatility, a 15°C increase in temperature would lead to the evaporation of 60% of nitrate mass (Huffman et al., 2009). In addition to volatility, the winter enhancement of inorganic nitrates is related to higher NO_x levels, which is the major source for inorganic nitrates and largely elevated in winter in the southeastern US (Blanchard et al., 2013). For example, as shown in Table 1, the NO_x concentration in JST_Nov (50.5 ppb) is 3.5 times higher than that in JST_May (14.4 ppb). Thus, the lower temperature and higher NO_x levels in winter than summer likely compensate for the weaker photooxidation and result in the increase in inorganic nitrates. Interestingly, we observe a rush hour peak (around 9am) in the diurnal trend of total nitrates at urban sites in winter (JST_Nov and RS_Jan). This rush hour peak is primarily from inorganic nitrates supported by the following evidence: 1) the R_{meas} is close to R_{AN} during the rush hour period (Fig. S15); 2) the rush hour peak only exists in the diurnal profile of $NO_{3,inorg}$ (Fig. 12); and 3) the coincident peak in the diurnal trend of NH_4 (Fig. 3). Early morning peaks in inorganic nitrates were also consistently seen by a variety of online instruments as part of the Atlanta Supersite Experiment at the JST site (Weber et al., 2003). In Mexico City, Hennigan et al. (2008) attributed the fast production of inorganic nitrates mainly to secondary formation from

photooxidation of NO_x and subsequent partitioning of HNO_3. The rush hour peak of inorganic nitrates disappears rapidly, which is likely caused by evaporation and dilution as the planetary boundary layer height increases (Hennigan et al., 2008).

The concentration of $NO_{3,org}$ is slightly higher in summer, but its seasonal variation is not as strong as $NO_{3,inorg}$ (Table 2 and Fig. 10). This is likely due to the compensating effects of source strength and gas/particle partitioning. The organic nitrates mainly originate from VOC oxidation by the nitrate radical and/or photooxidation in the presence of NO_x. The VOC concentrations are higher in summer due to stronger biogenic emissions, which would provide sources for organic nitrates. However, the temperature is higher in summer than winter, which would hinder the partitioning of organic nitrates into the particle phase.

4.3 Aerosol Spatial Variability

The spatial variability of organics, sulfate, ammonium, and total nitrate in the greater Atlanta area is investigated by comparing ACSM measurements (stationary at the Georgia Tech site) with HR-ToF-AMS measurements (rotating among different sites). Figure 13 shows the correlation coefficients for NR-PM_1 species between ACSM measurements (stationary at the Georgia Tech site) and HR-ToF-AMS measurements (rotating among different sites). Detailed comparisons, in terms of time series and scatter plots, are shown in Fig. S14. The ACSM and HR-ToF-AMS are compared side-by-side at the Georgia Tech (GT) site from 20 July to 4 September, 2012 and the time series of the species measured by the two instruments are well correlated (R=0.95, 0.93, 0.82, 0.85 for organics, sulfate, ammonium, and total nitrate, respectively) and agree within instrument uncertainty (i.e., 20-35%) (Bahreini et al., 2009).

As expected, the correlation gets weaker as the distance between the GT site and other sampling sites increases. Surprisingly, the organic correlation coefficient in July is 0.92 between GT and YRK sites, which have considerable spatial separation (i.e., 70 km), indicating that the organics are uniformly distributed in the greater Atlanta area in summer time. In contrast, the organic correlation coefficient between GT and YRK decreases to 0.66 in winter. Unlike organics, the correlation in SO_4 between GT and YRK is similarly good in both summer and winter (R=0.7 and 0.85 for summer and winter, respectively). Our observation is generally

850 consistent with the previous study by Zhang et al. (2012), who showed that WSOC, and to a less
851 extent SO_4, are spatially homogeneous in the southeastern US based on results from daily-
852 average filter measurements (one filter in every six days) in 2007. The authors attributed the
853 uniform distribution of WSOC and SO_4 largely to stagnant air masses in southeastern US during
854 summer time and both long-lived secondary WSOC and SO_4 eventually spread across the region,
855 although somewhat higher WSOC spatial correlations compared to sulfate were thought to be
856 due to widely distributed SOA precursor emissions compared to point sources for SO_2. Hidy et
857 al. (2014) also showed that secondary species, like SO_4, have weaker rural and urban contrast in
858 the southeastern US, though only yearly average data were considered in that study.

859 Although meteorology plays an important role in the spatial variability of aerosol, it alone
860 cannot explain the seasonality of the OA spatial variability. For example, meteorology should
861 have the same effect on the regional variability of SO_4 and OA. However, while SO_4 is
862 uniformly distributed in both summer and winter, OA is more uniform in summer than winter,
863 suggesting other factors also influence the spatial variability of OA. The seasonality of OA
864 spatial variability (i.e., more spatially homogeneous in summer compared to winter) is probably
865 affected by the seasonal variation of OA sources in addition to meteorology. As shown in Fig. 6,
866 SOA is the dominant source for total OA (69-100% of OA) in summer for both rural and urban
867 sites. This likely arises from the fact that biogenic VOCs, which are important precursors for
868 SOA, are abundant and widely distributed in the southeastern US during summer time (Guenther
869 et al., 2006). Thus, SOA is regional and the dominant component of OA, leading to the uniform
870 distribution of OA. In contrast, POA concentration varies greatly between urban and rural sites.
871 In winter, while the SOA still dominates total OA at rural sites, the POA is comparable with
872 SOA at urban sites (Fig. 6). This is because that the concentration of regional SOA decreases due
873 to weaker photochemical activity and lower biogenic VOCs emissions in winter, but the
874 concentration of POA (HOA+BBOA+COA) is relatively constant, or even increases. This is
875 likely due to elevated emission from biomass burning and reduced evaporation and dispersion,
876 which are associated with lower temperatures in winter (Fig. 6). Thus, the facts that POA is not
877 uniformly distributed and that the concentration of POA is comparable to SOA possibly lead to
878 the spatial non-uniformity of OA in winter.

879

880 4.4 Interpretation of long-term measurements

881 In this section, we compare our observations from short-term detailed aerosol chemical
882 measurements with those from long-term and more basic measurements to test the validity of our
883 conclusions. Further, based on our extensive measurements, we attempt to provide insights into
884 interpreting long-term observations.

885 4.4.1 OA Diurnal Variation

886 By investigating the diurnal pattern of organic carbon (OC) from 1 June – 15 July of each
887 year (from 2000 to 2013) in Centreville, rural Alabama, Hidy et al. (2014) observed that OC
888 shows consistently weak diurnal variability. Similarly, Zhang et al. (2012) observed that water-
889 soluble organic carbon (WSOC), which is a surrogate for SOA (in summer), only shows a
890 moderate increase in the daytime in Jefferson Street and Yorkville, GA, during 2008 summer. In
891 this study, we find that OA shows little diurnal variability in summer datasets (Fig. 3), which is
892 consistent with long-term observations and previous studies.

893 The lack of a prominent daytime increase in the OA in summer could appear to discount
894 the role of photochemistry-driven secondary OA formation. However, a number of factors need
895 to be considered, such as the changes in planetary boundary layer height, contribution of various
896 sources to OA, and temperature-dependent gas/particle partitioning. Firstly, the rapid expansion
897 of the boundary layer during the day may dilute the OA concentration. In Centreville, the
898 boundary layer height (BLH) was measured by a ceilometer. The diurnal variation of BLH is
899 shown in Fig. 14. The BLH typically peaks (i.e., 1300m) at 17:00 and exhibits a daily minimum
900 (i.e., 375m) at 07:00. In order to remove the effect of BLH-driven dilution on the diurnal
901 variation of OA, we multiply the OA diurnal profile by BLH. The interpretation of the product of
902 the concentration of OA (i.e., $\mu g\ m^{-3}$) times BLH (i.e., m) is the integrated column concentration
903 of OA (i.e., $\mu g\ m^{-2}$) from ground to the top of boundary layer over a unit surface area, assuming
904 the OA is well-mixed in the boundary layer. The value of OA*BLH would be conserved if there
905 is no gain or loss of OA in the column regardless of the change of BLH. Thus, this value could
906 indicate the net gain or loss of OA in the column without the effect of BLH-driven dilution. As
907 shown in Fig. 3d, the OA*BLH increases rapidly starting at ~7:00 and reaches a daily maximum
908 at ~17:00. The evident peak in the diurnal variation of OA*BLH suggests a substantial OA

production in the day, and that the relatively flat OA diurnal variation (i.e., μg m^{-3}) is largely caused by the BLH-driven dilution. For the cases where boundary layer height data are not available, normalizing OA by CO is often utilized in the literature to minimize the effect of dilution, considering CO as an inert species. By using this method, Blanchard et al. (2011) and Zhang et al. (2012) showed that OC/CO and WSOC/CO exhibit pronounced daytime increase, suggesting that the expansion of boundary layer would weaken the OA diurnal variation. The fact that both OC/CO and WSOC/CO peaks in the day implies that photochemistry-driven SOA production is an important source of OA.

Secondly, the time-dependent contributions of various sources to total OA could also affect its diurnal profile. As shown in Fig. 5, the various OA sources resolved by PMF analysis have distinctly different diurnal trends, indicating that their contributions to total OA vary throughout the day. Primary sources, such as HOA and COA, peak during rush hours and meal-time, respectively. The contributions of Isoprene-OA and MO-OOA to total OA are largest in the afternoon and decrease after sunset. In contrast, another SOA source, LO-OOA, peaks in the early morning and at night, as the formation of LO-OOA is proposed to mainly correspond to nocturnal nitrate radical oxidation of biogenic VOCs in summer (Xu et al., 2015). Therefore, different diurnal trends of various OA sources compensate each other, which possibly results in the weak diurnal variation of total OA.

Specifically, LO-OOA, which exhibits a daily maximum at night, compensates for the decrease of other OA sources after sunset and results in the relatively flat total OA diurnal profile. This has important implication in interpreting non-speciated OC measurements. For example, Hennigan et al. (2009) observed a substantial nocturnal increase of gas-phase WSOC, but not an accompanied increase in particle-phase WSOC in Atlanta during summer. The authors hypothesized that the differences between gas-phase and particle-phase WSOC are caused by the oxidation of α-pinene and isoprene by $NO_3^{\bullet}$ radical producing substantial amount of gas-phase WSOC but little particle-phase WSOC. Though it is plausible that α-pinene+$NO_3^{\bullet}$ and isoprene+$NO_3^{\bullet}$ reactions produce more volatile products than low-volatility products, our study shows that there is indeed substantial nocturnal SOA production (i.e., LO-OOA), which likely corresponds to the nocturnal increase in gas-phase WSOC in Hennigan et al. (2009), but not

clearly discernible in particle-phase WSOC due to the compensation by the decreasing concentrations of other OA sources at night.

In addition, temperature-dependent gas/particle partitioning also plays a role in OA diurnal variation. As the temperature is higher during day, the gas/particle partitioning would favor the gas-phase and hence lower the particle-phase concentration. Taken together, the weak diurnal variation of OA in summer is likely caused by changes in boundary layer height and the varying contribution of various OA sources throughout the day, which does not contradict the importance of photochemistry-driven SOA production. Especially, LO-OOA, which is likely related to $NO_3^{\bullet}$ chemistry, peaks at night and compensates the nocturnal decrease of other SOA sources. In fact, the importance of photochemistry can be gained by comparing OA diurnal profile of summer and winter. As the photochemistry is relatively weaker in winter, daytime SOA production is suppressed, which results in OA reaching a daily minimum during daytime in winter datasets (Fig. 3).

4.4.2 Urban and rural contrast of OA seasonality

In this study, we observed that the seasonality of OA behaves differently between urban and rural sites. For example, while the OA concentration is relatively constant between summer and winter for the urban JST site (9.1 μg m^{-3} in May vs 7.9 μg m^{-3} in November), the OA concentration is ~4 times higher in summer than winter for the rural YRK site (11.2 μg m^{-3} in July vs 3.2 μg m^{-3} in December). Our observations are consistent with the long-term measurements from the SEARCH network. Fig. 15 shows the seasonal average OC concentration measured in JST and YRK from 1999 to 2013. Despite the decreasing trend of OC in the past 14 years, which has been noted and discussed extensively in Hidy et al. (2014), we note that the OC concentration is similar between summer and winter at the JST site, but OC is elevated in summer compared to winter for the YRK site. The urban and rural contrast of OA seasonality is likely caused by the fact that OA sources are different at urban and rural sites. As shown by PMF analysis on our short-term measurements, the total OA at the rural YRK site is dominant by SOA in both summer and winter (SOA/OA = 100% and 78% for summer and winter, respectively, Fig. 6), but the concentration of SOA is lower in winter when the SOA formation is depressed due to low biogenic VOCs emissions and weak photochemical activity. For the urban JST site, in contrast, POA accounts for a large fraction of total OA (30-48%, depending on the month).

Though the SOA formation is also depressed in winter at urban sites, the decrease in SOA concentration is compensated by the increase in POA concentration from vehicles and cooking (Fig. 6). Thus, the OA at JST is relatively constant between summer and winter. The changing composition of the OA also implies differing aerosol toxicity and health impacts, not discernible from measurements of total OA (or OC) (Verma et al., 2015). The fairly flat seasonal trend in OA or OC at urban sites has not been captured by current models. All 31 models reviewed in a recent study by Tsigaridis et al. (2014) predicted higher OC concentration in summer than winter for urban monitoring sites in Georgia. One possible reason is that the anthropogenic emission inventories applied in current models do not take seasonal variation into account, resulting in an under-prediction of the pollution levels in urban area.

4.4.3 Correlation between OC and sulfate

Based on the OC and sulfate measurements (2005 – 2010) from three SEARCH network sites (Centreville, Jefferson Street, and Yorkville), we find that regardless of the sampling sites, the correlation between OC and sulfate has a distinct seasonal variation, with the best correlation in summer (R ranging 0.47-0.69) and worst in winter (R ranging 0.01-0.33) (Fig. 16). Since sulfate is mostly secondary in the southeastern US, one possible explanation for the seasonality of the correlation between OC and sulfate is that the majority of OC is secondary in summer, but not in winter, which is supported by the OA source apportionment in this study. It is also likely that sulfate is directly involved in the OA production in summer. Specifically, Xu et al. (2015) found that sulfate directly and largely mediates the formation of isoprene OA (18-36% of total OA in summer) in the southeastern US, instead of particle water content and/or particle acidity, as previous studies have suggested.

5. Conclusion

Nearly one-year of measurements were performed across multiple sites in the southeastern US with a variety of online instruments, with the focus on HR-ToF-AMS data in this study. We find that organics are the dominant components of the NR-PM_1 at both rural and urban sites throughout the year. The OA diurnal profile shows little variation in summer and peaks at night in winter datasets. The lack of midday enhancement in OA diurnal profile is likely caused by the expansion of boundary layer in the day and compensating effects of various OA

997 factors. The OA measured at different sampling sites and seasons has a similar degree of
998 oxidation. Sulfate contributes the second highest to NR-PM_1. Sulfate concentration is higher in
999 summer (3.0 to 4.0 μg m^{-3}) than winter (1.4 to 1.7 μg m^{-3}), probably due to stronger
1000 photochemistry in summer. In contrast to sulfate, the inorganic nitrate concentration is estimated
1001 to be three times higher in winter than summer. This is likely caused by higher NO_x levels in
1002 winter, which serves as the source for inorganic nitrates and the semi-volatile nature of inorganic
1003 nitrates, which tend to partitions into the particle phase when the temperature is low.

1004 Positive Matrix Factorization (PMF) analysis revealed that the organic aerosol has
1005 various sources in the southeastern US, which changes between seasons and sampling sites (rural
1006 vs urban). Hydrocarbon-like organic aerosol (HOA) and cooking organic aerosol (COA), which
1007 arise from primary vehicle emissions and cooking, respectively, are important but not dominant
1008 OA sources for urban sites. Biomass burning OA (BBOA) concentrations shows clear
1009 enhancements in winter compared to summer. In addition, biomass burning is found to be an
1010 important, but not exclusive, source for brown carbon in the southeastern US. Isoprene-derived
1011 OA (Isoprene-OA), which is from the reactive uptake of isoprene epoxides in the presence of
1012 hydrated sulfate, only exists in warmer months (May-August) when isoprene emissions are
1013 substantial. In addition to rural sites, Isoprene-OA is resolved from urban sites where the
1014 majority of peroxy radicals are believed to react with NO_x. We note that f_{C5H6O+}, which has been
1015 used as a marker for Isoprene-OA, ranges from 0.9-2.3% and is higher in the Isoprene-OA factor
1016 from rural sites than urban sites. One possible source of Isoprene-OA in urban sites is transport.
1017 However, transport would not likely result in the reproducible diurnal profile of Isoprene-OA,
1018 which peaks in early afternoon. Instead, Isoprene-OA in urban sites more likely comes from
1019 local production, as a recent study showed that IEPOX could be produced in the presence of NO_x
1020 (Jacobs et al., 2014). Less-oxidized oxygenated OA (LO-OOA) and more-oxidized oxygenated
1021 OA (MO-OOA) are resolved from both rural and urban sites throughout the year. LO-OOA
1022 shows improved correlation with estimated "nitrate functionality from organic nitrates" (i.e.,
1023 $NO_{3,org}$) than total nitrates. In addition, both LO-OOA and estimated $NO_{3,org}$ peaks at night (Figs.
1024 5 and 12), implying that LO-OOA could arise from nighttime oxidation of biogenic VOCs by
1025 nitrate radicals. Unlike isoprene, monoterpene emissions occur year-around and continue into the
1026 night. The prevalence of the LO-OOA factor at all sites year-around points to the important
1027 contribution of monoterpene SOA to the total OA budget in the southeastern US. As the most

oxidized OA factor, MO-OOA reaches a daily maximum in the afternoon and likely contains aged OA from various sources, such as vehicle emission, biomass burning, and aged OA from biogenic VOCs. We find that the correlation between MO-OOA and ozone is substantially better in summer than winter, suggesting that the sources of MO-OOA might vary with season.

In order to estimate the organic nitrate contribution to OA, we applied and evaluated three methods, i.e, NO_x^+ ratio method, PMF method, and AMS-IC method. Despite the uncertainty of the NO_x^+ ratio method (i.e., the values of R_{ON} and R_{AN}) and the PMF method (i.e., the separation of pure NIA factor), both methods provide reasonable results in separating the measured total nitrates into nitrate functionality from inorganic and organic nitrates. The "nitrate functionality from organic nitrates" (i.e., $NO_{3,org}$) accounts for about 63–100% and 10-20% of total measured nitrate (i.e., $NO_{3,meas}$) in summer and winter, respectively. Further, we estimate the contribution of organic nitrates to total OA based on estimated $NO_{3,org}$ and assumed molecular weigth of bulk organic nitrates. Depending on location, season and estimation method, organic nitrates account for about 5-25% of total OA, which indicates that organic nitrates are important components in the ambient aerosol.

The spatial distribution of OA is investigated by comparing ACSM measurements (stationary at the Georgia Tech site) and HR-ToF-AMS measurements (rotating among different sites). In summer, OA is spatially homogeneous as suggested by the good correlation (R=0.92) in July between the GT and YRK sites, which are 70km apart. The spatial homogeneity of OA in summer is likely caused by SOA being the dominant source of OA for both urban and rural sites. The parameters such as temperature, solar radiation, and precursor VOCs, which have great influences on SOA formation, are similar between urban and rural sites. Compared to summer, the OA is less spatially homogenous in winter. The correlation coefficient of OA between GT and YRK decreases to 0.66 in winter. This is likely due to the elevated contribution from POA to total OA in winter and the spatially inhomogeneous distribution of POA. Meteorology also plays a role in the OA spatial distribution, but alone is unlikely to explain the observation.

We show that short-term and extensive measurements can help interpret long-term basic measurements. For example, consistent with long-term (1999 – 2013) OC measurements from the SEARCH network, we also observed that the seasonal variation of OA has some urban and rural contrasts. While the OA concentration is similar between summer and winter for the urban

JST site, it increases by a factor of 4 from winter to summer for the rural YRK site, according to our year-long observations. PMF analysis suggests that the different OA seasonality between urban and rural sites is likely due to the varying strength of OA sources. For rural sites, SOA represents the dominant fraction of OA in both summer and winter, but SOA concentration is much lower in winter. For urban sites, in contrast, the decrease in SOA concentration in winter is compensated by the increase in POA concentration due to less dispersion from lower boundary layer heights, leading to a relatively constant total OA concentration compared to summer. In addition, analysis of long-term OC and sulfate measurements from the SEARCH network shows that the correlation between OC and sulfate is substantially better in summer than winter, consistent with our source apportionment results that show the majority of OA is secondary in summer. The better correlation of OC and sulfate in summer also supports that sulfate directly mediates the formation of isoprene SOA (Xu et al., 2015), which is only present in warmer months.

Acknowledgement

This publication was made possible by US EPA grant R834799. This publication's contents are solely the responsibility of the grantee and do not necessarily represent the official views of the US EPA. Further, US EPA does not endorse the purchase of any commercial products or services mentioned in the publication. Measurements in SOAS are supported by the NSF under grant number 1242258. S.S. acknowledges support from the Air Products Undergraduate Research Program and the President's Undergraduate Research Award (PURA) at Georgia Tech. The authors thank the SEARCH personnel for their many contributions. Without their support this work would not have been possible.

Reference

Aiken, A. C., Decarlo, P. F., Kroll, J. H., Worsnop, D. R., Huffman, J. A., Docherty, K. S., Ulbrich, I. M., Mohr, C., Kimmel, J. R., Sueper, D., Sun, Y., Zhang, Q., Trimborn, A., Northway, M., Ziemann, P. J., Canagaratna, M. R., Onasch, T. B., Alfarra, M. R., Prevot, A. S. H., Dommen, J., Duplissy, J., Metzger, A., Baltensperger, U., and Jimenez, J. L.: O/C and OM/OC ratios of primary, secondary, and ambient organic aerosols with high-resolution time-of-flight aerosol mass spectrometry, Environ Sci Technol, 42, 4478-4485, Doi 10.1021/Es703009q, 2008.

Aiken, A. C., Salcedo, D., Cubison, M. J., Huffman, J. A., DeCarlo, P. F., Ulbrich, I. M., Docherty, K. S., Sueper, D., Kimmel, J. R., Worsnop, D. R., Trimborn, A., Northway, M., Stone, E. A., Schauer, J. J., Volkamer, R. M., Fortner, E., de Foy, B., Wang, J., Laskin, A., Shutthanandan, V., Zheng, J., Zhang, R., Gaffney, J., Marley, N. A., Paredes-Miranda, G., Arnott, W. P., Molina, L. T., Sosa, G., and Jimenez, J. L.: Mexico City aerosol analysis during MILAGRO using high resolution aerosol mass spectrometry at the urban supersite (T0) – Part 1: Fine particle composition and organic source apportionment, Atmos. Chem. Phys., 9, 6633-6653, 10.5194/acp-9-6633-2009, 2009.

Allan, J. D., Bower, K. N., Coe, H., Boudries, H., Jayne, J. T., Canagaratna, M. R., Millet, D. B., Goldstein, A. H., Quinn, P. K., Weber, R. J., and Worsnop, D. R.: Submicron aerosol composition at Trinidad Head, California, during ITCT 2K2: Its relationship with gas phase volatile organic carbon and assessment of instrument performance, Journal of Geophysical Research: Atmospheres, 109, D23S24, 10.1029/2003JD004208, 2004.

Allan, J. D., Williams, P. I., Morgan, W. T., Martin, C. L., Flynn, M. J., Lee, J., Nemitz, E., Phillips, G. J., Gallagher, M. W., and Coe, H.: Contributions from transport, solid fuel burning and cooking to primary organic aerosols in two UK cities, Atmos. Chem. Phys., 10, 647-668, 10.5194/acp-10-647-2010, 2010.

Andreae, M. O., and Gelencsér, A.: Black carbon or brown carbon? The nature of light-absorbing carbonaceous aerosols, Atmos. Chem. Phys., 6, 3131-3148, 10.5194/acp-6-3131-2006, 2006.

Bae, M. S., Schwab, J. J., Zhang, Q., Hogrefe, O., Demerjian, K. L., Weimer, S., Rhoads, K., Orsini, D., Venkatachari, P., and Hopke, P. K.: Interference of organic signals in highly time resolved nitrate measurements by low mass resolution aerosol mass spectrometry, J Geophys Res-Atmos, 112, Artn D22305 Doi 10.1029/2007jd008614, 2007.

Bahreini, R., Ervens, B., Middlebrook, A. M., Warneke, C., de Gouw, J. A., DeCarlo, P. F., Jimenez, J. L., Brock, C. A., Neuman, J. A., Ryerson, T. B., Stark, H., Atlas, E., Brioude, J.,

1127 Fried, A., Holloway, J. S., Peischl, J., Richter, D., Walega, J., Weibring, P., Wollny, A. G., and
1128 Fehsenfeld, F. C.: Organic aerosol formation in urban and industrial plumes near Houston and
1129 Dallas, Texas, Journal of Geophysical Research: Atmospheres, 114, D00F16,
1130 10.1029/2008JD011493, 2009.
1131
1132 Beddows, D. C. S., Harrison, R. M., Green, D. C., and Fuller, G. W.: Receptor modelling of both
1133 particle composition and size distribution from a background site in London, UK, Atmos. Chem.
1134 Phys. Discuss., 15, 10123-10162, 10.5194/acpd-15-10123-2015, 2015.
1135
1136 Blanchard, C. L., Hidy, G. M., Tanenbaum, S., Edgerton, E., Hartsell, B., and Jansen, J.: Carbon
1137 in southeastern U.S. aerosol particles: Empirical estimates of secondary organic aerosol
1138 formation, Atmospheric Environment, 42, 6710-6720,
1139 dx.doi.org/10.1016/j.atmosenv.2008.04.011, 2008.
1140
1141 Blanchard, C. L., Hidy, G. M., Tanenbaum, S., and Edgerton, E. S.: NMOC, ozone, and organic
1142 aerosol in the southeastern United States, 1999-2007: 3. Origins of organic aerosol in Atlanta,
1143 Georgia, and surrounding areas, Atmospheric Environment, 45, 1291-1302, DOI
1144 10.1016/j.atmosenv.2010.12.004, 2011.
1145
1146 Blanchard, C. L., Hidy, G. M., Tanenbaum, S., Edgerton, E. S., and Hartsell, B. E.: The
1147 Southeastern Aerosol Research and Characterization (SEARCH) study: Spatial variations and
1148 chemical climatology, 1999–2010, J Air Waste Manage, 63, 260-275,
1149 10.1080/10962247.2012.749816, 2013.
1150
1151 Bougiatioti, A., Stavroulas, I., Kostenidou, E., Zarmpas, P., Theodosi, C., Kouvarakis, G.,
1152 Canonaco, F., Prévôt, A. S. H., Nenes, A., Pandis, S. N., and Mihalopoulos, N.: Processing of
1153 biomass-burning aerosol in the eastern Mediterranean during summertime, Atmos. Chem. Phys.,
1154 14, 4793-4807, 10.5194/acp-14-4793-2014, 2014.
1155
1156 Boyd, C. M., Sanchez, J., Xu, L., Eugene, A. J., Nah, T., Tuet, W. Y., Guzman, M. I., and Ng, N.
1157 L.: Secondary Organic Aerosol (SOA) formation from the β-pinene + NO3 system: effect of
1158 humidity and peroxy radical fate, Atmos. Chem. Phys. Discuss., 15, 2679-2744, 10.5194/acpd-
1159 15-2679-2015, 2015.
1160
1161 Bruns, E. A., Perraud, V., Zelenyuk, A., Ezell, M. J., Johnson, S. N., Yu, Y., Imre, D.,
1162 Finlayson-Pitts, B. J., and Alexander, M. L.: Comparison of FTIR and Particle Mass
1163 Spectrometry for the Measurement of Particulate Organic Nitrates, Environ Sci Technol, 44,
1164 1056-1061, 10.1021/es9029864, 2010.
1165
1166 Budisulistiorini, S. H., Canagaratna, M. R., Croteau, P. L., Marth, W. J., Baumann, K., Edgerton,
1167 E. S., Shaw, S. L., Knipping, E. M., Worsnop, D. R., Jayne, J. T., Gold, A., and Surratt, J. D.:

Real-Time Continuous Characterization of Secondary Organic Aerosol Derived from Isoprene Epoxydiols in Downtown Atlanta, Georgia, Using the Aerodyne Aerosol Chemical Speciation Monitor, Environ Sci Technol, 47, 5686-5694, Doi 10.1021/Es400023n, 2013.

Canagaratna, M. R., Jayne, J. T., Jimenez, J. L., Allan, J. D., Alfarra, M. R., Zhang, Q., Onasch, T. B., Drewnick, F., Coe, H., Middlebrook, A., Delia, A., Williams, L. R., Trimborn, A. M., Northway, M. J., DeCarlo, P. F., Kolb, C. E., Davidovits, P., and Worsnop, D. R.: Chemical and microphysical characterization of ambient aerosols with the aerodyne aerosol mass spectrometer, Mass Spectrometry Reviews, 26, 185-222, 10.1002/mas.20115, 2007.

Canagaratna, M. R., Jimenez, J. L., Kroll, J. H., Chen, Q., Kessler, S. H., Massoli, P., Hildebrandt Ruiz, L., Fortner, E., Williams, L. R., Wilson, K. R., Surratt, J. D., Donahue, N. M., Jayne, J. T., and Worsnop, D. R.: Elemental ratio measurements of organic compounds using aerosol mass spectrometry: characterization, improved calibration, and implications, Atmos. Chem. Phys., 15, 253-272, 10.5194/acp-15-253-2015, 2015.

Chen, Q., Farmer, D. K., Rizzo, L. V., Pauliquevis, T., Kuwata, M., Karl, T. G., Guenther, A., Allan, J. D., Coe, H., Andreae, M. O., Pöschl, U., Jimenez, J. L., Artaxo, P., and Martin, S. T.: Fine-mode organic mass concentrations and sources in the Amazonian wet season (AMAZE-08), Atmos. Chem. Phys. Discuss., 14, 16151-16186, 10.5194/acpd-14-16151-2014, 2014.

Cohan, D., Boylan, J., Marmur, A., and Khan, M.: An Integrated Framework for Multipollutant Air Quality Management and Its Application in Georgia, Environmental Management, 40, 545-554, 10.1007/s00267-006-0228-4, 2007.

Crippa, M., DeCarlo, P. F., Slowik, J. G., Mohr, C., Heringa, M. F., Chirico, R., Poulain, L., Freutel, F., Sciare, J., Cozic, J., Di Marco, C. F., Elsasser, M., Nicolas, J. B., Marchand, N., Abidi, E., Wiedensohler, A., Drewnick, F., Schneider, J., Borrmann, S., Nemitz, E., Zimmermann, R., Jaffrezo, J. L., Prévôt, A. S. H., and Baltensperger, U.: Wintertime aerosol chemical composition and source apportionment of the organic fraction in the metropolitan area of Paris, Atmos. Chem. Phys., 13, 961-981, 10.5194/acp-13-961-2013, 2013.

Crippa, M., Canonaco, F., Lanz, V. A., Äijälä, M., Allan, J. D., Carbone, S., Capes, G., Ceburnis, D., Dall'Osto, M., Day, D. A., DeCarlo, P. F., Ehn, M., Eriksson, A., Freney, E., Hildebrandt Ruiz, L., Hillamo, R., Jimenez, J. L., Junninen, H., Kiendler-Scharr, A., Kortelainen, A. M., Kulmala, M., Laaksonen, A., Mensah, A. A., Mohr, C., Nemitz, E., O'Dowd, C., Ovadnevaite, J., Pandis, S. N., Petäjä, T., Poulain, L., Saarikoski, S., Sellegri, K., Swietlicki, E., Tiitta, P., Worsnop, D. R., Baltensperger, U., and Prévôt, A. S. H.: Organic aerosol components derived from 25 AMS data sets across Europe using a consistent ME-2 based source apportionment approach, Atmos. Chem. Phys., 14, 6159-6176, 10.5194/acp-14-6159-2014, 2014.

1209 Day, D. A., Wooldridge, P. J., Dillon, M. B., Thornton, J. A., and Cohen, R. C.: A thermal
1210 dissociation laser-induced fluorescence instrument for in situ detection of NO2, peroxy nitrates,
1211 alkyl nitrates, and HNO3, Journal of Geophysical Research: Atmospheres, 107, ACH 4-1-ACH
1212 4-14, 10.1029/2001JD000779, 2002.
1213

1214 DeCarlo, P. F., Kimmel, J. R., Trimborn, A., Northway, M. J., Jayne, J. T., Aiken, A. C., Gonin,
1215 M., Fuhrer, K., Horvath, T., Docherty, K. S., Worsnop, D. R., and Jimenez, J. L.: Field-
1216 Deployable, High-Resolution, Time-of-Flight Aerosol Mass Spectrometer, Anal Chem, 78,
1217 8281-8289, 10.1021/ac061249n, 2006.
1218

1219 DeWitt, H. L., Hellebust, S., Temime-Roussel, B., Ravier, S., Polo, L., Jacob, V., Buisson, C.,
1220 Charron, A., André, M., Pasquier, A., Besombes, J. L., Jaffrezo, J. L., Wortham, H., and
1221 Marchand, N.: Direct measurements of near-highway emissions in a high diesel environment,
1222 Atmos. Chem. Phys. Discuss., 14, 27373-27424, 10.5194/acpd-14-27373-2014, 2014.
1223

1224 Eddingsaas, N. C., VanderVelde, D. G., and Wennberg, P. O.: Kinetics and Products of the Acid-
1225 Catalyzed Ring-Opening of Atmospherically Relevant Butyl Epoxy Alcohols, J Phys Chem A,
1226 114, 8106-8113, Doi 10.1021/Jp103907c, 2010.
1227

1228 Edgerton, E. S., Hartsell, B. E., Saylor, R. D., Jansen, J. J., Hansen, D. A., and Hidy, G. M.: The
1229 southeastern aerosol research and characterization study: Part II. Filter-based measurements of
1230 fine and coarse particulate matter mass and composition, J Air Waste Manage, 55, 1527-1542,
1231 2005.
1232

1233 Ehn, M., Thornton, J. A., Kleist, E., Sipila, M., Junninen, H., Pullinen, I., Springer, M., Rubach,
1234 F., Tillmann, R., Lee, B., Lopez-Hilfiker, F., Andres, S., Acir, I.-H., Rissanen, M., Jokinen, T.,
1235 Schobesberger, S., Kangasluoma, J., Kontkanen, J., Nieminen, T., Kurten, T., Nielsen, L. B.,
1236 Jorgensen, S., Kjaergaard, H. G., Canagaratna, M., Maso, M. D., Berndt, T., Petaja, T., Wahner,
1237 A., Kerminen, V.-M., Kulmala, M., Worsnop, D. R., Wildt, J., and Mentel, T. F.: A large source
1238 of low-volatility secondary organic aerosol, Nature, 506, 476-479, 10.1038/nature13032, 2014.
1239

1240 El Haddad, I., D'Anna, B., Temime-Roussel, B., Nicolas, M., Boreave, A., Favez, O., Voisin, D.,
1241 Sciare, J., George, C., Jaffrezo, J. L., Wortham, H., and Marchand, N.: Towards a better
1242 understanding of the origins, chemical composition and aging of oxygenated organic aerosols:
1243 case study of a Mediterranean industrialized environment, Marseille, Atmos. Chem. Phys., 13,
1244 7875-7894, 10.5194/acp-13-7875-2013, 2013.
1245

1246 Farmer, D. K., Matsunaga, A., Docherty, K. S., Surratt, J. D., Seinfeld, J. H., Ziemann, P. J., and
1247 Jimenez, J. L.: Response of an aerosol mass spectrometer to organonitrates and organosulfates
1248 and implications for atmospheric chemistry, Proceedings of the National Academy of Sciences,
1249 107, 6670-6675, 10.1073/pnas.0912340107, 2010.

Feng, Y., Ramanathan, V., and Kotamarthi, V. R.: Brown carbon: a significant atmospheric absorber of solar radiation?, Atmos. Chem. Phys., 13, 8607-8621, 10.5194/acp-13-8607-2013, 2013.

Ford, B., and Heald, C. L.: Aerosol loading in the Southeastern United States: reconciling surface and satellite observations, Atmos Chem Phys, 13, 9269-9283, DOI 10.5194/acp-13-9269-2013, 2013.

Fry, J. L., Kiendler-Scharr, A., Rollins, A. W., Wooldridge, P. J., Brown, S. S., Fuchs, H., Dube, W., Mensah, A., dal Maso, M., Tillmann, R., Dorn, H. P., Brauers, T., and Cohen, R. C.: Organic nitrate and secondary organic aerosol yield from NO3 oxidation of beta-pinene evaluated using a gas-phase kinetics/aerosol partitioning model, Atmos Chem Phys, 9, 1431-1449, 2009.

Fry, J. L., Draper, D. C., Zarzana, K. J., Campuzano-Jost, P., Day, D. A., Jimenez, J. L., Brown, S. S., Cohen, R. C., Kaser, L., Hansel, A., Cappellin, L., Karl, T., Roux, A. H., Turnipseed, A., Cantrell, C., Lefer, B. L., and Grossberg, N.: Observations of gas- and aerosol-phase organic nitrates at BEACHON-RoMBAS 2011, Atmos Chem Phys, 13, 8585-8605, DOI 10.5194/acp-13-8585-2013, 2013.

Gaston, C. J., Riedel, T. P., Zhang, Z., Gold, A., Surratt, J. D., and Thornton, J. A.: Reactive Uptake of an Isoprene-Derived Epoxydiol to Submicron Aerosol Particles, Environ Sci Technol, 48, 11178-11186, 10.1021/es5034266, 2014.

Geron, C., Rasmussen, R., Arnts, R. R., and Guenther, A.: A review and synthesis of monoterpene speciation from forests in the United States, Atmospheric Environment, 34, 1761-1781, Doi 10.1016/S1352-2310(99)00364-7, 2000.

Grieshop, A. P., Donahue, N. M., and Robinson, A. L.: Laboratory investigation of photochemical oxidation of organic aerosol from wood fires 2: analysis of aerosol mass spectrometer data, Atmos. Chem. Phys., 9, 2227-2240, 10.5194/acp-9-2227-2009, 2009.

Guenther, A., Karl, T., Harley, P., Wiedinmyer, C., Palmer, P. I., and Geron, C.: Estimates of global terrestrial isoprene emissions using MEGAN (Model of Emissions of Gases and Aerosols from Nature), Atmos Chem Phys, 6, 3181-3210, 2006.

Guo, H., Xu, L., Bougiatioti, A., Cerully, K. M., Capps, S. L., Hite Jr, J. R., Carlton, A. G., Lee, S. H., Bergin, M. H., Ng, N. L., Nenes, A., and Weber, R. J.: Fine-particle water and pH in the southeastern United States, Atmos. Chem. Phys., 15, 5211-5228, 10.5194/acp-15-5211-2015, 2015.

Hansen, D. A., Edgerton, E. S., Hartsell, B. E., Jansen, J. J., Kandasamy, N., Hidy, G. M., and Blanchard, C. L.: The southeastern aerosol research and characterization study: Part 1-overview, J Air Waste Manage, 53, 1460-1471, 2003.

Hao, L. Q., Kortelainen, A., Romakkaniemi, S., Portin, H., Jaatinen, A., Leskinen, A., Komppula, M., Miettinen, P., Sueper, D., Pajunoja, A., Smith, J. N., Lehtinen, K. E. J., Worsnop, D. R., Laaksonen, A., and Virtanen, A.: Atmospheric submicron aerosol composition and particulate organic nitrate formation in a boreal forestland–urban mixed region, Atmos. Chem. Phys., 14, 13483-13495, 10.5194/acp-14-13483-2014, 2014.

Hayes, P. L., Ortega, A. M., Cubison, M. J., Froyd, K. D., Zhao, Y., Cliff, S. S., Hu, W. W., Toohey, D. W., Flynn, J. H., Lefer, B. L., Grossberg, N., Alvarez, S., Rappenglueck, B., Taylor, J. W., Allan, J. D., Holloway, J. S., Gilman, J. B., Kuster, W. C., De Gouw, J. A., Massoli, P., Zhang, X., Liu, J., Weber, R. J., Corrigan, A. L., Russell, L. M., Isaacman, G., Worton, D. R., Kreisberg, N. M., Goldstein, A. H., Thalman, R., Waxman, E. M., Volkamer, R., Lin, Y. H., Surratt, J. D., Kleindienst, T. E., Offenberg, J. H., Dusanter, S., Griffith, S., Stevens, P. S., Brioude, J., Angevine, W. M., and Jimenez, J. L.: Organic aerosol composition and sources in Pasadena, California, during the 2010 CalNex campaign, J Geophys Res-Atmos, 118, 9233-9257, Doi 10.1002/Jgrd.50530, 2013.

Hecobian, A., Zhang, X., Zheng, M., Frank, N., Edgerton, E. S., and Weber, R. J.: Water-Soluble Organic Aerosol material and the light-absorption characteristics of aqueous extracts measured over the Southeastern United States, Atmos. Chem. Phys., 10, 5965-5977, 10.5194/acp-10-5965-2010, 2010.

Hennigan, C. J., Sullivan, A. P., Fountoukis, C. I., Nenes, A., Hecobian, A., Vargas, O., Peltier, R. E., Case Hanks, A. T., Huey, L. G., Lefer, B. L., Russell, A. G., and Weber, R. J.: On the volatility and production mechanisms of newly formed nitrate and water soluble organic aerosol in Mexico City, Atmos. Chem. Phys., 8, 3761-3768, 10.5194/acp-8-3761-2008, 2008.

Hennigan, C. J., Bergin, M. H., Russell, A. G., Nenes, A., and Weber, R. J.: Gas/particle partitioning of water-soluble organic aerosol in Atlanta, Atmos Chem Phys, 9, 3613-3628, 2009.

Hennigan, C. J., Miracolo, M. A., Engelhart, G. J., May, A. A., Presto, A. A., Lee, T., Sullivan, A. P., McMeeking, G. R., Coe, H., Wold, C. E., Hao, W. M., Gilman, J. B., Kuster, W. C., de Gouw, J., Schichtel, B. A., Collett Jr, J. L., Kreidenweis, S. M., and Robinson, A. L.: Chemical and physical transformations of organic aerosol from the photo-oxidation of open biomass burning emissions in an environmental chamber, Atmos. Chem. Phys., 11, 7669-7686, 10.5194/acp-11-7669-2011, 2011.

1331 Heringa, M. F., DeCarlo, P. F., Chirico, R., Tritscher, T., Dommen, J., Weingartner, E., Richter,
1332 R., Wehrle, G., Prévôt, A. S. H., and Baltensperger, U.: Investigations of primary and secondary
1333 particulate matter of different wood combustion appliances with a high-resolution time-of-flight
1334 aerosol mass spectrometer, Atmos. Chem. Phys., 11, 5945-5957, 10.5194/acp-11-5945-2011,
1335 2011.
1336

1337 Hidy, G. M., Blanchard, C. L., Baumann, K., Edgerton, E., Tanenbaum, S., Shaw, S., Knipping,
1338 E., Tombach, I., Jansen, J., and Walters, J.: Chemical climatology of the southeastern United
1339 States, 1999–2013, Atmos. Chem. Phys., 14, 11893-11914, 10.5194/acp-14-11893-2014,
1340 2014.
1341

1342 Hildebrandt, L., Engelhart, G. J., Mohr, C., Kostenidou, E., Lanz, V. A., Bougiatioti, A.,
1343 DeCarlo, P. F., Prevot, A. S. H., Baltensperger, U., Mihalopoulos, N., Donahue, N. M., and
1344 Pandis, S. N.: Aged organic aerosol in the Eastern Mediterranean: the Finokalia Aerosol
1345 Measurement Experiment-2008, Atmos Chem Phys, 10, 4167-4186, DOI 10.5194/acp-10-4167-
1346 2010, 2010.
1347

1348 Huang, X. F., He, L. Y., Hu, M., Canagaratna, M. R., Sun, Y., Zhang, Q., Zhu, T., Xue, L., Zeng,
1349 L. W., Liu, X. G., Zhang, Y. H., Jayne, J. T., Ng, N. L., and Worsnop, D. R.: Highly time-
1350 resolved chemical characterization of atmospheric submicron particles during 2008 Beijing
1351 Olympic Games using an Aerodyne High-Resolution Aerosol Mass Spectrometer, Atmos Chem
1352 Phys, 10, 8933-8945, DOI 10.5194/acp-10-8933-2010, 2010.
1353

1354 Huffman, J. A., Docherty, K. S., Aiken, A. C., Cubison, M. J., Ulbrich, I. M., DeCarlo, P. F.,
1355 Sueper, D., Jayne, J. T., Worsnop, D. R., Ziemann, P. J., and Jimenez, J. L.: Chemically-resolved
1356 aerosol volatility measurements from two megacity field studies, Atmos Chem Phys, 9, 7161-
1357 7182, 2009.
1358

1359 Isaacman, G., Kreisberg, N. M., Yee, L. D., Worton, D. R., Chan, A. W. H., Moss, J. A., Hering,
1360 S. V., and Goldstein, A. H.: Online derivatization for hourly measurements of gas- and particle-
1361 phase semi-volatile oxygenated organic compounds by thermal desorption aerosol gas
1362 chromatography (SV-TAG), Atmos. Meas. Tech., 7, 4417-4429, 10.5194/amt-7-4417-2014,
1363 2014.
1364

1365 Jacobs, M. I., Burke, W. J., and Elrod, M. J.: Kinetics of the reactions of isoprene-derived
1366 hydroxynitrates: gas phase epoxide formation and solution phase hydrolysis, Atmos. Chem.
1367 Phys., 14, 8933-8946, 10.5194/acp-14-8933-2014, 2014.
1368

1369 Jaeckels, J. M., Bae, M.-S., and Schauer, J. J.: Positive Matrix Factorization (PMF) Analysis of
1370 Molecular Marker Measurements to Quantify the Sources of Organic Aerosols, Environ Sci
1371 Technol, 41, 5763-5769, 10.1021/es062536b, 2007.

1372

1373 Janssen, R. H. H., Vilà-Guerau de Arellano, J., Jimenez, J. L., Ganzeveld, L. N., Robinson, N. H.,
1374 Allan, J. D., Coe, H., and Pugh, T. A. M.: Influence of boundary layer dynamics and isoprene
1375 chemistry on the organic aerosol budget in a tropical forest, Journal of Geophysical Research:
1376 Atmospheres, 118, 9351-9366, 10.1002/jgrd.50672, 2013.
1377

1378 Jathar, S. H., Gordon, T. D., Hennigan, C. J., Pye, H. O. T., Pouliot, G., Adams, P. J., Donahue,
1379 N. M., and Robinson, A. L.: Unspeciated organic emissions from combustion sources and their
1380 influence on the secondary organic aerosol budget in the United States, P Natl Acad Sci USA,
1381 111, 10473-10478, DOI 10.1073/pnas.1323740111, 2014.
1382

1383 Jayne, J. T., Leard, D. C., Zhang, X. F., Davidovits, P., Smith, K. A., Kolb, C. E., and Worsnop,
1384 D. R.: Development of an aerosol mass spectrometer for size and composition analysis of
1385 submicron particles, Aerosol Sci Tech, 33, 49-70, Doi 10.1080/027868200410840, 2000.
1386

1387 Jimenez, J. L., Canagaratna, M. R., Donahue, N. M., Prevot, A. S. H., Zhang, Q., Kroll, J. H.,
1388 DeCarlo, P. F., Allan, J. D., Coe, H., Ng, N. L., Aiken, A. C., Docherty, K. S., Ulbrich, I. M.,
1389 Grieshop, A. P., Robinson, A. L., Duplissy, J., Smith, J. D., Wilson, K. R., Lanz, V. A., Hueglin,
1390 C., Sun, Y. L., Tian, J., Laaksonen, A., Raatikainen, T., Rautiainen, J., Vaattovaara, P., Ehn, M.,
1391 Kulmala, M., Tomlinson, J. M., Collins, D. R., Cubison, M. J., Dunlea, E. J., Huffman, J. A.,
1392 Onasch, T. B., Alfarra, M. R., Williams, P. I., Bower, K., Kondo, Y., Schneider, J., Drewnick, F.,
1393 Borrmann, S., Weimer, S., Demerjian, K., Salcedo, D., Cottrell, L., Griffin, R., Takami, A.,
1394 Miyoshi, T., Hatakeyama, S., Shimono, A., Sun, J. Y., Zhang, Y. M., Dzepina, K., Kimmel, J. R.,
1395 Sueper, D., Jayne, J. T., Herndon, S. C., Trimborn, A. M., Williams, L. R., Wood, E. C.,
1396 Middlebrook, A. M., Kolb, C. E., Baltensperger, U., and Worsnop, D. R.: Evolution of Organic
1397 Aerosols in the Atmosphere, Science, 326, 1525-1529, DOI 10.1126/science.1180353, 2009.
1398

1399 Kroll, J. H., Ng, N. L., Murphy, S. M., Flagan, R. C., and Seinfeld, J. H.: Secondary organic
1400 aerosol formation from isoprene photooxidation, Environ Sci Technol, 40, 1869-1877, Doi
1401 10.1021/Es0524301, 2006.
1402

1403 Kroll, J. H., Donahue, N. M., Jimenez, J. L., Kessler, S. H., Canagaratna, M. R., Wilson, K. R.,
1404 Altieri, K. E., Mazzoleni, L. R., Wozniak, A. S., Bluhm, H., Mysak, E. R., Smith, J. D., Kolb, C.
1405 E., and Worsnop, D. R.: Carbon oxidation state as a metric for describing the chemistry of
1406 atmospheric organic aerosol, Nat Chem, 3, 133-139, Doi 10.1038/Nchem.948, 2011.
1407

1408 Lack, D. A., Bahreini, R., Langridge, J. M., Gilman, J. B., and Middlebrook, A. M.: Brown
1409 carbon absorption linked to organic mass tracers in biomass burning particles, Atmos. Chem.
1410 Phys., 13, 2415-2422, 10.5194/acp-13-2415-2013, 2013.
1411

1412 Lanz, V. A., Alfarra, M. R., Baltensperger, U., Buchmann, B., Hueglin, C., and Prevot, A. S. H.:
1413 Source apportionment of submicron organic aerosols at an urban site by factor analytical
1414 modelling of aerosol mass spectra, Atmos Chem Phys, 7, 1503-1522, 2007.
1415

1416 Li, Y. J., Lee, B. P., Su, L., Fung, J. C. H., and Chan, C. K.: Seasonal characteristics of fine
1417 particulate matter (PM) based on high-resolution time-of-flight aerosol mass spectrometric (HR-
1418 ToF-AMS) measurements at the HKUST Supersite in Hong Kong, Atmos. Chem. Phys., 15, 37-
1419 53, 10.5194/acp-15-37-2015, 2015.
1420

1421 Lim, H.-J., and Turpin, B. J.: Origins of Primary and Secondary Organic Aerosol in Atlanta:
1422 Results of Time-Resolved Measurements during the Atlanta Supersite Experiment, Environ Sci
1423 Technol, 36, 4489-4496, 10.1021/es0206487, 2002.
1424

1425 Lin, Y.-H., Budisulistiorini, S. H., Chu, K., Siejack, R. A., Zhang, H., Riva, M., Zhang, Z., Gold,
1426 A., Kautzman, K. E., and Surratt, J. D.: Light-Absorbing Oligomer Formation in Secondary
1427 Organic Aerosol from Reactive Uptake of Isoprene Epoxydiols, Environ Sci Technol, 48, 12012-
1428 12021, 10.1021/es503142b, 2014.
1429

1430 Lin, Y. H., Zhang, Z. F., Docherty, K. S., Zhang, H. F., Budisulistiorini, S. H., Rubitschun, C. L.,
1431 Shaw, S. L., Knipping, E. M., Edgerton, E. S., Kleindienst, T. E., Gold, A., and Surratt, J. D.:
1432 Isoprene Epoxydiols as Precursors to Secondary Organic Aerosol Formation: Acid-Catalyzed
1433 Reactive Uptake Studies with Authentic Compounds, Environ Sci Technol, 46, 250-258, Doi
1434 10.1021/Es202554c, 2012.
1435

1436 Liu, J., Scheuer, E., Dibb, J., Ziemba, L. D., Thornhill, K. L., Anderson, B. E., Wisthaler, A.,
1437 Mikoviny, T., Devi, J. J., Bergin, M., and Weber, R. J.: Brown carbon in the continental
1438 troposphere, Geophysical Research Letters, 41, 2013GL058976, 10.1002/2013GL058976, 2014.
1439

1440 Liu, S., Day, D. A., Shields, J. E., and Russell, L. M.: Ozone-driven daytime formation of
1441 secondary organic aerosol containing carboxylic acid groups and alkane groups, Atmos Chem
1442 Phys, 11, 8321-8341, DOI 10.5194/acp-11-8321-2011, 2011.
1443

1444 Liu, Y., Kuwata, M., Strick, B. F., Geiger, F. M., Thomson, R. J., McKinney, K. A., and Martin,
1445 S. T.: Uptake of Epoxydiol Isomers Accounts for Half of the Particle-Phase Material Produced
1446 from Isoprene Photooxidation via the HO2 Pathway, Environ Sci Technol, 49, 250-258,
1447 10.1021/es5034298, 2015.
1448

1449 Mao, J., Ren, X., Zhang, L., Van Duin, D. M., Cohen, R. C., Park, J. H., Goldstein, A. H., Paulot,
1450 F., Beaver, M. R., Crounse, J. D., Wennberg, P. O., DiGangi, J. P., Henry, S. B., Keutsch, F. N.,
1451 Park, C., Schade, G. W., Wolfe, G. M., Thornton, J. A., and Brune, W. H.: Insights into hydroxyl

measurements and atmospheric oxidation in a California forest, Atmos. Chem. Phys., 12, 8009-8020, 10.5194/acp-12-8009-2012, 2012.

Matthew, B. M., Middlebrook, A. M., and Onasch, T. B.: Collection efficiencies in an Aerodyne Aerosol Mass Spectrometer as a function of particle phase for laboratory generated aerosols, Aerosol Sci Tech, 42, 884-898, Doi 10.1080/02786820802356797, 2008.

May, A. A., Saleh, R., Hennigan, C. J., Donahue, N. M., and Robinson, A. L.: Volatility of Organic Molecular Markers Used for Source Apportionment Analysis: Measurements and Implications for Atmospheric Lifetime, Environ Sci Technol, 46, 12435-12444, 10.1021/es302276t, 2012.

Middlebrook, A. M., Bahreini, R., Jimenez, J. L., and Canagaratna, M. R.: Evaluation of Composition-Dependent Collection Efficiencies for the Aerodyne Aerosol Mass Spectrometer using Field Data, Aerosol Sci Tech, 46, 258-271, Doi 10.1080/02786826.2011.620041, 2012.

Mohr, C., Huffman, J. A., Cubison, M. J., Aiken, A. C., Docherty, K. S., Kimmel, J. R., Ulbrich, I. M., Hannigan, M., and Jimenez, J. L.: Characterization of Primary Organic Aerosol Emissions from Meat Cooking, Trash Burning, and Motor Vehicles with High-Resolution Aerosol Mass Spectrometry and Comparison with Ambient and Chamber Observations, Environ Sci Technol, 43, 2443-2449, 10.1021/es8011518, 2009.

Mohr, C., DeCarlo, P. F., Heringa, M. F., Chirico, R., Slowik, J. G., Richter, R., Reche, C., Alastuey, A., Querol, X., Seco, R., Peñuelas, J., Jiménez, J. L., Crippa, M., Zimmermann, R., Baltensperger, U., and Prévôt, A. S. H.: Identification and quantification of organic aerosol from cooking and other sources in Barcelona using aerosol mass spectrometer data, Atmos. Chem. Phys., 12, 1649-1665, 10.5194/acp-12-1649-2012, 2012.

Ng, N. L., Canagaratna, M. R., Zhang, Q., Jimenez, J. L., Tian, J., Ulbrich, I. M., Kroll, J. H., Docherty, K. S., Chhabra, P. S., Bahreini, R., Murphy, S. M., Seinfeld, J. H., Hildebrandt, L., Donahue, N. M., DeCarlo, P. F., Lanz, V. A., Prevot, A. S. H., Dinar, E., Rudich, Y., and Worsnop, D. R.: Organic aerosol components observed in Northern Hemispheric datasets from Aerosol Mass Spectrometry, Atmos Chem Phys, 10, 4625-4641, DOI 10.5194/acp-10-4625-2010, 2010.

Ng, N. L., Herndon, S. C., Trimborn, A., Canagaratna, M. R., Croteau, P. L., Onasch, T. B., Sueper, D., Worsnop, D. R., Zhang, Q., Sun, Y. L., and Jayne, J. T.: An Aerosol Chemical Speciation Monitor (ACSM) for Routine Monitoring of the Composition and Mass Concentrations of Ambient Aerosol, Aerosol Sci Tech, 45, 780-794, Pii 934555189 Doi 10.1080/02786826.2011.560211, 2011.

1493 Nguyen, T. B., Coggon, M. M., Bates, K. H., Zhang, X., Schwantes, R. H., Schilling, K. A.,
1494 Loza, C. L., Flagan, R. C., Wennberg, P. O., and Seinfeld, J. H.: Organic aerosol formation from
1495 the reactive uptake of isoprene epoxydiols (IEPOX) onto non-acidified inorganic seeds, Atmos.
1496 Chem. Phys., 14, 3497-3510, 10.5194/acp-14-3497-2014, 2014.
1497

1498 Nordin, E. Z., Eriksson, A. C., Roldin, P., Nilsson, P. T., Carlsson, J. E., Kajos, M. K., Hellén,
1499 H., Wittbom, C., Rissler, J., Löndahl, J., Swietlicki, E., Svenningsson, B., Bohgard, M., Kulmala,
1500 M., Hallquist, M., and Pagels, J. H.: Secondary organic aerosol formation from idling gasoline
1501 passenger vehicle emissions investigated in a smog chamber, Atmos. Chem. Phys., 13, 6101-
1502 6116, 10.5194/acp-13-6101-2013, 2013.
1503

1504 Orsini, D. A., Ma, Y. L., Sullivan, A., Sierau, B., Baumann, K., and Weber, R. J.: Refinements to
1505 the particle-into-liquid sampler (PILS) for ground and airborne measurements of water soluble
1506 aerosol composition, Atmospheric Environment, 37, 1243-1259, Doi 10.1016/S1352-
1507 2310(02)01015-4, 2003.
1508

1509 Paatero, P., and Tapper, U.: Positive Matrix Factorization - a Nonnegative Factor Model with
1510 Optimal Utilization of Error-Estimates of Data Values, Environmetrics, 5, 111-126, DOI
1511 10.1002/env.3170050203, 1994.
1512

1513 Paatero, P.: A weighted non-negative least squares algorithm for three-way 'PARAFAC' factor
1514 analysis, Chemometr Intell Lab, 38, 223-242, Doi 10.1016/S0169-7439(97)00031-2, 1997.
1515

1516 Paglione, M., Kiendler-Scharr, A., Mensah, A. A., Finessi, E., Giulianelli, L., Sandrini, S.,
1517 Facchini, M. C., Fuzzi, S., Schlag, P., Piazzalunga, A., Tagliavini, E., Henzing, J. S., and
1518 Decesari, S.: Identification of humic-like substances (HULIS) in oxygenated organic aerosols
1519 using NMR and AMS factor analyses and liquid chromatographic techniques, Atmos. Chem.
1520 Phys., 14, 25-45, 10.5194/acp-14-25-2014, 2014.
1521

1522 Paulot, F., Crounse, J. D., Kjaergaard, H. G., Kurten, A., St Clair, J. M., Seinfeld, J. H., and
1523 Wennberg, P. O.: Unexpected Epoxide Formation in the Gas-Phase Photooxidation of Isoprene,
1524 Science, 325, 730-733, DOI 10.1126/science.1172910, 2009.
1525

1526 Perring, A. E., Pusede, S. E., and Cohen, R. C.: An Observational Perspective on the
1527 Atmospheric Impacts of Alkyl and Multifunctional Nitrates on Ozone and Secondary Organic
1528 Aerosol, Chem Rev, 113, 5848-5870, Doi 10.1021/Cr300520x, 2013.
1529

1530 Piletic, I. R., Edney, E. O., and Bartolotti, L. J.: A computational study of acid catalyzed aerosol
1531 reactions of atmospherically relevant epoxides, Phys Chem Chem Phys, 15, 18065-18076,
1532 10.1039/C3CP52851K, 2013.
1533

1534 Platt, S. M., El Haddad, I., Zardini, A. A., Clairotte, M., Astorga, C., Wolf, R., Slowik, J. G.,
1535 Temime-Roussel, B., Marchand, N., Jezek, I., Drinovec, L., Mocnik, G., Mohler, O., Richter, R.,
1536 Barmet, P., Bianchi, F., Baltensperger, U., and Prevot, A. S. H.: Secondary organic aerosol
1537 formation from gasoline vehicle emissions in a new mobile environmental reaction chamber,
1538 Atmos Chem Phys, 13, 9141-9158, DOI 10.5194/acp-13-9141-2013, 2013.
1539

1540 Presto, A. A., Gordon, T. D., and Robinson, A. L.: Primary to secondary organic aerosol:
1541 evolution of organic emissions from mobile combustion sources, Atmos. Chem. Phys., 14, 5015-
1542 5036, 10.5194/acp-14-5015-2014, 2014.
1543

1544 Raatikainen, T., Vaattovaara, P., Tiitta, P., Miettinen, P., Rautiainen, J., Ehn, M., Kulmala, M.,
1545 Laaksonen, A., and Worsnop, D. R.: Physicochemical properties and origin of organic groups
1546 detected in boreal forest using an aerosol mass spectrometer, Atmos. Chem. Phys., 10, 2063-
1547 2077, 10.5194/acp-10-2063-2010, 2010.
1548

1549 Robinson, A. L., Donahue, N. M., Shrivastava, M. K., Weitkamp, E. A., Sage, A. M., Grieshop,
1550 A. P., Lane, T. E., Pierce, J. R., and Pandis, S. N.: Rethinking organic aerosols: Semivolatile
1551 emissions and photochemical aging, Science, 315, 1259-1262, DOI 10.1126/science.1133061,
1552 2007.
1553

1554 Robinson, N. H., Hamilton, J. F., Allan, J. D., Langford, B., Oram, D. E., Chen, Q., Docherty, K.,
1555 Farmer, D. K., Jimenez, J. L., Ward, M. W., Hewitt, C. N., Barley, M. H., Jenkin, M. E., Rickard,
1556 A. R., Martin, S. T., McFiggans, G., and Coe, H.: Evidence for a significant proportion of
1557 Secondary Organic Aerosol from isoprene above a maritime tropical forest, Atmos Chem Phys,
1558 11, 1039-1050, DOI 10.5194/acp-11-1039-2011, 2011a.
1559

1560 Robinson, N. H., Newton, H. M., Allan, J. D., Irwin, M., Hamilton, J. F., Flynn, M., Bower, K.
1561 N., Williams, P. I., Mills, G., Reeves, C. E., McFiggans, G., and Coe, H.: Source attribution of
1562 Bornean air masses by back trajectory analysis during the OP3 project, Atmos. Chem. Phys., 11,
1563 9605-9630, 10.5194/acp-11-9605-2011, 2011b.
1564

1565 Rollins, A. W., Fry, J. L., Hunter, J. F., Kroll, J. H., Worsnop, D. R., Singaram, S. W., and
1566 Cohen, R. C.: Elemental analysis of aerosol organic nitrates with electron ionization high-
1567 resolution mass spectrometry, Atmos Meas Tech, 3, 301-310, 2010.
1568

1569 Rollins, A. W., Browne, E. C., Min, K.-E., Pusede, S. E., Wooldridge, P. J., Gentner, D. R.,
1570 Goldstein, A. H., Liu, S., Day, D. A., Russell, L. M., and Cohen, R. C.: Evidence for NOx
1571 Control over Nighttime SOA Formation, Science, 337, 1210-1212, 10.1126/science.1221520,
1572 2012.
1573 Russell, A., Holmes, H., Friberg, M., Ivey, C., Hu, Y., Balachandran, S., Mulholland, J., Tolbert,
1574 P., Sarnat, J., Sarnat, S., Strickland, M., Chang, H., and Liu, Y.: Use of Air Quality Modeling

Results in Health Effects Research, in: Air Pollution Modeling and its Application XXIII, edited by: Steyn, D., and Mathur, R., Springer Proceedings in Complexity, Springer International Publishing, 1-5, 2014.

Sato, K., Takami, A., Isozaki, T., Hikida, T., Shimono, A., and Imamura, T.: Mass spectrometric study of secondary organic aerosol formed from the photo-oxidation of aromatic hydrocarbons, Atmospheric Environment, 44, 1080-1087, dx.doi.org/10.1016/j.atmosenv.2009.12.013, 2010.

Schichtel, B. A., Malm, W. C., Bench, G., Fallon, S., McDade, C. E., Chow, J. C., and Watson, J. G.: Fossil and contemporary fine particulate carbon fractions at 12 rural and urban sites in the United States, Journal of Geophysical Research: Atmospheres, 113, D02311, 10.1029/2007JD008605, 2008.

Schneider, J., Weimer, S., Drewnick, F., Borrmann, S., Helas, G., Gwaze, P., Schmid, O., Andreae, M. O., and Kirchner, U.: Mass spectrometric analysis and aerodynamic properties of various types of combustion-related aerosol particles, Int J Mass Spectrom, 258, 37-49, dx.doi.org/10.1016/j.ijms.2006.07.008, 2006.

Setyan, A., Zhang, Q., Merkel, M., Knighton, W. B., Sun, Y., Song, C., Shilling, J. E., Onasch, T. B., Herndon, S. C., Worsnop, D. R., Fast, J. D., Zaveri, R. A., Berg, L. K., Wiedensohler, A., Flowers, B. A., Dubey, M. K., and Subramanian, R.: Characterization of submicron particles influenced by mixed biogenic and anthropogenic emissions using high-resolution aerosol mass spectrometry: results from CARES, Atmos Chem Phys, 12, 8131-8156, DOI 10.5194/acp-12-8131-2012, 2012.

Slowik, J. G., Vlasenko, A., McGuire, M., Evans, G. J., and Abbatt, J. P. D.: Simultaneous factor analysis of organic particle and gas mass spectra: AMS and PTR-MS measurements at an urban site, Atmos Chem Phys, 10, 1969-1988, 2010.

Slowik, J. G., Brook, J., Chang, R. Y. W., Evans, G. J., Hayden, K., Jeong, C. H., Li, S. M., Liggio, J., Liu, P. S. K., McGuire, M., Mihele, C., Sjostedt, S., Vlasenko, A., and Abbatt, J. P. D.: Photochemical processing of organic aerosol at nearby continental sites: contrast between urban plumes and regional aerosol, Atmos Chem Phys, 11, 2991-3006, DOI 10.5194/acp-11-2991-2011, 2011.

Sun, Y. L., Zhang, Q., Schwab, J. J., Chen, W. N., Bae, M. S., Hung, H. M., Lin, Y. C., Ng, N. L., Jayne, J., Massoli, P., Williams, L. R., and Demerjian, K. L.: Characterization of near-highway submicron aerosols in New York City with a high-resolution aerosol mass spectrometer, Atmos. Chem. Phys., 12, 2215-2227, 10.5194/acp-12-2215-2012, 2012a.

1615 Sun, Y. L., Zhang, Q., Schwab, J. J., Yang, T., Ng, N. L., and Demerjian, K. L.: Factor analysis
1616 of combined organic and inorganic aerosol mass spectra from high resolution aerosol mass
1617 spectrometer measurements, Atmos. Chem. Phys., 12, 8537-8551, 10.5194/acp-12-8537-2012,
1618 2012b.
1619

1620 Surratt, J. D., Lewandowski, M., Offenberg, J. H., Jaoui, M., Kleindienst, T. E., Edney, E. O.,
1621 and Seinfeld, J. H.: Effect of acidity on secondary organic aerosol formation from isoprene,
1622 Environ Sci Technol, 41, 5363-5369, Doi 10.1021/Es0704176, 2007.
1623

1624 Tsigaridis, K., Daskalakis, N., Kanakidou, M., Adams, P. J., Artaxo, P., Bahadur, R., Balkanski,
1625 Y., Bauer, S. E., Bellouin, N., Benedetti, A., Bergman, T., Berntsen, T. K., Beukes, J. P., Bian,
1626 H., Carslaw, K. S., Chin, M., Curci, G., Diehl, T., Easter, R. C., Ghan, S. J., Gong, S. L., Hodzic,
1627 A., Hoyle, C. R., Iversen, T., Jathar, S., Jimenez, J. L., Kaiser, J. W., Kirkevåg, A., Koch, D.,
1628 Kokkola, H., Lee, Y. H., Lin, G., Liu, X., Luo, G., Ma, X., Mann, G. W., Mihalopoulos, N.,
1629 Morcrette, J. J., Müller, J. F., Myhre, G., Myriokefalitakis, S., Ng, N. L., O'Donnell, D., Penner,
1630 J. E., Pozzoli, L., Pringle, K. J., Russell, L. M., Schulz, M., Sciare, J., Seland, Ø., Shindell, D. T.,
1631 Sillman, S., Skeie, R. B., Spracklen, D., Stavrakou, T., Steenrod, S. D., Takemura, T., Tiitta, P.,
1632 Tilmes, S., Tost, H., van Noije, T., van Zyl, P. G., von Salzen, K., Yu, F., Wang, Z., Wang, Z.,
1633 Zaveri, R. A., Zhang, H., Zhang, K., Zhang, Q., and Zhang, X.: The AeroCom evaluation and
1634 intercomparison of organic aerosol in global models, Atmos. Chem. Phys., 14, 10845-10895,
1635 10.5194/acp-14-10845-2014, 2014.
1636

1637 Ulbrich, I. M., Canagaratna, M. R., Zhang, Q., Worsnop, D. R., and Jimenez, J. L.: Interpretation
1638 of organic components from Positive Matrix Factorization of aerosol mass spectrometric data,
1639 Atmos. Chem. Phys., 9, 2891-2918, 10.5194/acp-9-2891-2009, 2009.
1640

1641 Verma, V., Fang, T., Guo, H., King, L., Bates, J. T., Peltier, R. E., Edgerton, E., Russell, A. G.,
1642 and Weber, R. J.: Reactive oxygen species associated with water-soluble PM2.5 in the
1643 southeastern United States: spatiotemporal trends and source apportionment, Atmos. Chem.
1644 Phys., 14, 12915-12930, 10.5194/acp-14-12915-2014, 2014.
1645

1646 Verma, V., Fang, T., Xu, L., Peltier, R. E., Russell, A. G., Ng, N. L., and Weber, R. J.: Organic
1647 Aerosols Associated with the Generation of Reactive Oxygen Species (ROS) by Water-Soluble
1648 PM2.5, Environ Sci Technol, 10.1021/es505577w, 2015.
1649

1650 Virkkula, A., Mäkelä, T., Hillamo, R., Yli-Tuomi, T., Hirsikko, A., Hämeri, K., and Koponen, I.
1651 K.: A Simple Procedure for Correcting Loading Effects of Aethalometer Data, J Air Waste
1652 Manage, 57, 1214-1222, 10.3155/1047-3289.57.10.1214, 2007.
1653

1654 Visser, S., Slowik, J. G., Furger, M., Zotter, P., Bukowiecki, N., Canonaco, F., Flechsig, U.,
1655 Appel, K., Green, D. C., Tremper, A. H., Young, D. E., Williams, P. I., Allan, J. D., Coe, H.,

1656 Williams, L. R., Mohr, C., Xu, L., Ng, N. L., Nemitz, E., Barlow, J. F., Halios, C. H., Fleming, Z.
1657 L., Baltensperger, U., and Prévôt, A. S. H.: Advanced source apportionment of size-resolved
1658 trace elements at multiple sites in London during winter, Atmos. Chem. Phys. Discuss., 15,
1659 14733-14781, 10.5194/acpd-15-14733-2015, 2015.
1660

1661 Washenfelder, R. A., Attwood, A. R., Brock, C. A., Guo, H., Xu, L., Weber, R. J., Ng, N. L.,
1662 Allen, H. M., Ayres, B. R., Baumann, K., Cohen, R. C., Draper, D. C., Duffey, K. C., Edgerton,
1663 E., Fry, J. L., Hu, W. W., Jimenez, J. L., Palm, B. B., Romer, P., Stone, E. A., Wooldridge, P. J.,
1664 and Brown, S. S.: Biomass burning dominates brown carbon absorption in the rural southeastern
1665 United States, Geophysical Research Letters, 2014GL062444, 10.1002/2014GL062444, 2015.
1666

1667 Weber, R.: Short-Term Temporal Variation in PM2.5 Mass and Chemical Composition during
1668 the Atlanta Supersite Experiment, 1999, J Air Waste Manage, 53, 84-91,
1669 10.1080/10473289.2003.10466123, 2003.
1670

1671 Weber, R., Orsini, D., Duan, Y., Baumann, K., Kiang, C. S., Chameides, W., Lee, Y. N.,
1672 Brechtel, F., Klotz, P., Jongejan, P., ten Brink, H., Slanina, J., Boring, C. B., Genfa, Z., Dasgupta,
1673 P., Hering, S., Stolzenburg, M., Dutcher, D. D., Edgerton, E., Hartsell, B., Solomon, P., and
1674 Tanner, R.: Intercomparison of near real time monitors of PM2.5 nitrate and sulfate at the U.S.
1675 Environmental Protection Agency Atlanta Supersite, Journal of Geophysical Research:
1676 Atmospheres, 108, 8421, 10.1029/2001JD001220, 2003.
1677

1678 Weber, R. J., Orsini, D., Daun, Y., Lee, Y. N., Klotz, P. J., and Brechtel, F.: A particle-into-
1679 liquid collector for rapid measurement of aerosol bulk chemical composition, Aerosol Sci Tech,
1680 35, 718-727, Doi 10.1080/02786820152546761, 2001.
1681

1682 Weber, R. J., Sullivan, A. P., Peltier, R. E., Russell, A., Yan, B., Zheng, M., de Gouw, J.,
1683 Warneke, C., Brock, C., Holloway, J. S., Atlas, E. L., and Edgerton, E.: A study of secondary
1684 organic aerosol formation in the anthropogenic-influenced southeastern United States, J Geophys
1685 Res-Atmos, 112, Artn D13302 Doi 10.1029/2007jd008408, 2007.
1686

1687 Winquist, A., Kirrane, E., Klein, M., Strickland, M., Darrow, L. A., Sarnat, S. E., Gass, K.,
1688 Mulholland, J., Russell, A., and Tolbert, P.: Joint Effects of Ambient Air Pollutants on Pediatric
1689 Asthma Emergency Department Visits in Atlanta, 1998–2004, Epidemiology, 25, 666-673,
1690 10.1097/ede.0000000000000146, 2014.
1691

1692 Xu, L., Kollman, M. S., Song, C., Shilling, J. E., and Ng, N. L.: Effects of NOx on the Volatility
1693 of Secondary Organic Aerosol from Isoprene Photooxidation, Environ Sci Technol, 48, 2253-
1694 2262, 10.1021/es404842g, 2014.
1695

Xu, L., Guo, H., Boyd, C. M., Klein, M., Bougiatioti, A., Cerully, K. M., Hite, J. R., Isaacman-VanWertz, G., Kreisberg, N. M., Knote, C., Olson, K., Koss, A., Goldstein, A. H., Hering, S. V., de Gouw, J., Baumann, K., Lee, S.-H., Nenes, A., Weber, R. J., and Ng, N. L.: Effects of anthropogenic emissions on aerosol formation from isoprene and monoterpenes in the southeastern United States, Proceedings of the National Academy of Sciences, 112, 37-42, 10.1073/pnas.1417609112, 2015.

Zhang, Q., Alfarra, M. R., Worsnop, D. R., Allan, J. D., Coe, H., Canagaratna, M. R., and Jimenez, J. L.: Deconvolution and Quantification of Hydrocarbon-like and Oxygenated Organic Aerosols Based on Aerosol Mass Spectrometry, Environ Sci Technol, 39, 4938-4952, 10.1021/es048568l, 2005.

Zhang, Q., Jimenez, J. L., Canagaratna, M. R., Ulbrich, I. M., Ng, N. L., Worsnop, D. R., and Sun, Y. L.: Understanding atmospheric organic aerosols via factor analysis of aerosol mass spectrometry: a review, Anal Bioanal Chem, 401, 3045-3067, DOI 10.1007/s00216-011-5355-y, 2011.

Zhang, X., Hecobian, A., Zheng, M., Frank, N. H., and Weber, R. J.: Biomass burning impact on PM 2.5 over the southeastern US during 2007: integrating chemically speciated FRM filter measurements, MODIS fire counts and PMF analysis, Atmos. Chem. Phys., 10, 6839-6853, 10.5194/acp-10-6839-2010, 2010.

Zhang, X., Liu, Z., Hecobian, A., Zheng, M., Frank, N. H., Edgerton, E. S., and Weber, R. J.: Spatial and seasonal variations of fine particle water-soluble organic carbon (WSOC) over the southeastern United States: implications for secondary organic aerosol formation, Atmos. Chem. Phys., 12, 6593-6607, 10.5194/acp-12-6593-2012, 2012.

Zhao, R., Mungall, E. L., Lee, A. K. Y., Aljawhary, D., and Abbatt, J. P. D.: Aqueous-phase photooxidation of levoglucosan – a mechanistic study using aerosol time-of-flight chemical ionization mass spectrometry (Aerosol ToF-CIMS), Atmos. Chem. Phys., 14, 9695-9706, 10.5194/acp-14-9695-2014, 2014.

Zheng, M., Cass, G. R., Schauer, J. J., and Edgerton, E. S.: Source Apportionment of PM2.5 in the Southeastern United States Using Solvent-Extractable Organic Compounds as Tracers, Environ Sci Technol, 36, 2361-2371, 10.1021/es011275x, 2002.

Zheng, M., Ke, L., Edgerton, E. S., Schauer, J. J., Dong, M., and Russell, A. G.: Spatial distribution of carbonaceous aerosol in the southeastern United States using molecular markers and carbon isotope data, Journal of Geophysical Research: Atmospheres, 111, D10S06, 10.1029/2005JD006777, 2006.

Zotter, P., El-Haddad, I., Zhang, Y., Hayes, P. L., Zhang, X., Lin, Y.-H., Wacker, L., Schnelle-Kreis, J., Abbaszade, G., Zimmermann, R., Surratt, J. D., Weber, R., Jimenez, J. L., Szidat, S., Baltensperger, U., and Prévôt, A. S. H.: Diurnal cycle of fossil and nonfossil carbon using radiocarbon analyses during CalNex, Journal of Geophysical Research: Atmospheres, 119, 2013JD021114, 10.1002/2013JD021114, 2014.

Table Captions

Table 1: Sampling sites and periods for the SCAPE and SOAS studies. Campaign average meteorological conditions, mixing ratios of gas-phase species, and mass concentrations of black carbon and NR-PM_1 species for all datasets. Average ± one standard deviation are reported.

Table 2: A summary of organic nitrates estimation from NO_x^+ ratio method. R_{AN} represents the NO_x^+ ratio (=NO^+/NO_2^+) for pure ammonium nitrate (AN). R_{meas} represents the NO_x^+ ratio from observation. $NO_{3,meas}$ represents the total nitrate functionality (from both organic and inorganic nitrates) as measured by the HR-ToF-AMS. $NO_{3,org}$ represents the nitrate functionality from organic nitrates, which is estimated from the NO_x^+ ratio method. ON and OA represent organic nitrate and organic aerosol, respectively.

1777 Table 1.

AMS sampling site		Jefferson Street	Centreville	Yorkville	Georgia Tech	Jefferson Street	Yorkville	Roadside
Sampling period		5/10/2012 - 6/2/2012	6/1/2013- 7/15/2013	6/26/2012 - 7/20/2012	7/20/2012 - 9/4/2012	11/6/2012 - 12/4/2012	12/5/2012 - 1/10/2013	1/26/2013 - 2/28/2013
Abbreviation		JST_May	CTR_June	YRK_July	GT_Aug	JST_Nov	YRK_Dec	RS_Jan
Met[a]	T (°C)[b]	23.0 ± 4.3	24.7 ± 4.3	26.9 ± 4.5	26.1 ± 3.5	11.3 ± 5.0	7.8 ± 5.5	8.1 ± 4.8
	RH(%)	65.8 ± 19.3	82.9 ± 15.3	61.9 ± 18.5	71.2 ± 17.2	64.5 ± 20.6	74.2 ± 20.1	64.6 ± 25.3
	WS ($m\ s^{-1}$)	1.6 ± 1.1	1.9 ± 0.9	2.3 ± 1.1	1.3 ± 0.8	1.3 ± 0.9	3.4 ± 1.7	2.1 ± 1.4
Gas (ppb)	NO	4.1 ± 13.0	0.1 ± 0.2	0.1 ± 0.1	N/A	32.1 ± 60.2	0.3 ± 0.8	N/A
	NO_2	10.3 ± 10.3	0.6 ± 0.6	1.1 ± 0.8	N/A	18.4 ± 12.8	3.0 ± 3.0	N/A
	SO_2	0.4 ± 0.7	0.3 ± 0.7	0.4 ± 0.5	N/A	1.2 ± 1.7	0.6 ± 1.1	N/A
	O_3	39.0 ± 21.9	26.4 ± 12.4	41.1 ± 17.0	N/A	18.8 ± 14.5	28.8 ± 8.3	N/A
$PM_{2.5}$ ($\mu g\ m^{-3}$)	BC[c]	N/A	0.2 ± 0.2	N/A	0.9 ± 0.7	0.9 ± 1.0	0.4 ± 0.3	1.3 ± 1.0
NR-PM_1 ($\mu g\ m^{-3}$)	SO_4	3.0 ± 1.5	1.9 ± 1.4	3.5 ± 1.8	4.0 ± 2.1	1.7 ± 0.9	1.4 ± 1.0	1.6 ± 1.2
	NO_3	0.4 ± 0.3	0.1 ± 0.1	0.3 ± 0.2	0.4 ± 0.4	1.2 ± 1.1	0.8 ± 0.8	1.4 ± 1.3
	NH_4	1.1 ± 0.5	0.4 ± 0.3	1.1 ± 0.5	1.2 ± 0.6	0.9 ± 0.6	0.6 ± 0.5	0.9 ± 0.6
	Chl	0.03 ± 0.03	0.01 ± 0.01	0.03 ± 0.03	0.02 ± 0.01	0.06 ± 0.07	0.04 ± 0.07	0.06 ± 0.11
	Org	9.1 ± 4.3	5.0 ± 4.0	11.2 ± 6.4	9.6 ± 4.4	7.9 ± 5.1	3.2 ± 2.3	4.7 ± 3.6

1778

1779 [a] Meteorological data at JST and YRK are recorded by Atmospheric Research & Analysis (ARA). Meteorological data at GT and RS
1780 are from JST during the same periods.

1781 [b] The numbers reported in the table are campaign-averaged values based on high temporal resolution data (1 - 60min depending on
1782 instrument).

1783 [c] Black carbon concentration was measured by a seven-wavelength Aethalometer at GT_Aug and JST_Nov and by a multi-angle
1784 absorption photometer (MAAP) at CTR_June, YRK_Dec, and RS_Jan.

1785 Table 2.

Site	R_{AN}[a]	R_{meas}	R with LO-OOA		$NO_{3,org}$ conc. ($\mu g\ m^{-3}$)[d]		$NO_{3,org}/NO_{3,meas}$		ON/OA[e]	
			$NO_{3,meas}$	$NO_{3,org}$[b]	lower	upper	lower	upper	lower	upper
JST_May	1.73	4.47	0.68	0.78	0.19	0.27	0.55	0.76	0.07	0.14
CTR_June[c]	2.93	7.10	0.76	0.84	0.06	0.08	0.80	1.00	0.06	0.10
YRK_July	2.24	5.45	0.66	0.83	0.18	0.28	0.63	1.00	0.05	0.12
GT_Aug	2.26	6.17	0.56	0.70	0.21	0.33	0.64	0.99	0.07	0.16
JST_Nov	1.95	3.12	0.14	0.63	0.23	0.25	0.19	0.21	0.09	0.15
YRK_Dec	2.24	3.16	0.29	0.08	0.09	0.16	0.11	0.21	0.09	0.25
RS_Jan	2.62	2.78	0.46	-0.22	0.13	0.13	0.10	0.10	0.09	0.13

1786

1787 [a] R_{AN} is determined from IE calibrations at each site.

1788 [b] The Pearson's correlation coefficient (R) between LO-OOA and $NO_{3,org}$ are obtained by using
1789 $R_{ON} = 10$ in the NO_x^+ ratio method.

1790 [c] For CTR_June, only 6/24 - 7/15 data are reported in order to compare with results from AMS-
1791 IC method where a PM_1 cyclone was used.

1792 [d] For CTR_June and YRK_July, the NO_x^+ ratio method with $R_{ON} = 10$ and PMF method define
1793 the lower and upper bound for $NO_{3,org}$, respectively; for JST_Nov, YRK_Dec, the PMF method
1794 and NO_x^+ ratio method with $R_{ON} = 10$ define the lower and upper bound, respectively; for
1795 RS_Jan, the PMF method defines both the lower and upper bound; for JST_May and GT_Aug,
1796 the NO_x^+ ratio method with $R_{ON} = 10$ and 5 defines the lower and upper bound, respectively.

1797 [e] The lower and upper bounds correspond to an assumed MW of organic nitrates of 200 and 300
1798 g mol^{-1}.

1799

1800
1801
1802
1803
1804
1805
1806
1807
1808
1809
1810
1811
1812

Figure Captions

Figure 1: Sampling sites for SCAPE and SOAS studies. The gray circled region represents urban Atlanta.

Figure 2: Mass concentrations (a) and mass fractions (b) of non-refractory PM_1 (NR-PM_1) species measured by HR-ToF-AMS.

Figure 3: Diurnal profiles of non-refractory PM_1 (NR-PM_1) species measured by HR-ToF-AMS. Panel (d) shows the diurnal profiles of NR-PM_1 species after multiplying by the boundary layer height for the Centreville (CTR) site. The solid lines indicate the median concentration and the error bars indicate the standard error.

Figure 4: (a) f_{44} vs. f_{43} for total OA and OA factors resolved from PMF analysis. (b) The oxidation state of OA factors.

Figure 5: Diurnal profiles of OA factors resolved from PMF analysis on organic mass spectra. Panel (d) shows the diurnal profiles of OA factors after multiplying by the boundary layer height for the Centreville (CTR) site. The solid lines indicate the median concentration and the error bars indicate the standard error.

Figure 6: (a) Campaign-averaged mass concentrations of OA factors resolved from PMF analysis on organic mass spectra. (b) Campaign-averaged mass fractions of OA factors resolved from PMF analysis on organic mass spectra. SOA is the sum of Isoprene-OA, MO-OOA, and LO-OOA. POA is the sum of HOA, COA, and BBOA.

Figure 7: Scatter plot (left panel) and the time series (right panel) of BBOA and brown carbon light absorption for the datasets where a BBOA factor was resolved.

Figure 8: Scatter plot (left panel) and the time series (right panel) of MO-OOA and ozone.

Figure 9: Scatter plot of LO-OOA vs. the total measured nitrates (i.e., $NO_{3,meas}$) and LO-OOA vs. estimated concentration of "nitrate funcionality from organic nitrates" (i.e., $NO_{3,org}$) by using R_{ON} = 10 in the NO_x^+ ratio metod.

Figure 10. (a) Concentrations of total measured NO_3 (i.e., $NO_{3,meas}$), estimated "nitrate functionality from organic nitrates" (i.e., $NO_{3,org}$) by the NO_x^+ ratio method and the PMF method. (b) The contribution of $NO_{3,org}$ to $NO_{3,meas}$ (i.e., $NO_{3,org}/NO_{3,meas}$) from the NO_x^+ ratio method and the PMF method. Also shown are the estimated contribution of organic nitrates to total OA from the "best estimate" range of $NO_{3,org}$ and by assuming a MW of 200 and 300 g mol^{-1} for organic nitrates.

Figure 11. Comparion of estimated concentration of "nitrate functionality from organic nitrates" (i.e., $NO_{3,org}$) at the Centreville (CTR) site between the AMS-IC method and NO_x^+ ratio method with R_{ON} values of 5 and 10. The intercept and slope are obtained by orthogonal fit, which considers measurement errors in both dependent and independent variables. The correlation

coefficient R is obtained by linear least-squares fit. Intercepts are within the detection limit of PILS-IC nitrate (i.e., 0.03 μg m^{-3}). The 1:1 line is offset by the detection limit of PILS-IC nitrate (i.e., -0.03 μg m^{-3}) for visual clarity. The uncertainty of PILS-IC measurements is about 10% according to Weber et al. (2001).

Figure 12. Diurnal variation of $NO_{3,meas}$, $NO_{3,org}$, and $NO_{3,inorg}$ for all datasets. $NO_{3,org}$, and $NO_{3,inorg}$ are estimated by the NO_x^+ ratio method with an R_{ON} value of 10. The solid lines indicate the median concentration and the error bars indicate the standard error.

Figure 13. Correlation coefficients for NR-PM_1 species between ACSM measurements (stationary at the Georgia Tech site) and HR-ToF-AMS measuremens (rotating among different sites). Values are plotted vs. the relevant distance of the measurement site from the GT site, where the dotted lines represent the sampling sites where the HR-ToF-AMS measurements were made.

Figure 14. Diurnal variation of boundary layer height for CTR_June. The solid line indicates the median concentration and the error bars indicate the standard error.

Figure 15. Mean seasonal concentrations of organic carbon at the Jefferson Street (JST) and the Yorkville (YRK) sites. Summer: June – August. Winter: December – Februry.

Figure 16. The seasonality of the correlation between organic carbon and sulfate at the Jefferson Street (JST), Yorkville (YRK), and Centreville (CTR) sites. Seasons are by grouped by calendar months (Spring: March–May, Summer: June–August, Fall: September–November, and Winter: December–February).

1880 Fig. 1.

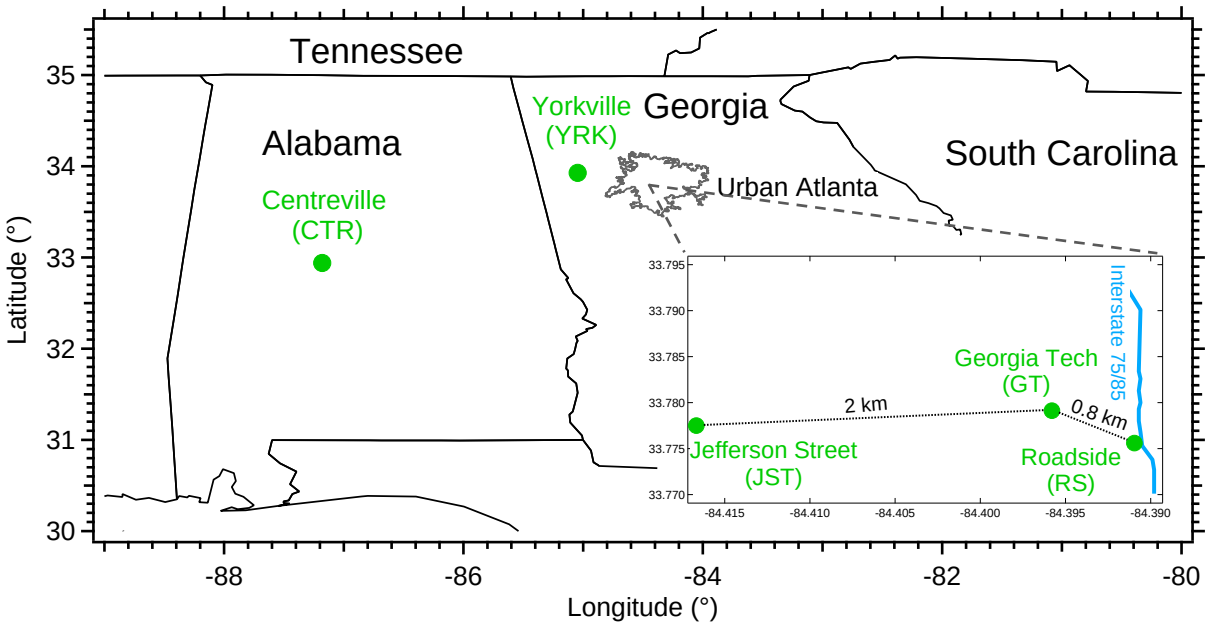

1881

1882

1883

1884

1885

1886

1887

1888

1889

1890

1891

1892

1893

1894

1895

1896

1897 Fig. 2.

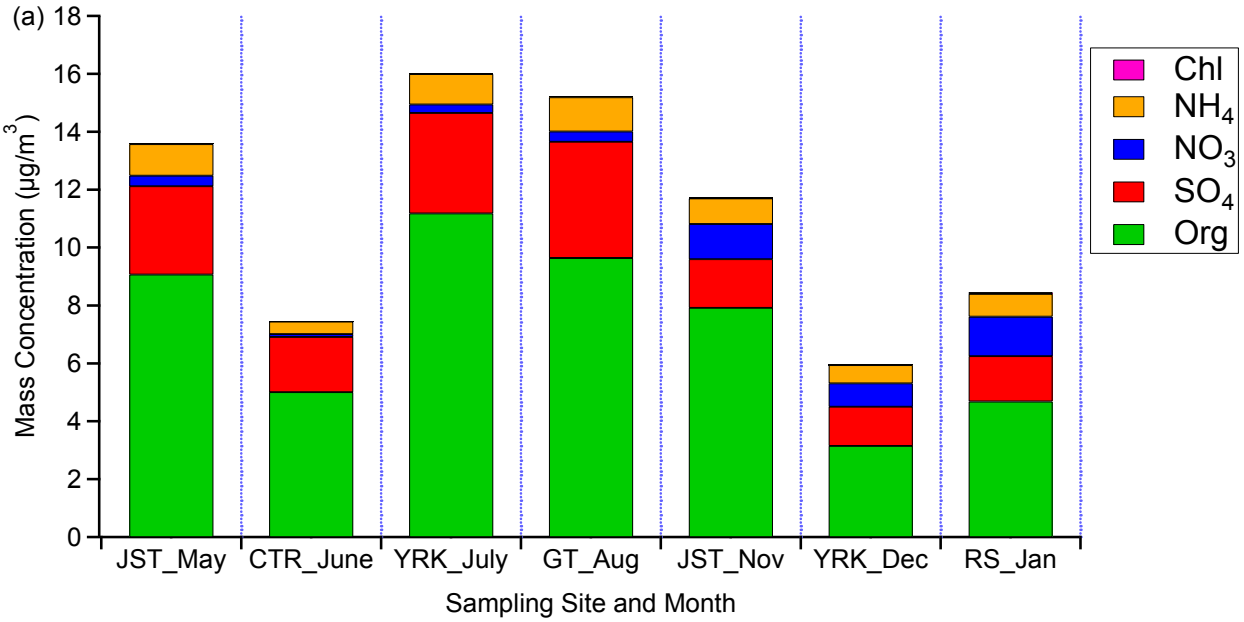

1898

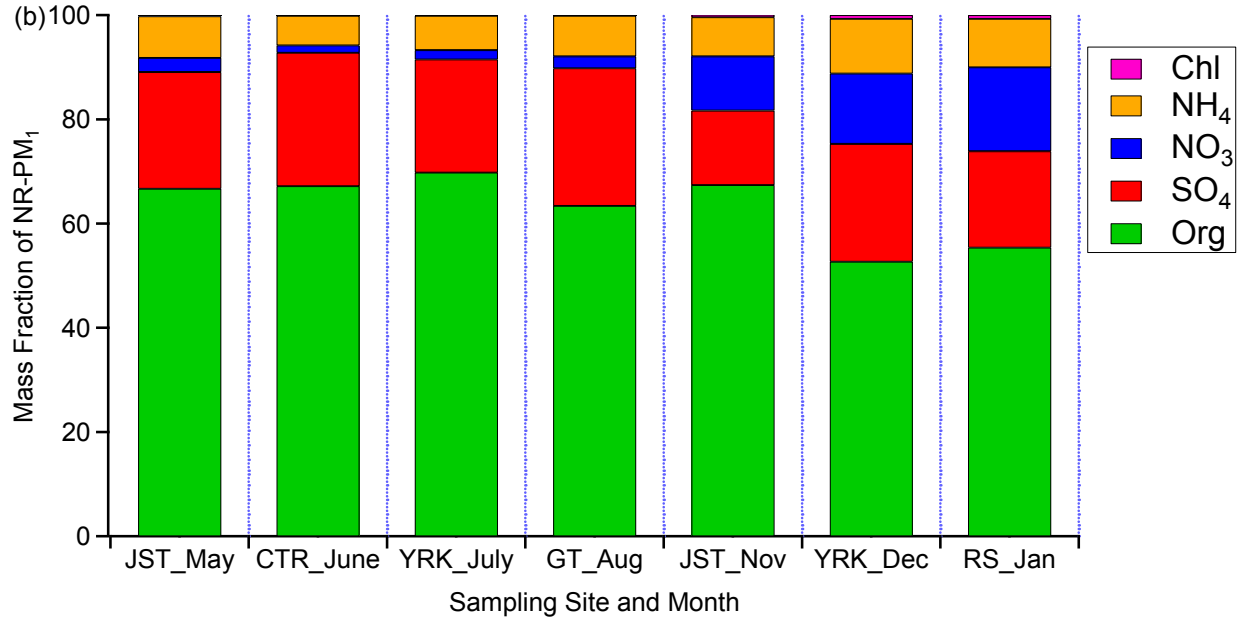

1899

1900

1901

1902

1903

1904

1905 Fig. 3.

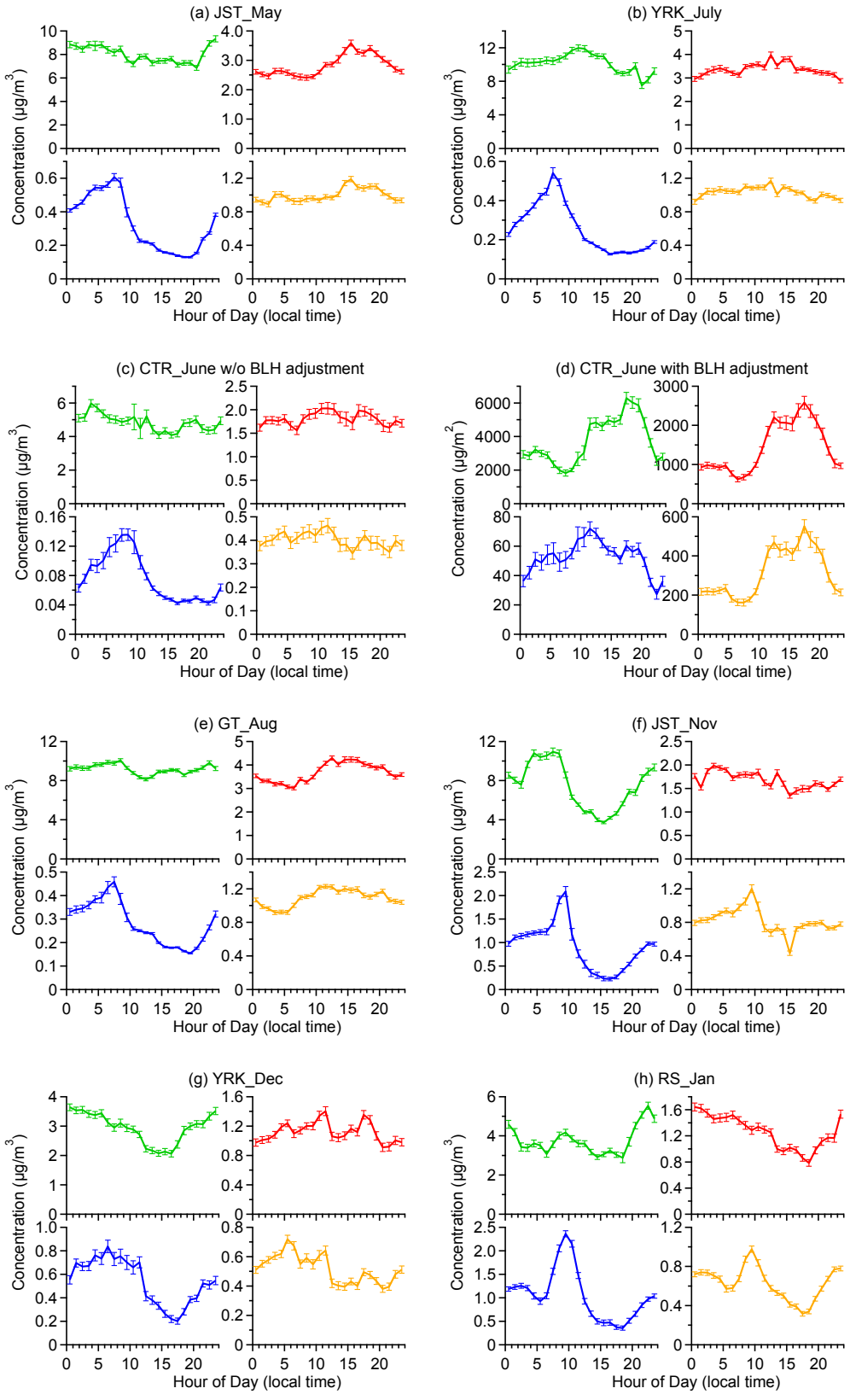

1906

1907

1908

1909

1910 Fig. 4.

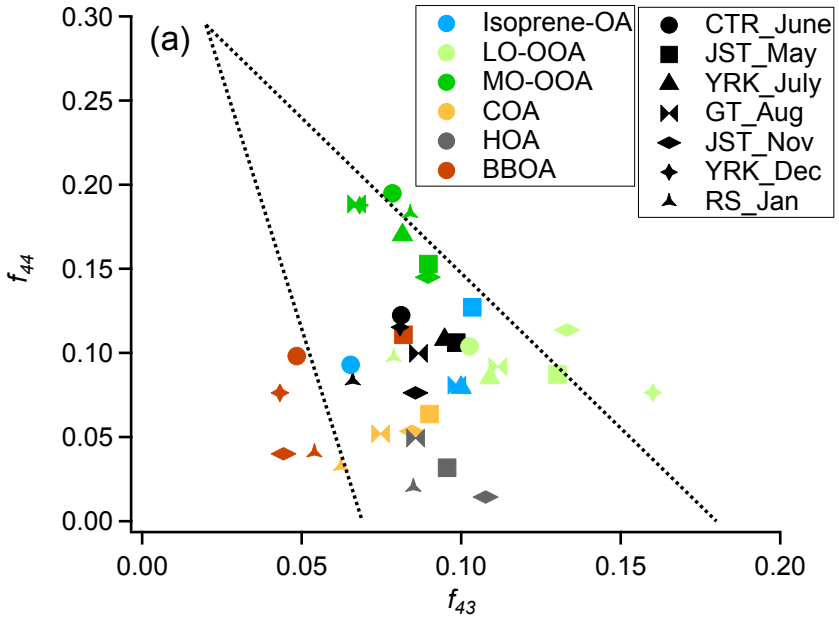

1911

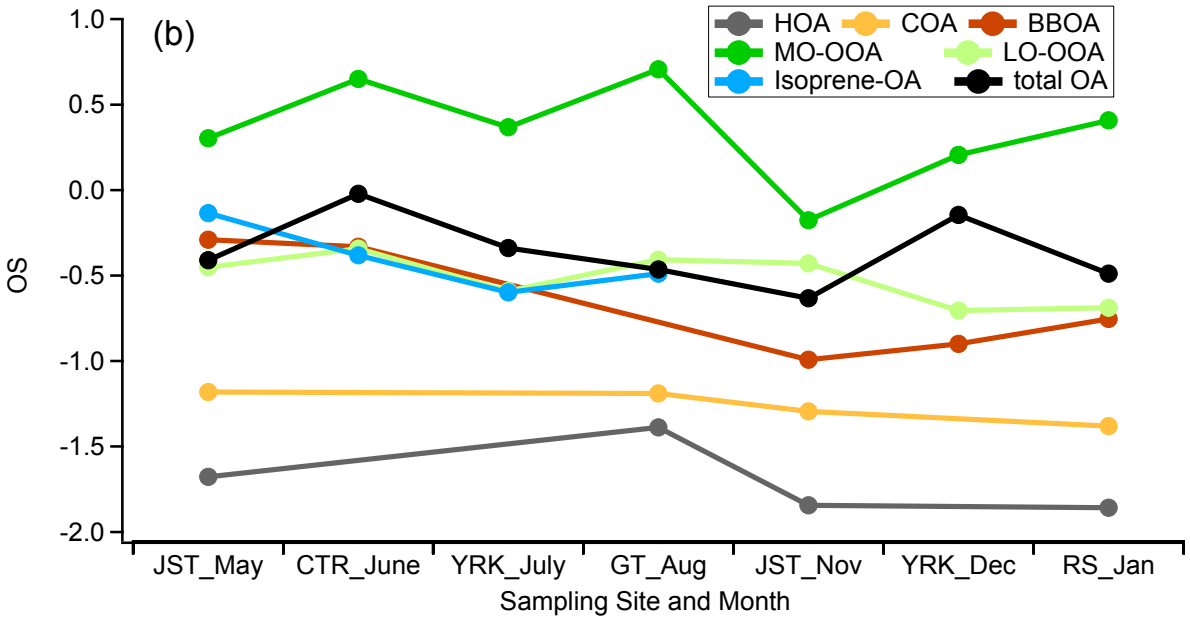

1912

1913

1914

1915

1916

1917

1918 Fig. 5.

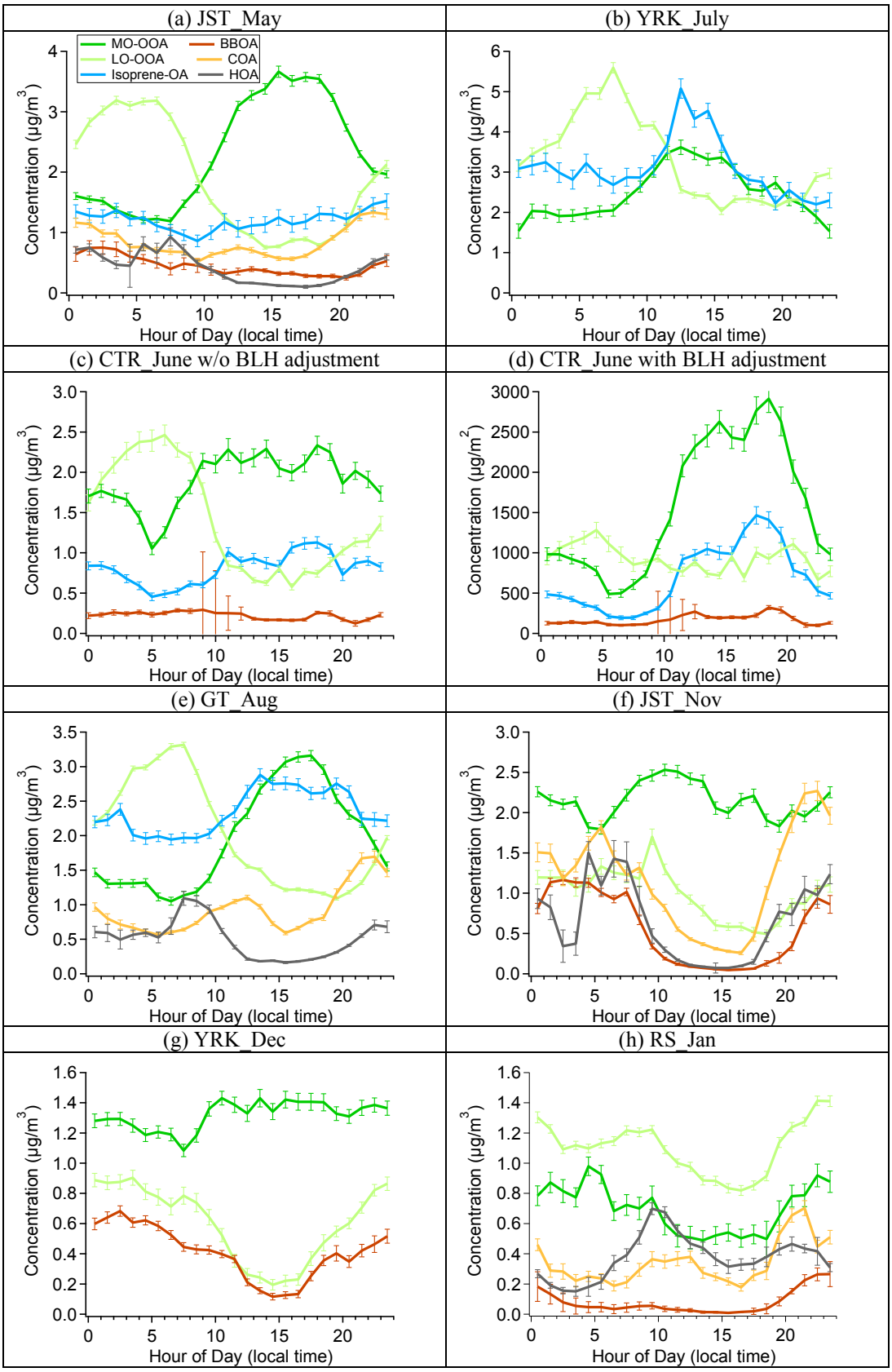
(a) JST_May
MO-OOA
LO-OOA
Isoprene-OA
BBOA
COA
HOA
Concentration (μg/m3)
Hour of Day (local time)
(b) YRK_July
Concentration (μg/m3)
Hour of Day (local time)
(c) CTR_June w/o BLH adjustment
Concentration (μg/m3)
Hour of Day (local time)
(d) CTR_June with BLH adjustment
Concentration (μg/m2)
Hour of Day (local time)
(e) GT_Aug
Concentration (μg/m3)
Hour of Day (local time)
(f) JST_Nov
Concentration (μg/m3)
Hour of Day (local time)
(g) YRK_Dec
Concentration (μg/m3)
Hour of Day (local time)
(h) RS_Jan
Concentration (μg/m3)
Hour of Day (local time)

1919 Fig. 6.

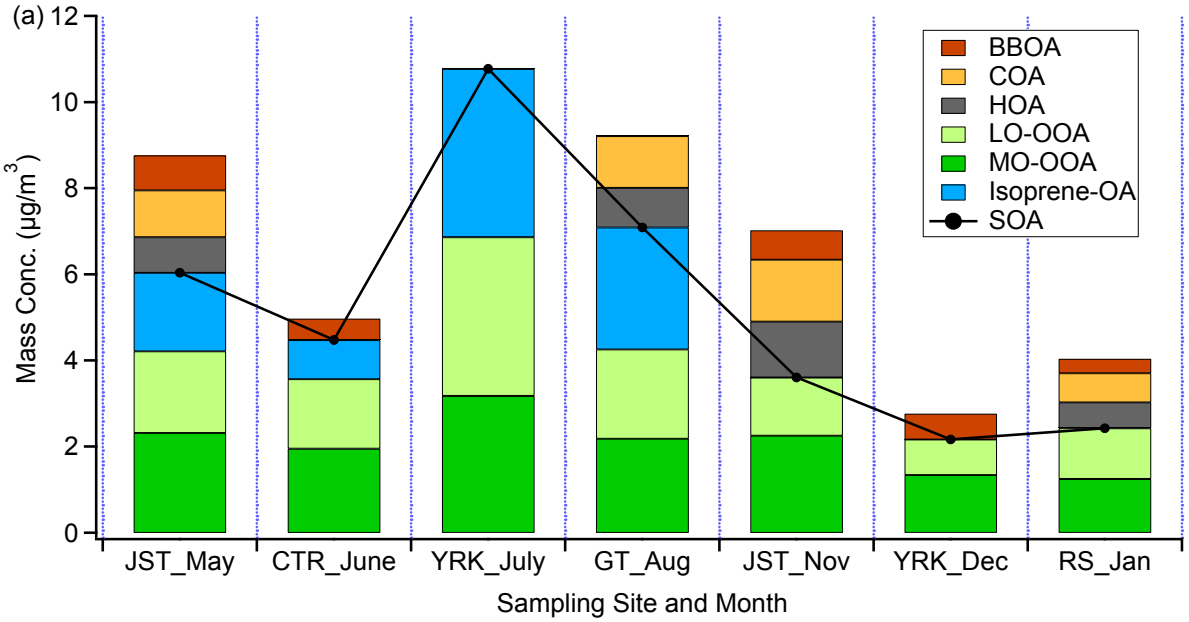

1920

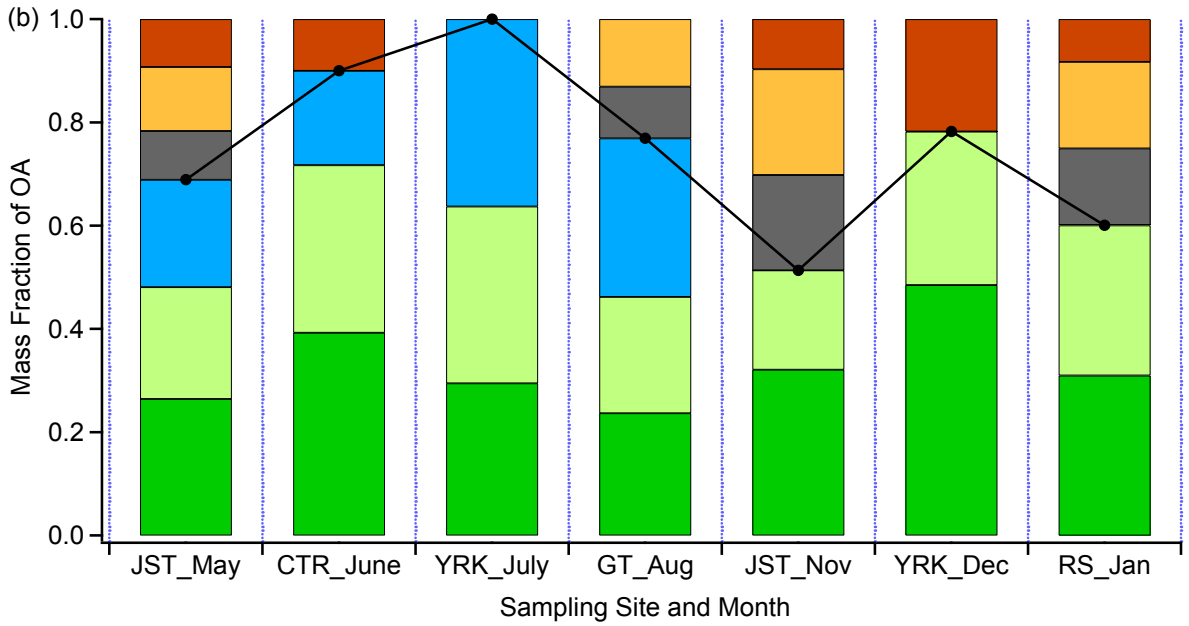

1921

1922

1923

1924

1925

1926

1927 Fig. 7.

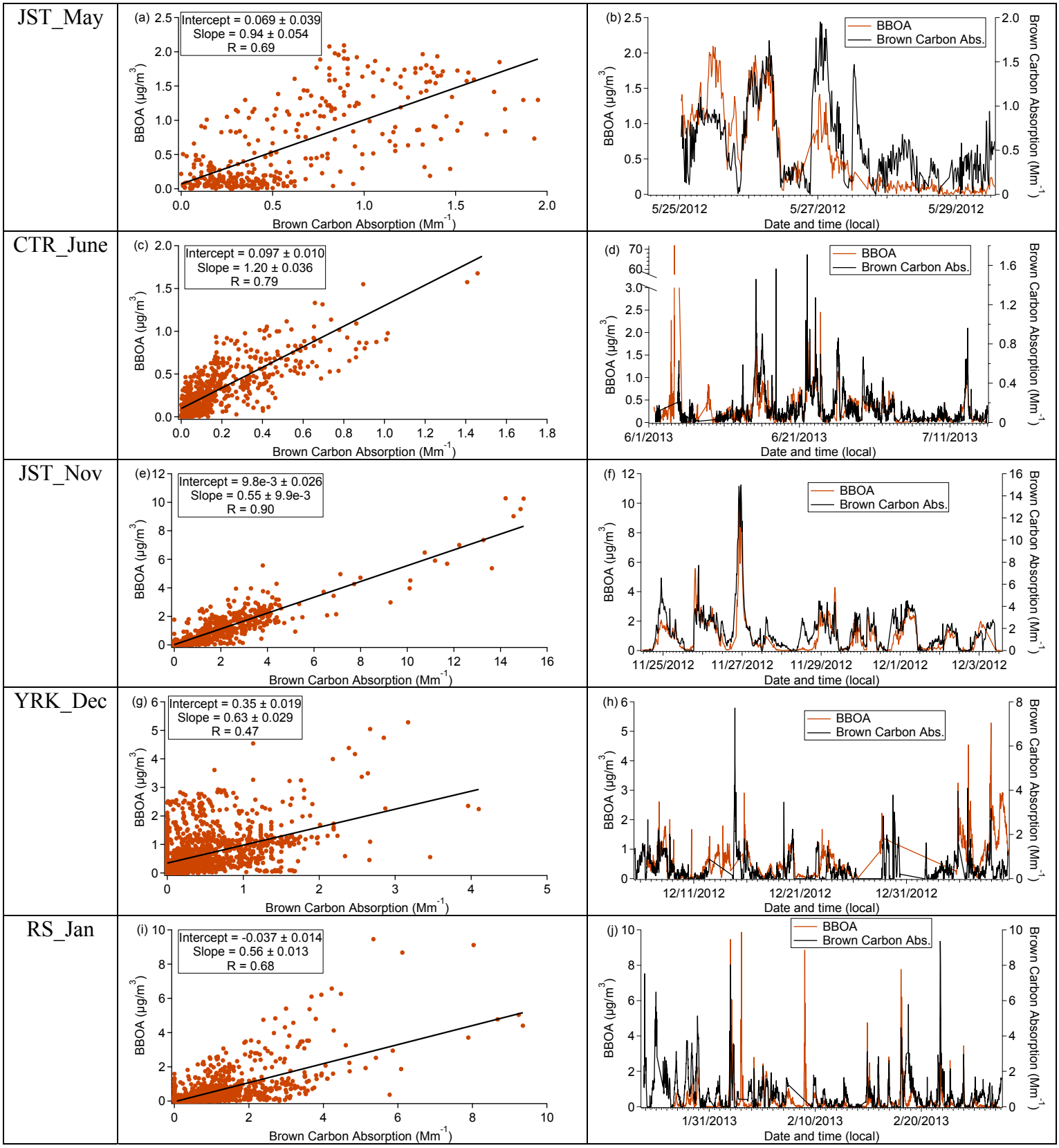
JST_May
CTR_June
JST_Nov
YRK_Dec
RS_Jan
(a)
Intercept = 0.069 ± 0.039
Slope = 0.94 ± 0.054
R = 0.69
BBOA (µg/m3)
Brown Carbon Absorption (Mm-1)
(b)
BBOA
Brown Carbon Abs.
BBOA (µg/m3)
Brown Carbon Absorption (Mm-1)
5/25/2012
5/27/2012
5/29/2012
Date and time (local)
(c)
Intercept = 0.097 ± 0.010
Slope = 1.20 ± 0.036
R = 0.79
BBOA (µg/m3)
Brown Carbon Absorption (Mm-1)
(d)
BBOA
Brown Carbon Abs.
BBOA (µg/m3)
Brown Carbon Absorption (Mm-1)
6/1/2013
6/21/2013
7/11/2013
Date and time (local)
(e)
Intercept = 9.8e-3 ± 0.026
Slope = 0.55 ± 9.9e-3
R = 0.90
BBOA (µg/m3)
Brown Carbon Absorption (Mm-1)
(f)
BBOA
Brown Carbon Abs.
BBOA (µg/m3)
Brown Carbon Absorption (Mm-1)
11/25/2012
11/27/2012
11/29/2012
12/1/2012
12/3/2012
Date and time (local)
(g)
Intercept = 0.35 ± 0.019
Slope = 0.63 ± 0.029
R = 0.47
BBOA (µg/m3)
Brown Carbon Absorption (Mm-1)
(h)
BBOA
Brown Carbon Abs.
BBOA (µg/m3)
Brown Carbon Absorption (Mm-1)
12/11/2012
12/21/2012
12/31/2012
Date and time (local)
(i)
Intercept = -0.037 ± 0.014
Slope = 0.56 ± 0.013
R = 0.68
BBOA (µg/m3)
Brown Carbon Absorption (Mm-1)
(j)
BBOA
Brown Carbon Abs.
BBOA (µg/m3)
Brown Carbon Absorption (Mm-1)
1/31/2013
2/10/2013
2/20/2013
Date and time (local)

1928 Fig. 8.

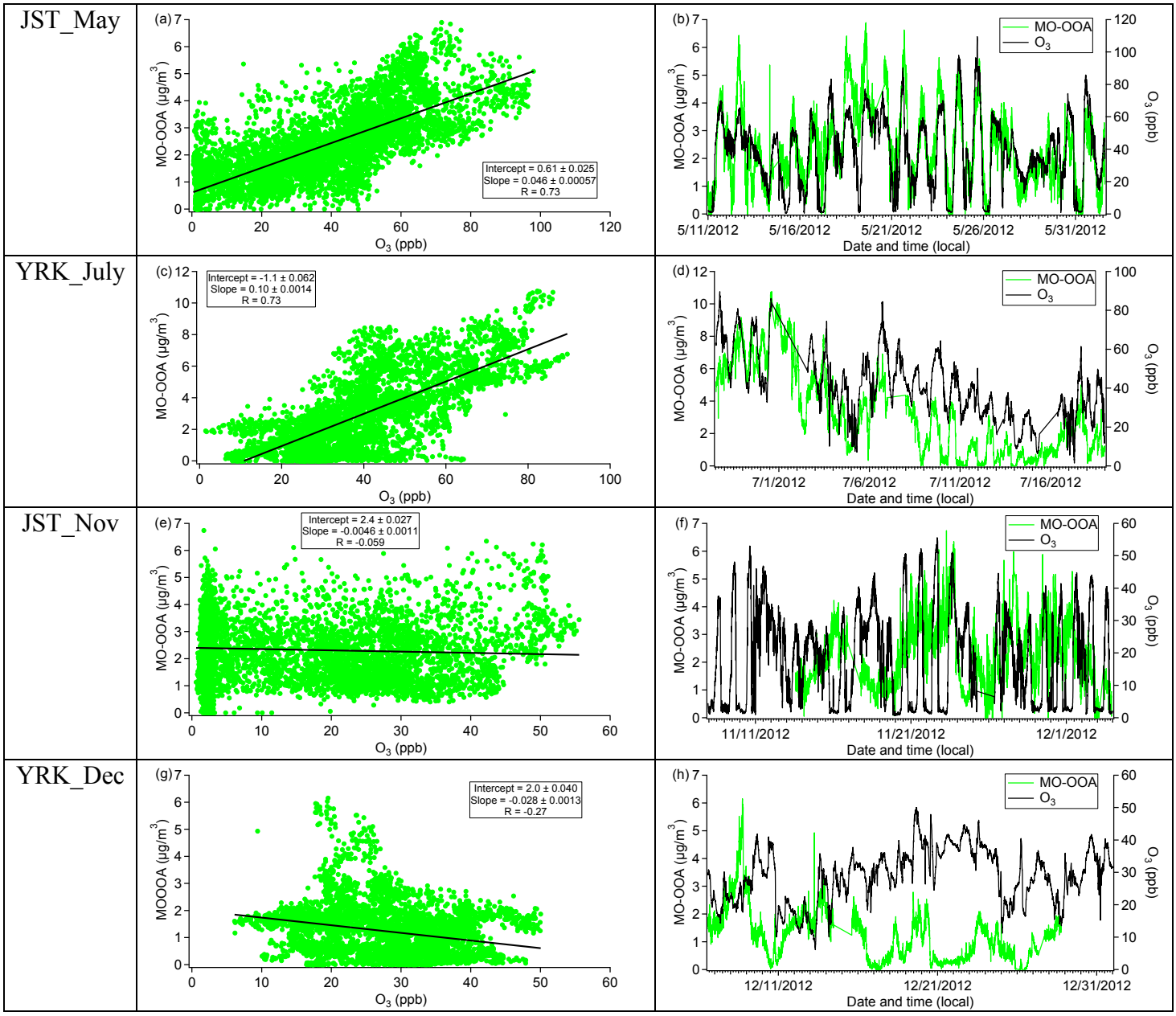

1929

1930

1931

1932

1933

1934

1935 Fig. 9.

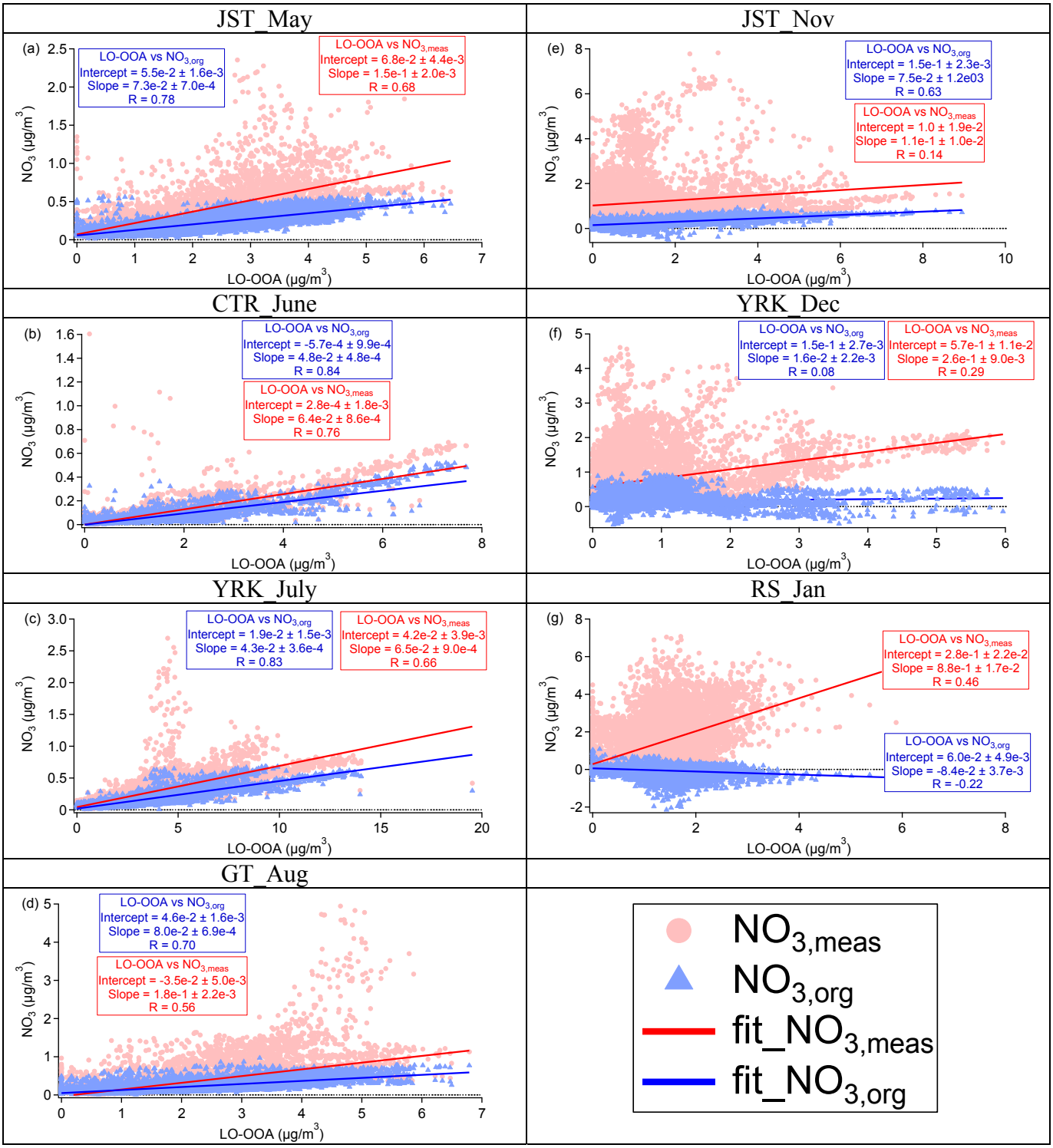

1936

1937

1938 Fig. 10.

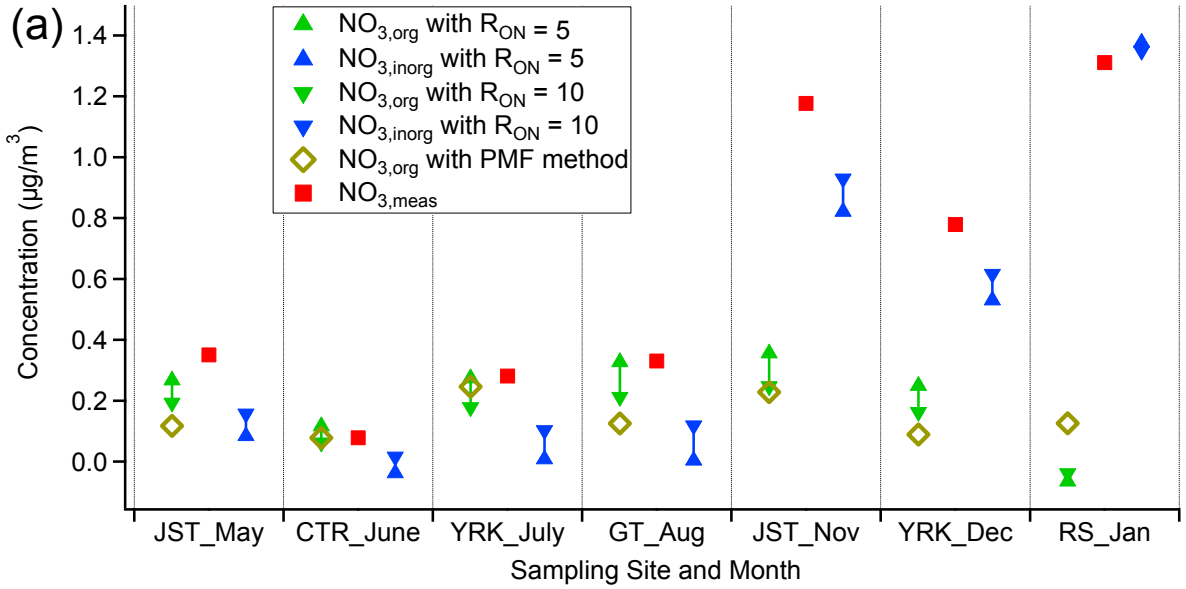

1939

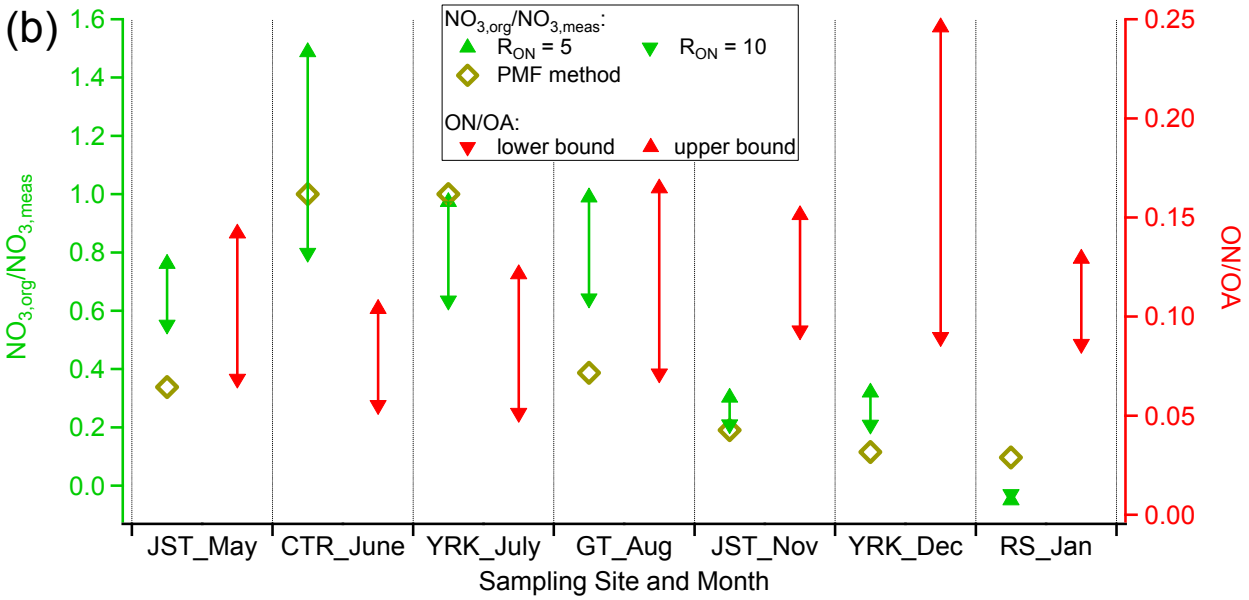

1940

1941

1942

1943

1944

1945

1946 Fig. 11.

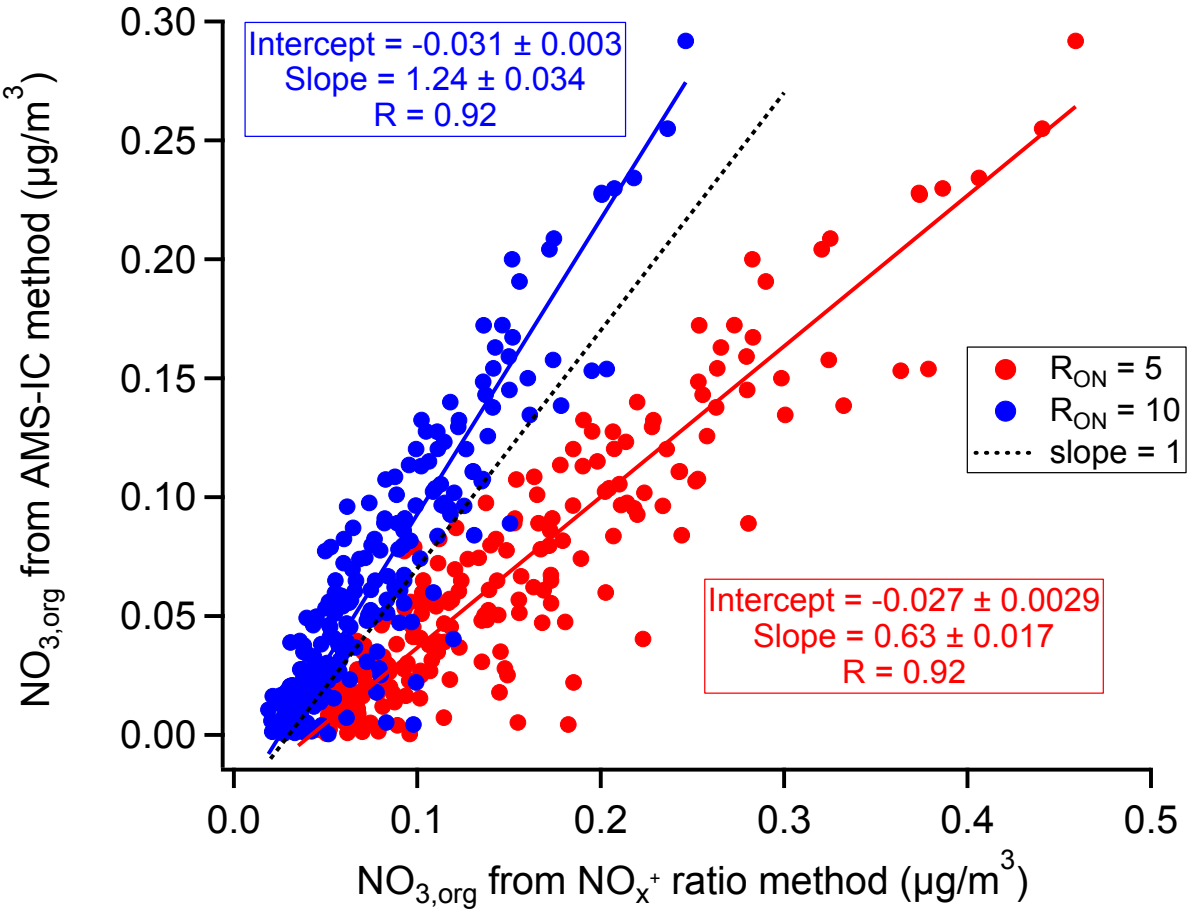

1947

1948

1949

1950

1951

1952

1953

1954

1955

1956

1957

1958 Fig. 12.

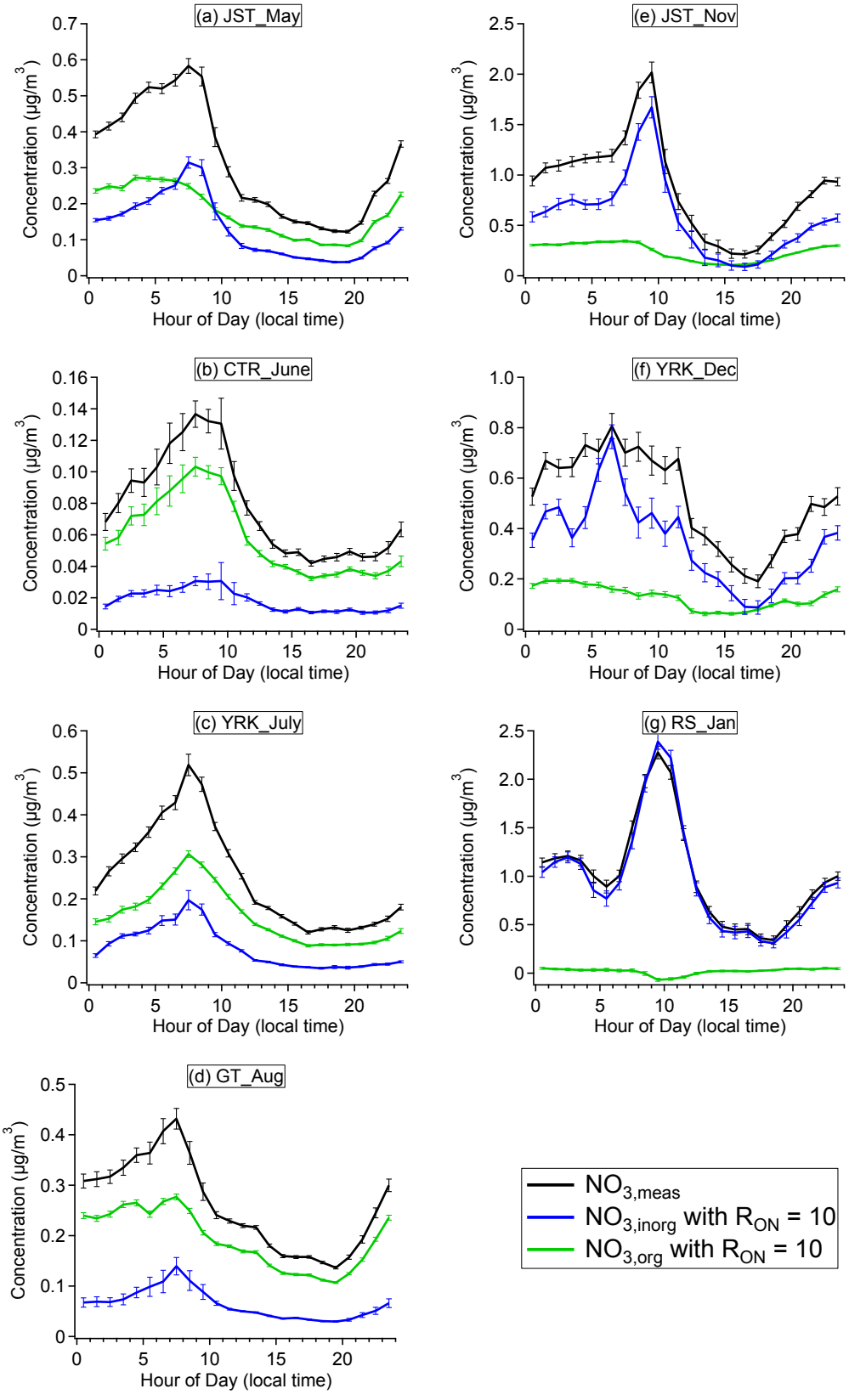

1959

1960

1961

1962

1963 Fig. 13.

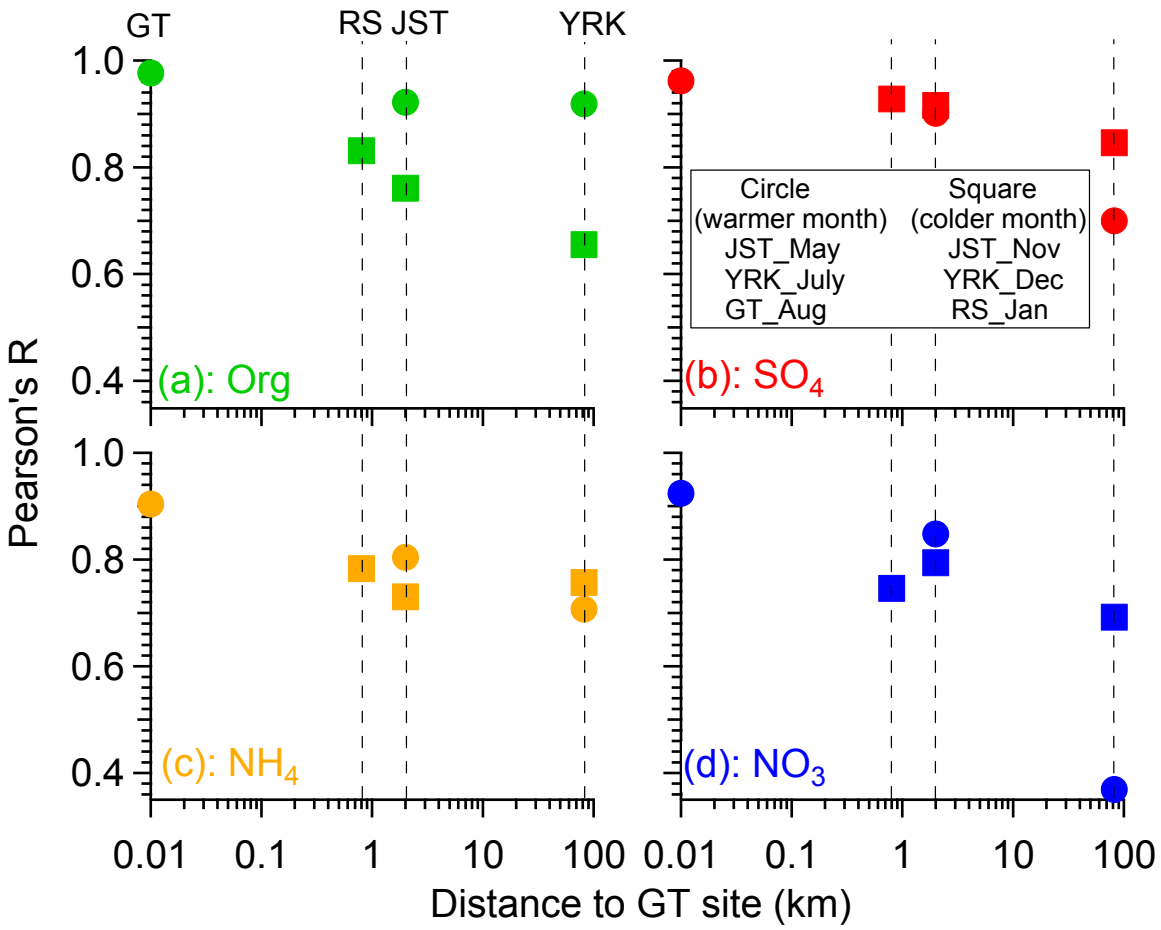

1964

1965

1966

1967

1968

1969

1970

1971

1972

1973

1974

1975 Fig. 14.

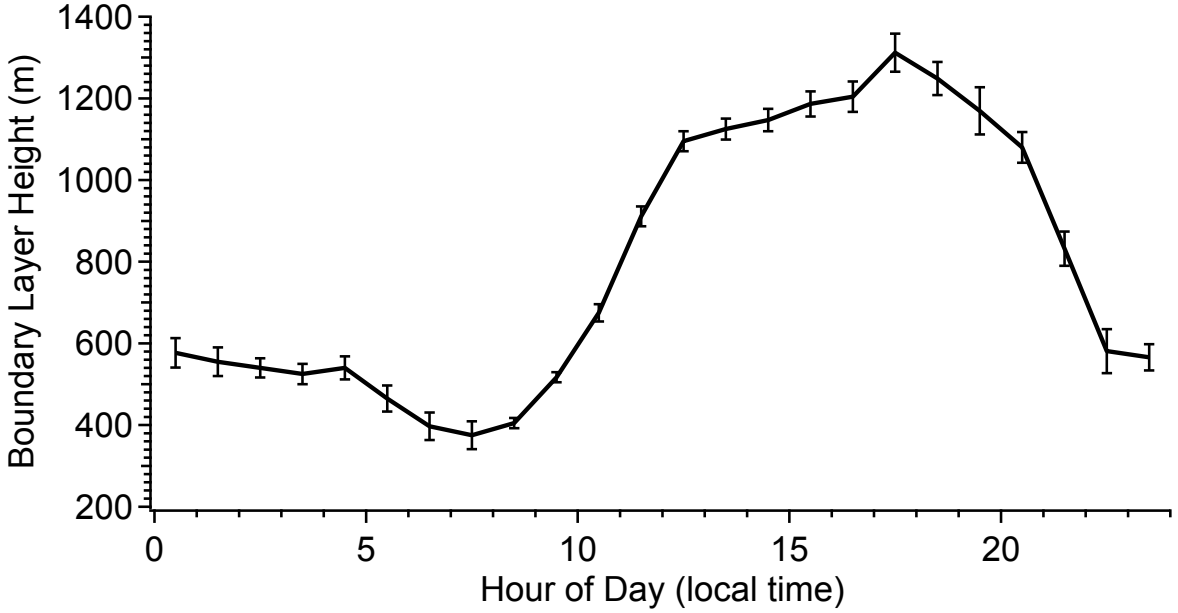

1976

1977

1978

1979

1980

1981

1982

1983

1984

1985

1986

1987

1988

1989

1990

1991 Fig.15.

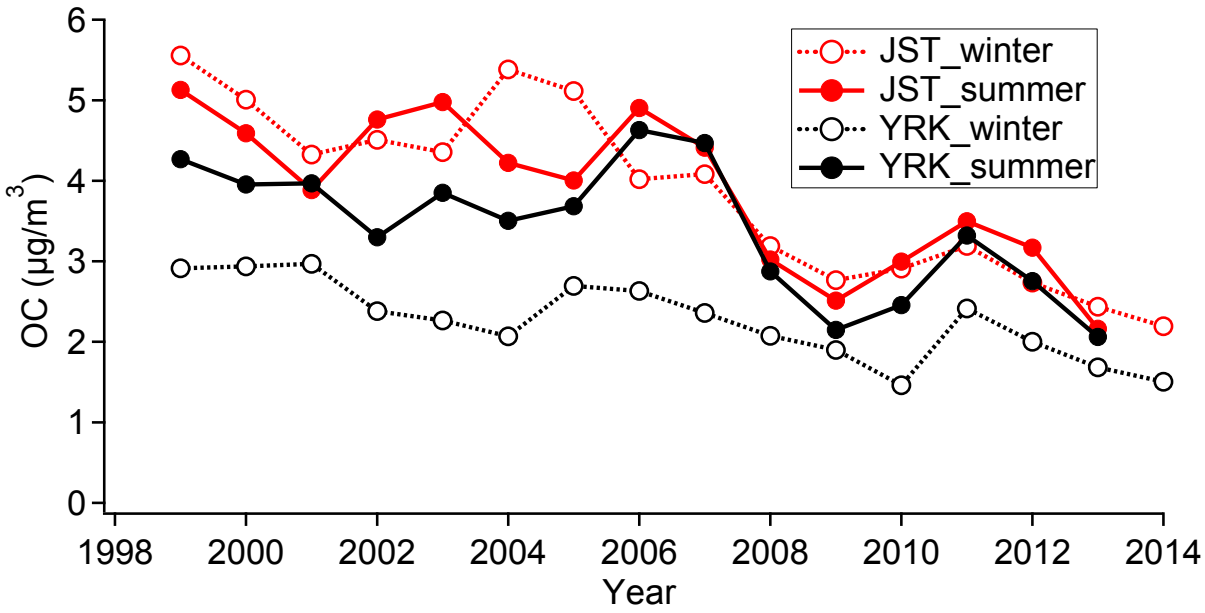

1992

1993

1994

1995

1996

1997

1998

1999

2000

2001

2002

2003

2004

2005

2006

2007 Fig.16.

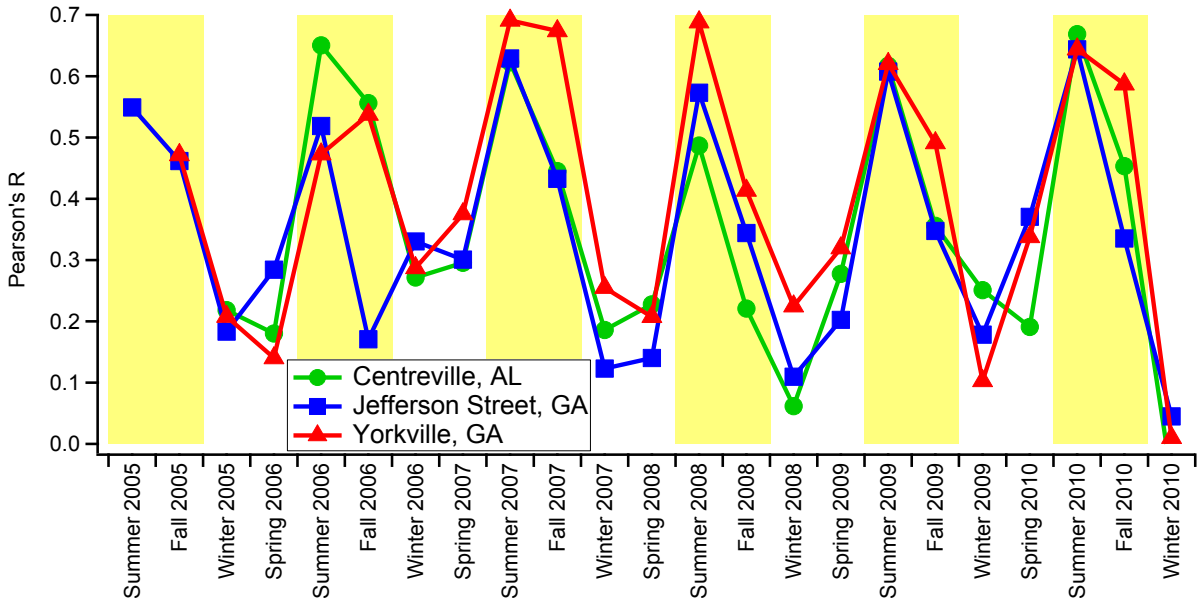

2008

2009

2010

2011

2012

2013

2014

2015

2016

2017

2018

2019

2020

2021

2022

2023